Shape Design and Operation of Microreactors

Osamu Tonomura

2015

Contents

Part II : Operation of Microreactors

Acknowledgments

First of all, I am indebted to my supervisor, Professor Shinji Hasebe, who patiently guided me in completing my Ph.D. study. Little achievement would have been made without his expert advice and criticism. I am grateful to him not only for the deep scientific support and the help in writing my thesis but also for his numerous efforts for providing me the best working conditions.

Besides I would like to thank my thesis committee members, Professor Jun-ichi Yoshida and Professor Kazuhiro Mae for accepting my jury and their insightful comments and suggestions.

I am also grateful to Professor Iori Hashimoto, Professor Manabu Kano and Professor Masaru Noda for their help in planning my studies and the Department of Chemical Engineering at Kyoto University for the use of its facilities. I also wish to thank Mrs Yoshiko Nakanishi and Mr. Satoshi Taniguchi, whose support will never be forgotten.

This work would not have been done without the financial support from New Energy and Industrial Technology Development Organization (NEDO) projects, Grant-in-Aid for Scientific Research, and Kyoto University.

I am indebted to the students and researchers in PSE group. The depth and breadth of knowledge in the group has been impressive and exceedingly valuable. Friendships gained during my time at Kyoto University have made my student and working life enjoyable as well as fruitful.

Last but not least, the constant support of my family has been most invaluable in encouraging me to complete my study.

Osamu Tonomura

Kyoto, 2015

Introduction

This introductory chapter gives some background on microreactors, an overview of design and operation of microreactors, and the outline of this thesis. Section 0.1 provides brief history of micro chemical process technology. Section 0.2 introduces microreactors and numbering-up approach. Section 0.3 is given to transport phenomena in microreactors. Section 0.4 is concerned with reactions using microreactors. Section 0.5 provides basic characterization techniques for microreactors. Sections 0.6 and 0.7 discuss shape design and operation of microreactors, respectively. Finally, the objectives of this research are detailed.

0.1 Background on Micro Chemical Process Technology

For more than 10 years, micro chemical process technology has attracted considerable industrial and academic attention in various fields. The main characteristic of micro chemical processes is the small diameter of the channels ensuring short radial diffusion time. This leads to a narrow residence time distribution, high heat and mass transfer. In addition, micro chemical processes have a high surface to volume ratio allowing efficient heat removal and high molar fluxes. Microfabricated chip devices, usually called “μ-TAS”, have emerged as powerful tools for carrying out chemical and biomedical analysis. Such chip devices can achieve a significantly shorter separation time as well as a more accurate analysis compared to conventional laboratory scale systems. In addition, especially in the chemical industry, R&D on micro chemical processes has been energetically conducted for realizing the production of specialty products that have been difficult to produce in conventional chemical plants. The term microreactor is defined as a reactor containing microstructures for reactions. Such microstructures are often fabricated by using microfabrication processing in the electronics and semiconductor industries, and micromachining in the mechanical engineering, microelectromechanical systems (MEMS)

and microfluidics. The characteristic dimension of the microstructures of microreactors is typically less than several millimeters. A good overview of the state-of-the-art in micro chemical process technologies or microreactors is given by literature [1-4].

The first international conference on microreaction technology (IMRET) was held in 1997 by the German Society for Chemical Engineering and Biotechnology, DECHEMA. Since then, the IMRET conferences have been frequently held in Europe, US and Asia. In Japan, the first workshop on micro chemical plants was held in 2003, and since then, progress in microreactors and related fields has been reported at various workshops annually. Further emphasis is placed on several projects throughout the world. These projects have been launched to further accelerate industrial applications of micro chemical process technology. For example, in Japan, the research association of micro chemical process technology (MCPT) was established in 2002. MCPT realized several pilot-scale micro chemical plants based on the results of experimental and theoretical researches. In Europe, the integrated multiscale process unit with locally structured elements (IMPULSE) project was also started in 2005. IMPULSE aims at the integration of innovative process equipment to attain radical performance enhancement for whole process systems in chemical and pharmaceutical production. Besides these projects, there are many other activities in Europe, US and Asia.

0.2 Microreactors and Numbering-up Approach

A microreactor or microstructured reactor or microchannel reactor is a device in which chemical reactions take place. The microreactor is often split into a mixing zone and a reaction zone to ensure adequate mixing and long residence times. For example, Ratner et al. [5] have developed a microreactor for glycosylation, which has serpentine channels for mixing and reaction as shown in **Fig. 0.1**. Geometrically similar microreactors are also used for Diels-Alder reactions [6] and Oxidation reactions [7] and are on sale from company (e.g., mikroglas chemtech GmbH).

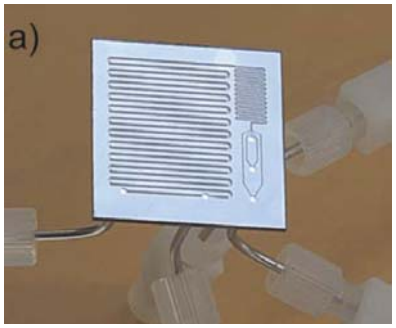

Fig. 0.1 Microreactor with serpentine channel [5]

In micro chemical plants, a micromixer is also a key component. There are a great variety of micromixers that use different principle of minimizing diffusional distances to induce fast mixing between fluid steams. The T-mixers, the jet mixers, the flow focusing mixers, the caterpillar mixers, the K-M mixers, and other types of mixers have been developed so far. These micromixers are mainly classified in two basic concepts: active mixers and passive mixers [8]. A detailed list of these mixers can be found in papers [9-11].

It is necessary to transfer laboratory microprocess operation to the production scale. The ability to replicate flow, transport and reaction conditions from a single microchannel to many parallel microchannels is vital in microreactors. The parallelization of microchannels or microreactors is often referred to as numbering-up. The numbering-up approach is divided into two: internal and external numbering-up structure [12]. Internal numbering-up is the parallelization of some components such as microchannels in one microdevice as shown in **Fig. 0.2**, and external numbering-up is the parallel setup of some microdevices as shown in **Fig. 0.3**.

Fig. 0.4 shows a plate-fin microreactor, which was used for methanol oxidation reforming in the previous research [13]. The plate-fin microreactor is as a representative example of microreactors with internal numbering-up structure. Moreover, the plate-fin microreactors are stacked together for gas-phase reactions [14] and are arranged alternately with a comparable number of plates that comprise cooling-medium channels [15].

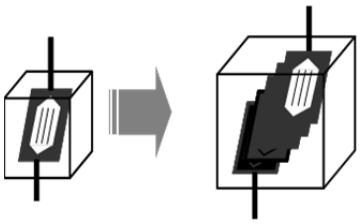

Fig. 0.2 Internal numbring-up

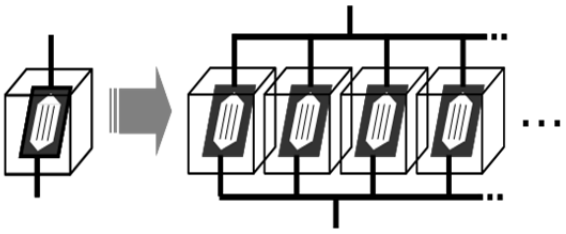

Fig. 0.3 External numbering-up

Fig. 0.4 Plate-fin microreactor [13]

As an example of external numbering-up, a pilot plant was designed by Axiva [16]. Four tubular reactors are parallelized and 28 micromixers are used to mix the inlet flows of them. Togashi et al. [17] also developed a pilot plant using numbering-up of 20 microreactors.

The above mentioned numbering-up approach stands in contrast to scale-up for large-scale conventional plants in which reactor design and dimensions are increased through a series of time-consuming steps. Although the numbering-up approach increases the number of channels, plates with microstructures or devices to enlarge the capacity, the flow distribution must be considered and is a requirement for successful use of microreactors [18]. In other words, the major obstacle in numbering-up – internally or externally – is to provide precise reagent flow rates for each reactor [19]. There are conceptually different ways to control the flows in a plant with numbering-up structure. A pump and/or a mass flow controller is used for each line. This is a very precise method to control the streams, but not available to internally parallelized reactors and certainly an expensive option [19]. In such a case, alternately, one pump/regulator is used for each stream followed by accurate flow distributor. This configuration is less expensive than dedicating a pump or a mass flow controller for each stream [19]. However, the similar pressure drop across every single stream and/or the appropriately designed flow distributors is required. For example, as the number of channels becomes large in a device, the adequate design of manifolds becomes important. If the flow distribution in micro heat exchangers varies by about 5 %, the performance is 5% less than the design value [4]. Multiple channel devices demand new design methodology to increase channel number and provide safe operation conditions.

0.3 Transport Phenomena in Microreactors

Transport phenomena are crucial in the scale-up of conventional chemical reactors because many processes are heat and/or mass transfer controlled. Process engineering calculations and process equipment design begins with the conservation and balance equations of mass, species, momentum, and energy. The conservation laws of mass and energy are valid in the scope of micro chemical processes.

As reactors are miniaturized, the characteristic length and time scales shift to different regimes (see **Table 0.1** [20]) , but almost all transport processes are in the continuum range. Small channels allow short transport lengths for heat and mass transfer. The transport length by diffusion mixing in gas and in liquids is displayed over the corresponding time in **Fig. 0.5** [21]. Microdevices such as micromixers and microreactors provide fluid structures with length scales of approximate 1 μm. These small fluid structures lead to mixing times shorter than 100 μs in

gases and approximate 1 ms in liquids. This is the main reason for the enhanced selectivity and yield of chemical reactions in microreactors [21].

Table 0.1 Scaling effect of transport properties [20]

	nm	μm	mm	m
Length (L)	10^{-9}	10^{-6}	10^{-3}	1
Surface area (L^2)	10^{-18}	10^{-12}	10^{-6}	1
Volume (L^3)	10^{-27}	10^{-18}	10^{-9}	1
Specific surface area (L^{-1})	10^{9}	10^{6}	10^{3}	1
Rate ($\propto L$)	10^{-9}	10^{-6}	10^{-3}	1
Inertial force ($\propto L^4$)	10^{-36}	10^{-24}	10^{-12}	1
Viscous force ($\propto L^2$)	10^{-18}	10^{-12}	10^{-6}	1
Interfacial tension ($\propto L$)	10^{-9}	10^{-6}	10^{-3}	1
Viscous force/inertial force ($\propto L^{-2}$)	10^{18}	10^{12}	10^{6}	1
Interfacial tension/inertial force ($\propto L^{-3}$)	10^{27}	10^{18}	10^{9}	1

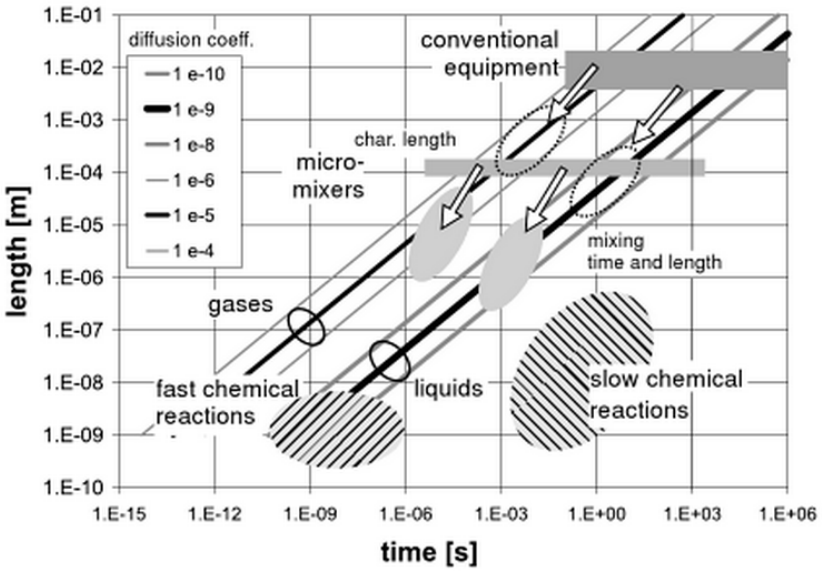

Fig. 0.5 Characteristic length and time scales for mixing in microdevices [21]

In single-phase flows, the fluid motion in microreactors is determined by wall friction, viscous forces and inertial forces. The basic equations are valid for laminar flow with a typical Re number below the critical Re number at transition from laminar to turbulent flow. The critical Re number for flows are in the range of $O(10^3)$. There is still some discussion whether the critical Re number for microchannels is lower than that for conventional geometries. The order-of-magnitude is generally accepted, however, surface roughness and entrance effects should definitely be taken into consideration. For laminar flow, the channel friction factor coefficient is inversely proportional to the flow velocity, i.e. Re number. The channel friction factor coefficients for various cross sections are given in Shah and London [22].

Multiphase flows provide several mechanisms for enhancing and extending the performance of single-phase flow systems [23]. For example, the broad dispersion bands associated with single-phase flows can be reduced by adding a second, immiscible, fluid stream. Various flow patterns have been obtained for two-phase flow in microchannels. Most researchers present representative pictures along with the observed flow pattern map for clarity. The most common flow patterns are bubbly flow, segmented or slug flow, annular flow, and churn flow. Depending on the wetting properties of the microchannel walls, the lubricating films of the continuous phase are observed in segmented and annular flow. The segmented flow gives a number of favorable conditions, including enhanced mixing, increased mass transfer and reduced dispersion. These effects enhance reaction yield and selectivity.

0.4 Reaction using Microreactors

For example, fast reactions are usually highly exothermic. Therefore, heat removal is an important factor in controlling fast reactions. Heat transfer takes place through the surface of the reactor. By taking advantage of the fact that microspaces have a large surface area per unit volume compared with macrospaces, heat transfer occurs very rapidly in microscale systems, making precise temperature control possible.

There are many applications of microreactors in various fields. Hessel et al. [3] give a comprehensive overview of chemical reaction applications. In addition, the concept of flash chemistry was coined by Yoshida [24] for fast reactions. The features of microreactors are quite useful in controlling fast reactions involving highly reactive unstable intermediates. Therefore, chemical conversions that are impossible in conventional reactors should be made possible using microreactors.

The reaction examples using microreactors are introduced as follows [25]. Friedel-Crafts alkylations are investigated by using short mixing time and good temperature control. Aromatic and heteroaromatic compounds react as nucleophiles to give Friedel-Crafts-type alkylation products in rapid reactions. These mixing and temperature-sensitive reactions serve as good examples for flash chemistry. Halogenations and metal organic reactions such as Grignard or lithiation are further prominent examples. Higher temperature in a pressurized system accelerates chemical reactions and makes slow reactions suitable for micro flow synthesis. Also polymerizations have been performed successfully in microreactors. The concept of Novel Process Windows is well described by Hessel et al. [26], giving the chemists more opportunities for synthesizing and processing complex molecules. The container approach for chemical production is followed by chemical companies. The Evotrainer concept [27] was developed for small-scale production of specialty chemicals. The container serves for process development, personal training as well as production of early market supply.

Currently, several guides through the multitude of chemical reactions can be found in literature. The Flow Chemistry Society, which publishes the Journal of Flow Chemistry, was formed in 2010 by flow chemistry researchers to unite and represent those who are actively working on this rapidly developing field. A more recent book of Wiles and Watts [28] covers many chemical reactions investigated in their research group, performed in their reaction system, and gathered from open literature. The reactions are categorized according to the involved phases, i.e., gas-liquid multiphase and solid formation, as well as for reaction initiation. Special emphasis is also given to droplet and particle formation as well as industrial applications and continuous-flow separation techniques.

0.5 Characterization Techniques for Microreactors

This section describes numerical and experimental techniques for the characterization of microscale flow. One of the most often used experimental techniques is imaging technique, for example, brightfield microscopy [29], fluorescence microscopy [30], and confocal microscopy [31]. Since the imaging technique offers a noninvasive mean of measurement in microscale flow, it is the key tool for characterizing microreactors. The most common technique for measuring the velocity field inside a microreactor is particle image velocimetry (PIV). The PIV measurement is carried out by recording two images of particles at two different time instances. In addition, the efficiency of mixing is indirectly measured on the basis of the products of chemical reactions or the change of fluorescent intensity. Parallel competing reactions can be used for evaluating mixing efficiency. For example, a mixture of iodate, iodine, sodium

hydroxide, and boric acid is mixed with sulfuric acid, the so-called Dushman reaction occurs [32].

In order to facilitate interpretation of the experimental measurements, numerical modeling and simulation is often performed. Fluid dynamics determines the characteristics of microreactors with pressure drop, residence time, heat transfer, and mixing. Particularly, mixing in laminar flow is quite complex and needs a high mathematical effort [21]. For example, a model for convective mixing in T-shaped micromixers and combined meandering micromixers was proposed [33]. It is important to know how mixing can influence the selectivity of chemical reactions, and computational fluid dynamics (CFD) simulations are quite helpful in providing a deeper insight into this issue. Apart from microreactors, in the field of MEMS, efficient simulators have been developed to predict device performance[34–37] . A lumped-parameter system is usually used in MEMS simulators to describe flow behavior, because a model should be simple in order to enhance design efficiency. But, when micro chemical plants are analyzed and designed, microreactors need to be treated as distributed-parameter systems in order to analyze rigorously the characteristics of flow and heat transfer in them. Thus, not MEMS simulators but CFD simulators are suitable for designing microreactors.

CFD is concerned with obtaining numerical solution to fluid flow problems by using the high-speed and large-memory computers. The differential equations governing the fluid flow are transformed into a set of algebraic equations, which can be solved with the aid of a digital computer. The well known discretization methods used in CFD are Finite Difference Method (FDM), Finite Volume Method (FVM) and Finite Element Method (FEM). CFD not only predicts fluid flow behavior, but also the transfer of heat and mass, phase change, and chemical reaction. CFD analysis often shows the phenomena happening within a system or device that would not otherwise be visible through any other means. In design and development, CFD is now considered to be standard numerical tool, widely used within industry, and it is an essential tool for shortening the design and development cycles.

For single-phase flows, there exit a number of commercial CFD codes that can be used to investigate mass and heat transfer phenomena. In multi-phase systems, numerical simulations can be also performed using commercially available codes [38]. For example, phase-field methods, which use a phase order parameter to indicate the location of interfaces, are applied to the analysis of breakup and coalescence phenomena [39]. Lattice-Boltzmann methods are also used to simulate a flow-focusing device [40]. In addition, volume-of-fluid methods keep track of the volumetric fraction of each phase and are used to analyze segmented flow in

microchannels [41].

0.6 Shape Design of Microreactors

The design of microreactors is largely a trial-and-error process resulting in inefficiencies and suboptimal designs [42]. Through the R&D activities on microreactors, the necessity of developing a systematic design method of microreactors has been recognized. Microreactor design problems are different from those of conventional reactors. In a conventional design problem, the unit operations are modeled by using terms such as perfect mixing and overall heat transfer coefficient. In other words, each unit operation is modeled as a lumped parameter system. However, the desired performance of microreactors can be achieved by the precise control of the temperature, the residence time distribution and/or the degree of mixing. Hence, each microreactor is modeled as a distributed parameter system. And then, the shape of the reactor must be included in the design variables in addition to the size of the reactor. The existent papers [1, 43] convey the fact that the manifold shape of a plate-fin microreactor affects the flow distribution in the parallelized microchannels, through CFD simulation. Amador et al. [44] investigated the effects of channel blockages and manifold structures on flow distribution in microchannel reactors by using an analytical model based on electrical resistance networks. J. Aubin et al. [45] investigate the effect of various geometrical parameters of a grooved staggered herringbone micromixer on the mixing performance by using CFD. The grooved staggered herringbone micromixer and creates a transverse velocity component in the flow field. In addition, in segmented flows, the film menisci shape between the channel and dispersed phase is influenced by cross-sectional shape of channels [46]. The different thickness of inner and outer film menisci is given by the serpentine channels [47]. In addition, such non-straight channels break symmetry and enhance mixing in bubbles [48]. This enhanced mixing is due to chaotic advection in flow. According to these reports, a design problem of microreactors is regarded as a shape optimization problem, in which a cost function defined on a flow domain and/or on its boundary is minimized or maximized under several constraints.

Most things can be improved, so engineers and scientists optimize. Optimization is a key enabling tools for decision making in chemical engineering. An optimal design problem is basically formulated as follows:

$$\text{Minimize} \quad I = I(\boldsymbol{x}) \qquad \text{with respect to} \quad \boldsymbol{x}$$

$$\text{subject to} \quad \begin{cases} h(\boldsymbol{x}) = 0 \\ c(\boldsymbol{x}) \le 0 \end{cases}$$

In the case of a fluid-dynamic optimization problem, the cost function I depends on design variables and state variables. The design variables represent the shape of channels. The cost function I is minimized, subject to partial differential equation (PDE) constraints, h, such as Navier-Stokes equations. and geometric constraints, c.

With the advances in computational resources and algorithms, CFD-based optimal shape design is an interesting field for industrial applications such as aerospace, car, train, and ship building [49-54]. In such design, the computation of the cost function gradient, namely the sensitivity of some performance measure, is the heart of the optimization. Recently, the adjoint variable method has attracted the attention as an efficient sensitivity analysis method [55-57], since it allows successfully obtaining the shape gradient functions independently of the number of design variables. Therefore, one of objectives of this thesis is placed on the development of a shape optimization system using the adjoint variable method.

0.7 Operation and Control of Microreactors

The performance of micro chemical plants with numbering-up structure depends on the flow distribution among the parallelized microchannels/microreactors [58]. It is desired to achieve the equalization of flow rates of all the microchannels/microreactors because the flow maldistribution deteriorates reaction selectivity, heat transfer efficiency, and so on. Blockage or clogging is the most recognized trouble with microreactors. For example, Bayer et al. [59], who developed a continuous radical polymerization process having micro pre-mixers, mentioned that poor mixing conditions cause blockage in a reactor. Ju et al. [60] applied a stainless steel microchannel reactor for the continuous synthesis of zeolite NaA, and they found that aging the synthesis solution was a key procedure for avoiding blockage of the microchannel. In these literatures and others, one of the critical operation problems was blockage in microreactors, which negatively affects the flow distribution in the whole micro chemical plants with numbering-up structure. The flowrate in each microreactor can be kept at a desired value by installing flow controllers, but it is not practical to install flow controllers in all the microreactors. To accelerate industrial application of micro chemical process technology, it is

necessary to develop a process monitoring and control system for microreactors.

Although conventional physical sensors and actuators can be miniaturized and connected to microreactors, several other monitoring and control methods for continuous flow processes are introduced in literature [61]. Temperature can be measured through integrated sensors and controlled with on-chip or modular components. For example, thin layers of platinum are deposited on microreactors to record and adjust reactor temperatures [62]. Resistive electrical heaters [63] is also used to control temperatures. In addition, flow rates can be measured with micropressure sensors [64] and optical fiber cantilevers [65]. Flow control methods include not only commercial syringe pumps but also pneumatic [66] and passive pumping [67] systems. Furthermore, several research groups have monitored the streams of microreactors by using spectroscopic tools such as IR [68], Raman [69] and NMR [70]. These monitoring and control methods basically can be applied to a single microreactor for laboratory use, and it will not be assumed that they are directly installed to microreactors with numbering-up structure. Therefore, simpler and more reasonable monitoring and control methods need to be developed for production units.

0.8 Objective and Thesis Structure

This thesis is outlined according to the design and operation of microreactors. Part I presents the design of appropriate microreactor geometries and is composed of three chapters. Part II presents the operation of microreactors with numbering-up structure and is composed of four chapters.

Most microreactors are usually developed ad hoc, on the basis of engineers' experience. In other words, there is no systematic procedure for developing a microreactor. In Chapter 1, as the first step of the systematic design of microreactors, a design problem of a plate-fin microreactor is focused on, and characteristics of flow pattern inside plate-fin microreactors are investigated by using CFD. In addition, a CFD-based optimization method is proposed for the design of plate-fin microreactors.

CFD is often used to rigorously examine the influence of the shape of microchannels on heat and mass transport phenomena in the flow field. However, the rash combination of CFD and the optimization technique based on evaluating gradients of the cost function requires enormous computation time when the number of design variables is large. Recently, the adjoint variable method has attracted the attention as an efficient sensitivity analysis method, particularly for

aeronautical shape design, since it allows one to successfully obtain the shape gradient functions independently of the number of design variables. In Chapter 2, an automatic shape optimization system based on the adjoint variable method is developed. The major drawbacks of microreactors are high pressure drop, which conflicts with industrial production [4]. Therefore, to validate the effectiveness of the developed system, pressure drop minimization problems of a U-shaped microchannel and a branched microchannel in incompressible flows under constant volume conditions are solved.

For larger and complicated geometries of microreactors, the numerical simulation of transport phenomena is too elaborate and time-consuming for CFD. Alternatively, simplified modeling helps to reduce the complexity and leads to an efficient analysis and design. Therefore, a new systematic design approach based on a simplified thermo-fluid model is developed in Chapter 3. The developed approach is applied to the optimal design problem of a plate-fin microreactor with uniform temperature and residence time distributions.

When the production capacity of micro chemical plants is increased by numbering-up approach, it is important to realize the uniform flow distribution among the parallelized microreactors. In Chapter 4, test plants are constructed to analyze the influence of blockage on the flow distribution among the parallelized microreactors under two types of operation policies, pressure drop control and total flow control.

In addition, a blocked microreactor needs to be identified as early as possible to achieve the stable long-term operation of micro chemical plants. In Chapter 5, two types of blockage diagnosis systems are developed to identify a blocked plate among stacked microreactors by using two temperature sensors. In Chapter 6, the flow uniformity in a new type of flow distributor, split-and-recombine-type flow distributor (SRFD), which has three or more bifurcation points and one or more junction points, is examined through CFD simulation, and another blockage diagnosis system is developed to isolate a blocked microreactor from the externally parallelized microreactors by using two flow sensors, which are embedded in the SRFD. In Chapter 7, two methods developed in Chapters 4 and 6 are combined to keep continuous operation of a plant without shutdown until it is returned to normal condition after detecting a blocked microreactor. In addition, the performance of the developed system is maximized by adjusting the channel size and sensor placement in the flow distributors. Finally, conclusions and final remarks are described.

References

[1] W. Ehrfeld, V. Hessel, H. Lowe, "Microreactors: new technology for modern chemistry," Wiley, VCH, Weinheim (2000)

[2] P.D.I. Fletcher, S.J. Haswell, E. Pombo-Villar, B.H. Warrington, P. Watts, S.Y.F. Wong, X. Zhang, "Micro reactors: principles and applications in organic synthesis," Tetrahedron **58**, 4735-4757 (2002)

[3] V. Hessel, S. Hardt, H. Lowe, "Chemical micro process engineering: fundamentals, modelling and reactions," Wiley, VCH, Weinheim (2005)

[4] N. Kockmann, "Micro process engineering: fundamentals, devices, fabrication, and applications," Wiley, VCH, Weinheim (2006)

[5] D.M. Ratner, E.R. Murphy, M. Jhunjhunwala, D.A. Snyder, K.F. Jensen, P.H. Seeberger, "Microreactor-based reaction optimization in organic chemistry - glycosylation as a challenge," Chemical Communications, 578-580 (2005)

[6] R.M. Tiggelaar, F. Benito-Lozpez, D.C. Hermes, H. Rathgen, R.J.M. Egberink, F.G. Mugele, D.N. Reinhoundt, A. van den Berg, W. Verboom, J.G.E. Gardeniers, "Fabrication, mechanical testing and application of high-pressure glass microreactor chips," Chemical Engineering Journal, **131**, 163-170 (2007)

[7] E. R. Delsman, M.H.J.M. de Croon, G.J. Kramer, P.D. Cobden, C. Hofmann, V. Cominos, J.C. Schouten, "Experiments and modeling of an integrated preferential oxidation - heat exchanger microdevice," Chemical Engineering Journal, **101**, 123–131 (2004)

[8] L. Falk and J.M. Commenge, "Performance comparison of micromixers," Chemical Engineering Science, **65**, 405-411 (2010)

[9] N.T. Nguyen and Z. Wu, "Micormixers - a review," Journal of Micromechanics and Microengineering, **15**, 1-16 (2005)

[10] T.M. Squires and S.R. Quake, "Microfluidics: fluid physics at the nanoliter scale," Reviews of Modern Physics, **77**, 977-1026 (2005)

[11] H. Lowe, W. Ehrfeld, W Hessel, V. Richter, J Schieve, Preprint of 4th Int. Conf. on Microreaction Technology, 441-445, Atlanta, US (2000)

[12] V. Hessel and H. Lowe; "Microchemical engineering: components, plant concepts, user acceptance-part Ⅲ," Chemical Engineering Technology, **26**(5), 531-544 (2003)

[13] G. Chen, S. Li, Q. Yuan, "Pd-Zn/Cu-Zn-Al catalysts prepared for methanol oxidation reforming in microchannel reactors," Catalysis Today, **120**, 63-70 (2007)

[14] N. Steinfeldt, N. Dropka, A. Wolf, M. Baerns, "Application of multichannel microreactors for studying heterogeneous catalyzed gas phase reactions," Chemical Engineering Research and Design, **81**(A7), 735-743 (2003)

[15] S. Schubert, R. Schellen, L. Mleczko, S. Laue, P. Lehner, US 2009093655 A1 (2009)

[16] T. Bayer, D. Pysall, O. Wachsen, "Micro mixing effects in continuous radical polymerization for the production of acrylates," Preprint of 3rd International Conference on Microreaction Technology, 165-170 (2000)

[17] S. Togashi, T. Miyamoto, T. Sano, M. Suzuki, "Development of a pilot plant using the numbering-up of microreactors," Preprint of 9th International Conference on Microreaction Technology, 222-223, Potsdam, Germany (2006)

[18] J. Yue, R. Boichot, L. Luo, Y. Gonthier, G. Chen and Q. Yuan, "Flow Distribution and Mass Transfer in a Parallel Microchannel Contactor Integrated with Constructal Distributors," AIChE, **56**, 298-317 (2010)

[19] T. Schwalbe, A. Kursawe, J. Sommer, "Application report on operating cellular process chemistry plants in fine chemical and contract manufacturing industries," Chemical Engineering and Technology, **28**(4) 408-419 (2005)

[20] K. Mae, "Advanced chemical processing using microspace," Chemical Engineering Science, **62**, 4842-4851 (2007)

[21] N. Kockmann, "Transport phenomena in micro process engineering," Springer (2008)

[22] R.K. Shah and A.L. London, "Laminar forced convection in ducts," Academic Press, New York (1978)

[23] A. Gunther and K.F. Jensen, "Multiphase microfluidics: from flow characteristics to chemical and materials synthesis," Lab on a Chip, **6**, 148-1503 (2006)

[24] J.-I. Yoshida, "Flash chemistry," WILEY (2008)

[25] T. Bieringer, S. Buchholz, N. Kockmann, "Future production concepts in the chemical industry: modular - small-scale - continuous," Chemical Engineering and Technology, **36**(6), 900-910 (2013)

[26] V. Hessel, I. Vural Gürsel, Q. Wang, T. Noël, J. Lang, "Potential analysis of smart flow processing and micro process technology for fastening process development: use of chemistry and process design as intensification fields," Chemical Engineering and Technology. **35**, 1184-1204 (2012)

[27] J. Lang, F. Stenger, H. Richert, Evonik Elements, **37**, 12-17 (2011)

[28] C. Wiles, P. Watts, "Micro Reaction Technology in Organic Synthesis," CRC Press, Boca Raton, FL (2011)

[29] D.R. Link, S.L. Anna, D.A. Weitz, H.A. Stone, "Geometrically mediated breakup of drops in microfluidic devices," Physical Review Letters, **92**, 054503 (2004)

[30] Y.F. Fan and I, Hassan, "Experimental and numerical investigation of a scaled-up passive micromixer using fluorescence technique," Experiments in fluids, **49**, 733-747 (2010)

[31] H. Kinoshita, S. Kaneda, T. Fujiia, M. Oshima, "Three-dimensional measurement and

visualization of internal flow of a moving droplet using confocal micro-PIV," Lab on a Chip, **7**, 338-346 (2007)

[32] M.C. Fournier, L. Falk, J. Villermaux, "A new parallel competing reaction system for assessing micromixing efficiency-determination of micromixing time by a sample mixing model," Journal of Fluid Mechanics, **555**, 5178-5192 (1996)

[33] N. Kockmann, T Kiefer, M. Engler and P Woias, Convective mixing and chemical reactions in microchannels with high flow rates, Sensors & Actuators B, **117**, 495-508 (2006)

[34] O. Nagler, M. Trost, B. Hillerich, F. Kozlowski, "Efficient design and optimization of MEMS by integrating commercial simulation tools," Sensors & Actuators A, **66**, 15-20 (1998)

[35] C.G. Schabmueller, M. Koch, A.G.R. Evans, A. Brunnschweiler, "Design and fabrication of a microfluidic circuitboad," Journal of Micromechanics and Microengineering, **9**, 176-179 (1999)

[36] A. Rasmussen, C. Marvriplis, M.E. Zaghloul, O. Mikulchenko, K. Mayaram, "Simulation and optimization of a microfluidic flow sensor," Sensors & Actuators A, **88**, 121-132 (2001)

[37] P. Schneider, A. Schneider, P. Schwarz, "A modular approach for simulation-based optimization of MEMS," Microelectronics Journal, **33**, 29-38 (2002)

[38] A.J. Abrahamse, A. van der Padt, R.M. Boom, W.B.C. de Heij, "Process fundamental of membrane emulsification: simulation with CFD," AIChE J., **47**(6), 1285-1291 (2001)

[39] De Menech, M., "Modeling of droplet breakup in a microfluidic T-shaped junction with a phase-field model," Physical Review E, **73**, 031505 (2006)

[40] Z. Yu, O. Heraminger, L.S. Fan, "Experiment and lattice Bltzmann simulation of two-phase gas-liquid flows in microchannels," Chemical Engineering Science, **62**, 7172-7183 (2007)

[41] D.Y. Qian and A. Lawal, "Numerical study on gas and liquid slugs for Taylor flow in a T-junction microchannel," Chemical Engineering Science, **61**, 7609-7625 (2006)

[42] L. Falk and J.M. Commenge, "Performance comparison of micromixers," Chemical Engineering Science, **65**, 405-411 (2010)

[43] G. Griffini and A. Gavriilidis, "Effect of microchannel plate design on fluid flow uniformity at low flow rates," Chemical Engineering and Technology, **30**, 395-406 (2007)

[44] C. Amador, A. Gavriilidis, P. Angeli, "Flow distribution in different microreactor scale-out geometries and the effect of manufacturing tolerances and channel blockage," Chemical Engineering Journal, **101**, 379–390 (2004)

[45] J. Aubin, D.F. Fletcher, C. Wuereb, "Design of micromixers using CFD modeling," Chemical Engineering Science, **60**, 2503-2516 (2005)

[46] M.T. Kreutzer, A. Gunther, K.F. Jensen, “Sample dispersion for segmented flow in microchannels with rectangular cross section,” Analytical Chemistry, **80**, 1558-1567 (2008)

[47] M. Muradoglu and H.A. Stone, “Motion of large bubbles in curved channels,” Journal of Fluid Mechanics, **570**, 455-466 (2007)

[48] A. Gunther, S.A. Khan, M. Thalmann, F. Trachsel, K.F. Jensen, “Transport and reaction in microscale segmented gas-liquid flow,” Lab on a Chip, **4**, 278-286 (2004)

[49] W.K. Anderson, V. Venkatakrishnan, “Aerodynamic design optimization on unstructured grids with a continuous adjoint formulation,” Computer & Fluids, **28**, 443-480 (1999)

[50] B. Mohammadi and O. Pironneau, “Applied shape optimization for fluids,” Oxford Science Publications (2001)

[51] O. Pironneau, “On optimum profiles in Stokes flow,” Journal of Fluid Mechanics, **59**(1), 117-128 (1973)

[52] O. Pironneau, “On optimum design in fluid mechanics,” Journal of Fluid Mechanics, **64**(1), 97-110 (1974)

[53] O. Pironneau, “Optimal shape design for elliptic systems,” Springer-Verlag, New York (1984)

[54] J. Reuther, J.J. Alonso, M.J. Rimlinger, A. Jameson, “Aerodynamic shape optimization of supersonic aircraft configurations via an adjoint formulation on distributed memory parallel computers,” Computer & Fluids, **28**, 675-700 (1999)

[55] M.B. Giles and N.A. Pierce, “An introduction to the adjoint approach to design,” Flow, Turbulence and Combustion, **65**, 393-415 (2000)

[56] A. Jameson, L. Martinelli, N.A. Pierce, “Optimum aerodynamic design using the Navier-Stokes equations,” Theoretical Computational Fluid Dynamics, **10**, 213-237 (1998)

[57] O. Soto, R. Löhner, C. Yang, “An adjoint-based design methodology for CFD problems,” International Journal of Numerical Methods for Heat & Fluid Flow, **14**(6), 734-559 (2004)

[58] Fujioka, T., M. Kano, O. Tonomura, S. Hasebe; "Data-Based and Model-Based Blockage Diagnosis Systems for Stacked Micro Chemical Plants", AIChE Annual Meeting, paper 570b, Cincinnati, OH, Oct. 30-Nov. 4 (2005)

[59] T. Bayer, D. Pysall, O. Wachesen, “Micro mixing effects in continuous radical polymerization,” Proceedings of 3rd International Conference o Microreaction Technology (IMRET3), Frankfurt, Germany, 165-170 (1999)

[60] Ju, J., Zeng, C., Zhang, L., Xu, N., “Continuous synthesis of zeolite NaA in a microchannel reactor,” Chemical Engineering Journal, **116**, 115-121 (2006)

[61] J.P. McMullen and K.F. Jensen, “Integrated microreactors for reaction automation: new approaches to reaction development,” Annual Review of Analytical Chemistry, **3**, 19-42 (2010)

[62] D.J. Quiram, K.F. Jensen, M.A. Schmidt, P.L. Mills, J.F. Ryley, "Integrated microreactor system for gas-phase catalytic reactions. 1. Scale-up microreactor design and fabrication," Industrial & Engineering Chemistry Research, **46**, 8292-305 (2007)

[63] M.W. Losey, R.J. Jackman, S.L. Firebaugh, M.A. Schmidt, K.F. Jensen, "Design and fabrication of microfluidic devices for multiphase mixing and reaction," Journal of Microelectromechanical Systems, **11**, 709-17 (2002)

[64] X. Zhang, P. Coupland, P.D.I. Fletcher, S.J. Haswell, "Monitoring of liquid flow through microtubes using a micropressure sensor," Chemical Engineering Research and Design, **87**, 19-24 (2009)

[65] V. Lien, F. Vollmer, "Microfluidic flow rate detection based on integrated optical fiber cantilever," Lab on a Chip, **7**, 1352-56 (2007)

[66] T. Braschler, L. Metref, R. Zvitov-Marabi, H. van Lintel, N. Demierre, "A simple pneumatic setup for driving microfluidics," Lab on a Chip, **7**, 420-22 (2007)

[67] G.M. Walker and D.J. Beebe, "A passive pumping method for microfluidic devices," Lab on a Chip, **2**,131-34 (2002)

[68] C.F. Carter, H. Lange, S.V. Ley, I.R. Baxendale, B. Wittkamp, J.G. Goode, N.L. Gaunt, "ReactIR Flow Cell: A New Analytical Tool for Continuous Flow Chemical Processing," Organic Process Research & Development, **14**, 393-404 (2010)

[69] S. Mechtilde, S. Eduard, F. Andreas, "Computer controlled chemical micro-reactor," Journal of Physics: Conference Series, **28**, 115-118 (2006)

[70] J. Bart, A.J. Kolkman, A.J. Oosthoek-de Vries, K. Koch, P.J. Nieuwland, H.J.W.G. Janssen, J.P.J.M. van Bentum, K.A.M. Ampt, F.P.J.T. Rutjes, S.S. Wijmenga, H.J.G.E. Gardeniers, A.P.M. Kentgens, "A microfluidic high-resolution NMR flow probe," Journal of the American Chemical Society, **131**, 5014-5015 (2009)

Part I

Shape Design of Microreactors

Chapter 1

Shape Design Using Sequential CFD-based Simulation

Most microreactors are usually developed ad hoc, on the basis of engineers' experience. In other words, there is no systematic procedure for developing a microreactor. In this chapter, as the first step of the systematic design of microreactors, a design problem of a plate-fin microreactor is focused on, and characteristics of flow pattern inside plate-fin microreactors are investigated by using CFD. In addition, a CFD-based optimization method is proposed for the design of plate-fin microreactors. By using the proposed method, the optimal shape of manifold which minimizes space time under the constraint on flow uniformity is automatically derived.

1.1 Necessity for Shape Design of Microreactors

The use of microreactors for industrial scale production requires a large number of parallel microchannels, because each microchannel provides only a small amount of products. At first glance, the repetition of a microchannel may appear to be simple, but there are issues that have not been addressed in the design and operation of conventional chemical plants. The inadequate shape design gives rise to poor uniformity in the temperature and residence time distributions among parallel microchannels, which will make product quality worse. To show how the device shape affects the flow pattern in the device, three-dimensional flow simulations are executed by using commercial CFD software (Fluent®).

Figure 1.1 shows the normalized mass flow rate at each parallel channel. Vertical axis denotes dimensionless mass flow rate, which is defined by

$$\bar{F} = \frac{1}{5}\sum_{i=1}^{5} F(i) \tag{1.1}$$

$$f(i) = \frac{F(i)}{\bar{F}} \tag{1.2}$$

where $F(i)$ is mass flow rate at channel i.

As $f(i)$ (i = 1, 2, . . . , 5) is closer to 1.0, flow uniformity becomes better. From the viewpoint of flow uniformity, Type B-2 is better than Type B-1. The sizes of inlet manifold in Types B-3 and B-4 are larger than those in Types B-1 and B-2. The flow uniformity in parallel channels is not sensibly affected by magnifying the inlet manifold. These results fully demonstrate the importance of shape design for microdevices. Ehrfeld et al. [1] pointed out the importance of shape design through a similar result.

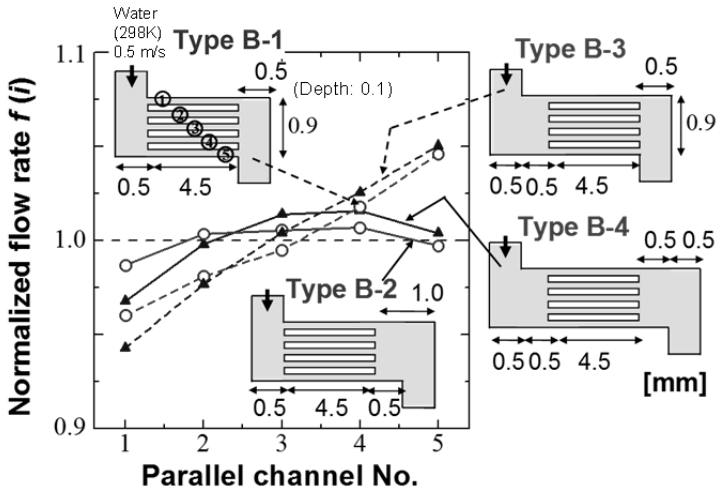

Fig. 1.1 Effect of device shape on flow distribution

1.2 Optimization of Manifold Shape

Uniform flow distribution can be realized by extending outlet manifold area as shown in Sec. 1.1. However, the extension of the outlet manifold increases dead volume inside the

microreactor, broadens residence time distribution, and makes space time long. In general, these characteristics caused by extending outlet manifold area are undesirable because they decrease the efficiency of microreactors. Therefore, both size and shape of the manifold should be optimized to realize uniform flow distribution, desirable space time, and desirable residence time distribution simultaneously. In this section, the optimization problem of designing inlet and outlet manifolds is discussed. This design problem is very difficult to solve because unlimited number of shape should be tested in theory and microreactors cannot be treated as a lumped-parameter system. In this work, the manifold shape is optimized by imposing constraints upon the shape and thereby reducing the degree of freedom.

1.2.1 Optimization of Discretized Shape

In the previous section, Type B-2 realizes the best flow distribution among four types. In this section, space time minimization problem is discussed under the condition that a device realizes the same or more uniform flow distribution than Type B-2. Since the space time can be shortened by reducing manifold area, the optimization problem is formulated as follows:

$$\text{Minimize} \quad \text{Manifold area} \ A \tag{1.3}$$

$$\text{Subject to} \quad \sum_{i=1}^{5} \left| \frac{F(i) - \overline{F}}{\overline{F}} \right| \leq 0.05 \tag{1.4}$$

Figure 1.2 shows the contour plot of velocity distribution in Type B-2. In this design, dead volume is formed around the corner of manifold denoted by dotted circles. Dead volume lengthens space time and broadens residence time distribution. Therefore, we focused on the design of manifold having less dead volume. In this work, the corner of manifold is trimmed away from the initial design Type B-2 in order to reduce the space time. The shape of removed area is described to simplify the design problem. That is, a corner generated by connecting two black points at each manifold shown in **Fig. 1.3** is removed manifold. By changing combination of two points at each manifold, a total 25 different shapes are generated. For all cases, flow patterns are simulated by CFD. As a result, more than half case does not satisfy the constraint of **Eq. (1.4)**. **Figure 1.4** illustrates the best design (Type B-O) which achieve uniform flow distribution while satisfying constraint on flow uniformity. The manifold area of Type B-O was reduced 25% compared with that of Type B-2. **Figure 1.5** shows flow distribution in Types B-2 and B-O.

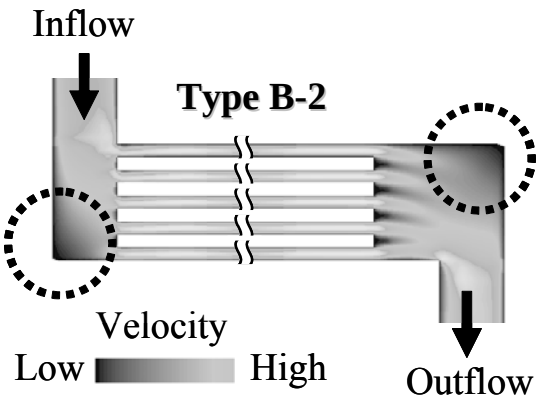

Fig. 1.2 Contour plot of velocity (Type B-2)

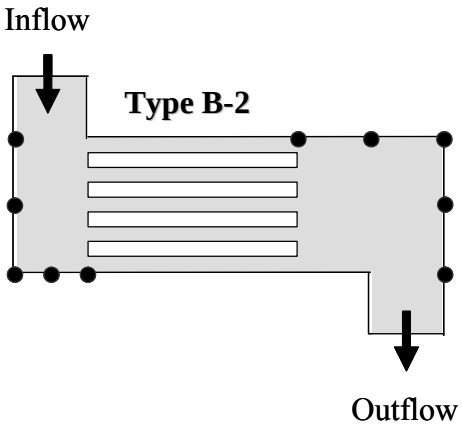

Fig. 1.3 Discrete model of manifolds

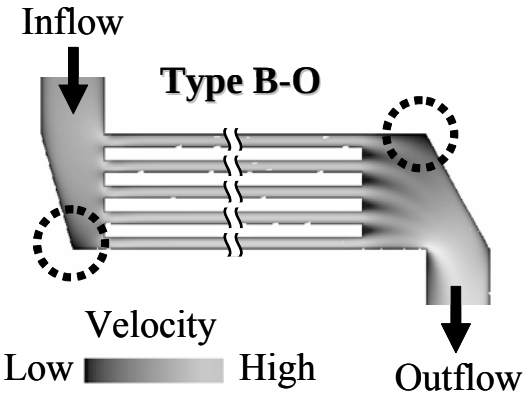

Fig. 1.4 Contour plot of velocity (Type B-O)

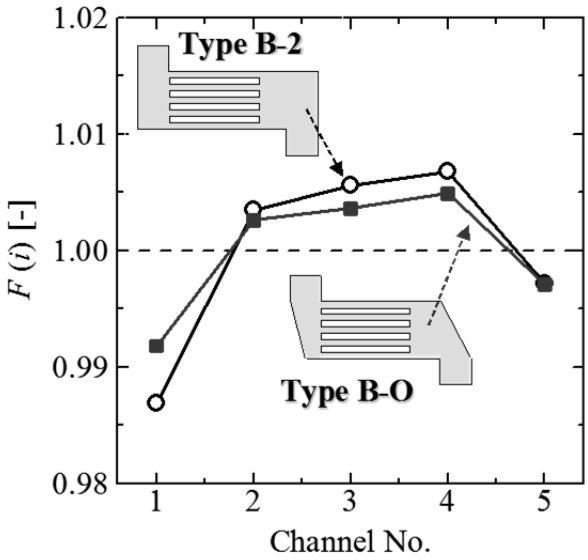

Fig. 1.5 Flow distribution (Types B-2 and B-O)

1.2.2 Automatic Shape Optimization

It takes much time and efforts to reach the optimal design if 3-dimensional structures and meshes used in CFD simulations are manually generated for each device shape. For efficient design, an automatic shape optimization method needs to be developed.

In optimization algorithm proposed in this section, the length of borderlines defining manifold shape is optimized as a continuous variable. **Figure 1.6** shows the flowchart of the proposed algorithm to optimize manifold shape. In the proposed method, the ranges of the optimization variables which define the shape of the device are given in advance. Then, initial device shape is defined and meshes are generated manually. After a CFD simulation, the performance index is calculated. While the result is not optimal, the shape is updated and meshes are regenerated. The shape update and the mesh regeneration can be automatically executed by integrating the model and mesh generator (Gambit 2.1) with the CFD simulator (Fluent® 6.0) through Visual Basic 6.0. As a result, automatic shape optimization is realized in this work.

As shown in **Fig. 1.7**, to simplify the problem, only the length of upper line that forms outlet manifold is treated as optimization variable. Golden section search method is used in the optimization algorithm. The objective function and constraint are **Eqs. (1.3)** and **(1.4)**, respectively. The second term of the objective function indicates the degree of flow maldistribution. P_e denotes a weighting factor. To derive the optimal solution (L= 390 μm),

fourteen rounds of iteration were required. It took about 60 minutes by a PC with a single processor running 2 GHz.

Minimize $$A + P_e \times \sum_{i=1}^{5} \left| \frac{F(i) - \bar{F}}{\bar{F}} \right| \tag{1.3}$$

Subject to $$11\mu\text{m} \leq L \leq 1000\mu\text{m} \tag{1.4}$$

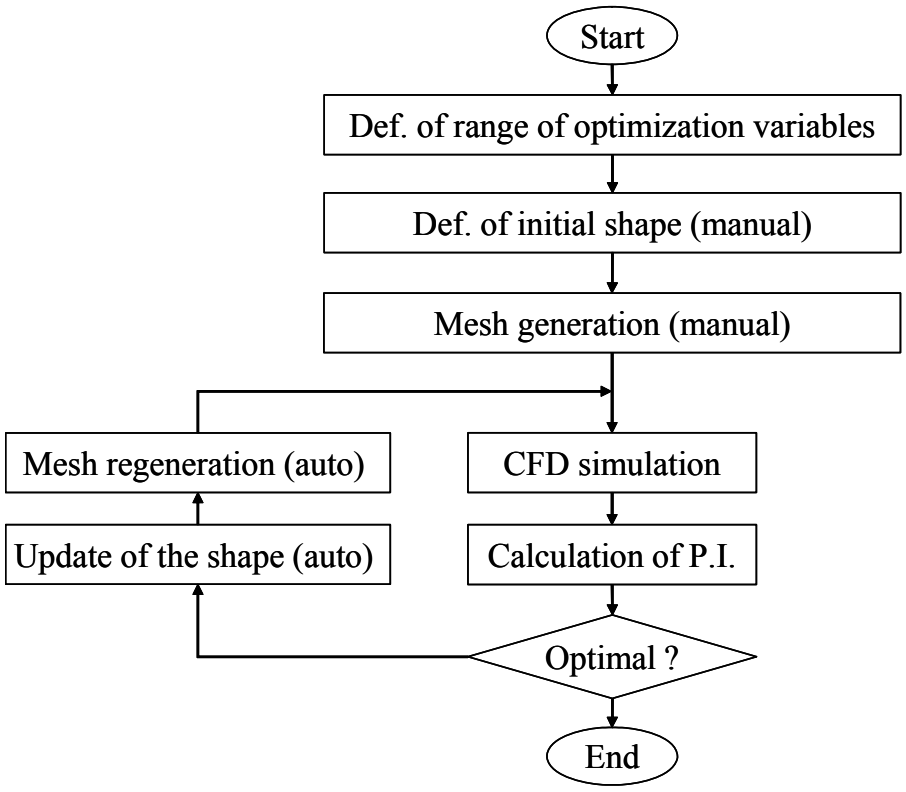

Fig. 1.6 Flowchart of shape optimization algorithm

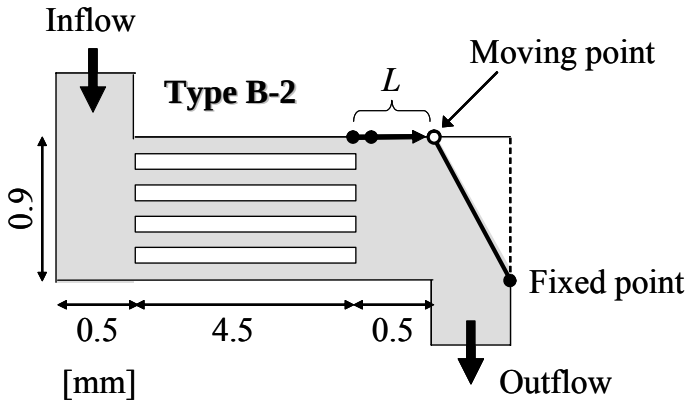

Fig. 1.7 Shape optimization of outlet manifold (Type B-2)

1.3 Results and Discussions

1.3.1 Shape Optimization

In the previous section, a shape optimization problem was formulated as one dimensional optimization problem and was solved by using the proposed method. The results of the CFD-based shape optimization give a lot of useful information on the design of microreactors to engineers. However, it requires a huge amount of computational time to obtain the optimal design when the number of design variables increases. Another approach for the shape optimization is to use an aggregated model. Commenge et al. [2] have proposed an approximate model of a microreactor by using a network of equivalent rectangular ducts. This model makes it possible to rapidly calculate the velocity distribution inside the device. The dominant drawback is the difficulty of embedding the effect of the inertia of flow in the model. For example, the model should not be used when the direction of the inlet flow plays an important role. Therefore, a sequential use of two methods is a promising approach. First, the shape of the device is roughly determined by using an aggregated method. Then, precise calculation is executed using the proposed CFD-based optimization method explained in the previous section. This kind of approach is discussed in Chapter 3.

1.3.2 Robust Design of Microreactors

The objective of using microreactors for chemical production is to achieve very high efficiency

that it is difficult for conventional chemical plants to reach. To maximize the performance of microreactors, operating conditions must be tightly controlled. However, installing sensors and actuators in each microreactor is not practical because the number of instruments becomes excessively large. Therefore, it is crucial to design robust microreactors against disturbances and changes in operating conditions. In this section, the influence of fin location on flow distribution is examined for various inlet flow rates, and the fin location increasing the robustness of the microreactors is derived. A new microreactor, Type C, is created to equalize flow pattern around inlet of each branched channel and thereby to realize uniform flow distribution. Each fin in Type C is shifted in parallel as shown in **Fig. 1.8**. The space time of fluid is the same for Types B-1 and C. CFD simulations were performed for three levels of inlet flow rates for reactors. The simulation results show that Type C is more robust than Type B-1 from the viewpoint of flow uniformity against changes in inlet flow rates. The maldistribution of fluid in Type B-1 seems to be caused by the influence of inertial force. Since the inertia force increases as inlet flow rate becomes higher, flow uniformity is deteriorated at the high inlet flow rate. Type C can realize more uniform flow distribution than Type B-1 by sifting fins, equalizing flow pattern around inlet of each branched channel, and reducing the influence of inertia force. These results suggest that a robust micro chemical plant can be actualized without installing sensors and actuators by investing individual devices with robustness.

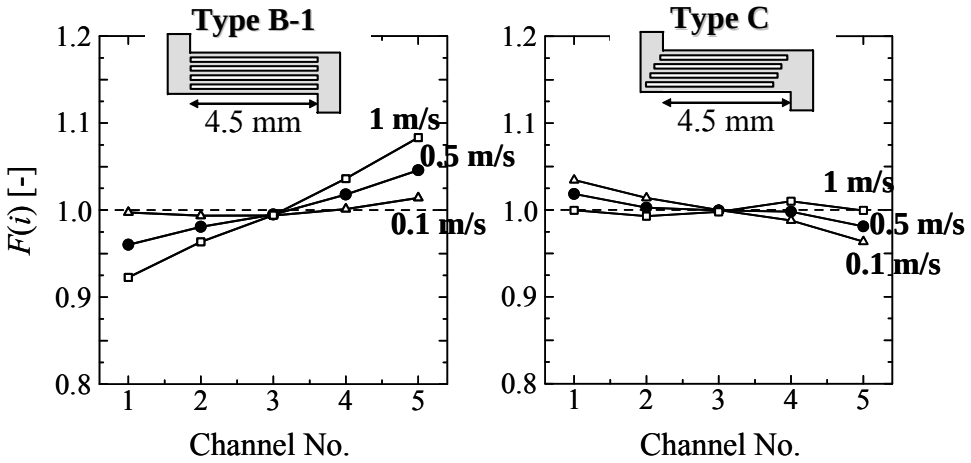

Fig. 1.8 Comparison between Type B-1 and Type C

1.4 Conclusions

A plate-fin microreactor is one of the dominant devices to be used in a micro chemical plant. In

this microreactor, the flow uniformity in branched channels is very important to realize the sharp residence time distribution. Flow distribution is strongly affected by shape of device. Therefore, in this chapter, effects of the design on the flow uniformity were discussed by using CFD simulation.

It was demonstrated that the magnification of outlet manifold area makes the flow distribution uniform. However, the extension of the outlet manifold increases dead volume inside the microreactor, broadens residence time distribution, and makes space time long.

In Sec. 1.2, the shape optimization problem to make space time short is solved under the constraint on flow uniformity. The result clarifies that a plate-fin microreactor with optimal manifold shape can achieve uniform flow distribution while realizing minimum space time. To derive optimal shape automatically, a new optimization method was developed by integration the model and mesh generator with the CFD simulator.

Furthermore, the effect of location of fins on flow uniformity is investigated for various inlet flow rates. The simulation results suggest the possibility of designing micro chemical plants with robustness.

In order to design an optimal micro chemical plant, an efficient design method needs to be developed. The CFD-based optimization approach proposed in this work can give rigorous results, but it requires a lot of computational time. To accelerate the design, a sequential design method would be useful. That is, a simplified model is used at initial design stage to roughly select good device shape, and then a rigorous CFD simulation is performed to determine an optimal design. At this stage of the development, it is not clear what kind of simplification of a device model is suitable for efficient design and is consistent with a rigorous model used in CFD simulation.

References

[1] W. Ehrfeld, V. Hessel, H. Löwe, “Extending the knowledge base in microfabrication towards chemical engineering and fluiddynamic simulation,” Proceedings of the 4th International Conference on Microreaction Technology (IMRET 4), Atlanta, USA, 3-20 (2000)

[2] J.M. Commenge, L. Falk, J.P. Corriou, M. Matlosz, “Optimal design for flow uniformity in microchannel reactors,” AIChE Journal, **48**(2), 345-358 (2002)

Chapter 2

Shape Design Using Adjoint Variable Method

The shape of microchannels is an important design variable to achieve the desired performance. Since most microchannels are, at present, designed by trial and error, a systematic optimal shape design method needs to be established. CFD is often used to rigorously examine the influence of the shape of microchannels on heat and mass transport phenomena in the flow field. However, the rash combination of CFD and the optimization technique based on evaluating gradients of the cost function requires enormous computation time when the number of design variables is large. Recently, the adjoint variable method has attracted the attention as an efficient sensitivity analysis method, particularly for aeronautical shape design, since it allows one to successfully obtain the shape gradient functions independently of the number of design variables. In this chapter, an automatic shape optimization system based on the adjoint variable method is developed using C language on a Windows platform. To validate the effectiveness of the developed system, pressure drop minimization problems of a U-shaped microchannel and a branched microchannel in incompressible flows under constant volume conditions are solved.

2.1 General Formulation of the Adjoint-based Shape Optimization

The optimization technique based on evaluating gradients of the cost function is the easiest way. For each design variable, its value is varied by a small amount, the cost function is recomputed, and the gradient with respect to it is measured. In this case, the number of CFD solutions required for N design variables is N+1. Consequently, the gradient-based method requires

enormous computation time when the number of design variables is large. In this study, the adjoint variable method is adopted to obtain gradients in a more expeditious manner.

In a fluid dynamic design optimization problem, the cost function depends on design parameters and flow variables. The cost function can be written as

$$I = I\left(\boldsymbol{W}(\boldsymbol{\beta}), \boldsymbol{\beta}\right) \tag{2.1}$$

where I is the cost function, $\boldsymbol{W}$ is the flow variable vector, and $\boldsymbol{\beta}$ is the design variable vector that represents the surface shape of channels. The cost function I is minimized or maximized subject to partial differential equation (PDE) constraints, geometric constraints, and physical constraints. Examples for the cost function I are drag or pressure drop, for PDE constraints $\boldsymbol{R}(\boldsymbol{W}, \boldsymbol{\beta})$ the Euler/Navier-Stokes equations, for geometric constraints $\boldsymbol{g}(\boldsymbol{\beta})$ the volume or cross sectional area, and for physical constraints $\boldsymbol{h}(\boldsymbol{W})$ a minimal pressure to prevent undesired phenomena.

The principles of the evaluation of gradients based on adjoint variables are given here [1-3]. A total differential in the cost function I and the PDE constraint $\boldsymbol{R}$ results in:

$$dI = \left(\frac{\partial I}{\partial \boldsymbol{W}}\right) d\boldsymbol{W} + \left(\frac{\partial I}{\partial \boldsymbol{\beta}}\right) d\boldsymbol{\beta}\,, \tag{2.2}$$

$$d\boldsymbol{R} = \left(\frac{\partial \boldsymbol{R}}{\partial \boldsymbol{W}}\right) d\boldsymbol{W} + \left(\frac{\partial \boldsymbol{R}}{\partial \boldsymbol{\beta}}\right) d\boldsymbol{\beta} = 0\,. \tag{2.3}$$

Next, a Lagrange multiplier $\boldsymbol{\lambda}$ is introduced to add the flow equation to the cost function:

$$\begin{aligned} dI &= \left(\frac{\partial I}{\partial \boldsymbol{W}}\right) d\boldsymbol{W} + \left(\frac{\partial I}{\partial \boldsymbol{\beta}}\right) d\boldsymbol{\beta} - \boldsymbol{\lambda}^T \left\{ \left(\frac{\partial \boldsymbol{R}}{\partial \boldsymbol{W}}\right) d\boldsymbol{W} + \left(\frac{\partial \boldsymbol{R}}{\partial \boldsymbol{\beta}}\right) d\boldsymbol{\beta} \right\} \\ &= \left\{ \left(\frac{\partial I}{\partial \boldsymbol{W}}\right) - \boldsymbol{\lambda}^T \left(\frac{\partial \boldsymbol{R}}{\partial \boldsymbol{W}}\right) \right\} d\boldsymbol{W} + \left\{ \left(\frac{\partial I}{\partial \boldsymbol{\beta}}\right) - \boldsymbol{\lambda}^T \left(\frac{\partial \boldsymbol{R}}{\partial \boldsymbol{\beta}}\right) \right\} d\boldsymbol{\beta} \end{aligned} \tag{2.4}$$

This implies that if we can solve:

$$\boldsymbol{\lambda}^T \left(\frac{\partial \boldsymbol{R}}{\partial \boldsymbol{W}} \right) = \left(\frac{\partial I}{\partial \boldsymbol{W}} \right), \tag{2.5}$$

the variation of I is given by:

$$dI = \left\{ \left(\frac{\partial I}{\partial \boldsymbol{\beta}} \right) - \boldsymbol{\lambda}^T \left(\frac{\partial \boldsymbol{R}}{\partial \boldsymbol{\beta}} \right) \right\} d\boldsymbol{\beta} = \boldsymbol{G} d\boldsymbol{\beta} . \tag{2.6}$$

Equation (2.6) means that the variation of I exhibits only derivatives with respect to $\boldsymbol{\beta}$, and that the shape gradient function $\boldsymbol{G}$ is independent of the number of design variables. In the case that $\boldsymbol{R}$ is PDE, the adjoint equation **(2.5)** is also PDE, and the appropriate boundary conditions must be determined. The effectiveness of the adjoint-based shape optimization is emphasized along with the increase in design variables.

2.2 A Shape Optimization System Development

In this research, an automatic shape optimization system based on the adjoint variable method is developed using C language on a Windows platform. The procedures for building the system are shown in **Fig. 2.1**. In principle, after a new shape is obtained, a new grid is generated, and the solution is restarted. For every design cycle, the following steps are required:

1) assume an initial shape,
2) generate computational grids,
3) solve the flow equations, viz. the Navier-Stokes equation and the continuity equation, for deriving the flow velocity and the pressure,
4) solve the adjoint equation to obtain the set of Lagrange multipliers,
5) calculate the shape gradient functions,
6) obtain a new shape by moving each point on the boundary,
7) go to step 2 unless the change in the cost function is smaller than a desired convergence parameter.

Each design cycle requires a numerical solution of both the flow and the adjoint equations, whose computational time is roughly twice that required to obtain the flow solution. In the following subsections, each one of these steps is described in more detail.

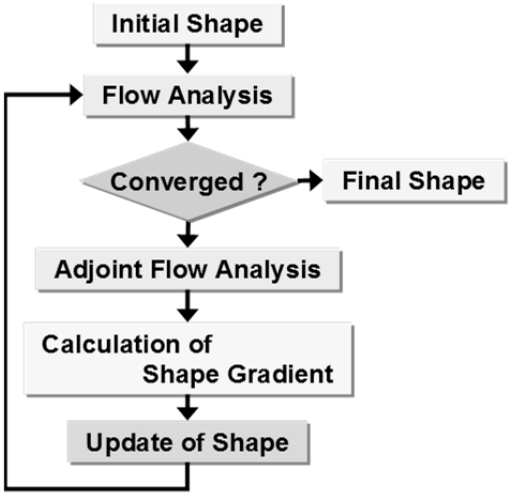

Fig. 2.1 Flow chart of shape optimization

2.2.1 Flow Analysis

Liquid flows in most microchannels are laminar and governed by the incompressible Navier-Stokes equation. Tretheway et al. [4] measured the velocity profile of water flowing through a microchannel with hydrophilic surface by using micron-resolution particle image velocimetry, and showed that the profile is consistent with the solution of Navier-Stokes equation under the no-slip condition. Using a Cartesian coordinate system (x, y) the main dimensionless governing equations of the flow model consist of the continuity and the Navier-Stokes equations:

$$\frac{\partial \tilde{u}}{\partial \tilde{x}} + \frac{\partial \tilde{v}}{\partial \tilde{y}} = 0 \tag{2.7}$$

$$\frac{\partial \tilde{u}}{\partial \tilde{t}} + \tilde{u}\frac{\partial \tilde{u}}{\partial \tilde{x}} + \tilde{v}\frac{\partial \tilde{u}}{\partial \tilde{y}} + \frac{\partial \tilde{p}}{\partial \tilde{x}} - \frac{1}{\mathrm{Re}}\nabla^2 \tilde{u} = 0 \tag{2.8}$$

$$\frac{\partial \tilde{v}}{\partial \tilde{t}} + \tilde{u}\frac{\partial \tilde{v}}{\partial \tilde{x}} + \tilde{v}\frac{\partial \tilde{v}}{\partial \tilde{y}} + \frac{\partial \tilde{p}}{\partial \tilde{y}} - \frac{1}{\mathrm{Re}}\nabla^2 \tilde{v} = 0 \tag{2.9}$$

where $\tilde{u}$ and $\tilde{v}$ are the components of the velocity field in the *x* and *y* direction respectively, $\tilde{p}$ the pressure, and Re Reynolds number. All velocities and lengths are scaled using the average inlet velocity $V_{ave.}$ and the inlet width W_{inlet} throughout this chapter. Hence the Reynolds number for the flow through the microchannels is defined as

$$\mathrm{Re} = \frac{V_{ave} W_{inlet} \rho}{\mu} \tag{2.10}$$

Re is used to quantify flow regimes and as an indicator of laminar or turbulent flow.

In this study, the two-dimensional incompressible Navier-Stokes equations in generalized coordinate systems are solved by using the fractional-step method, which was first suggested by Harlow and Welch [5] and Chorin [6]. The governing equations are discretized by finite volumes with a staggered mesh. The solution of the continuity equation is decoupled from the momentum equations by a fractional-step method which enforces mass conservation by solving a Poisson equation. Several two-dimensional laminar test cases are computed and compared with simulation results by commercial CFD software Fluent® to validate the developed solution method. As a result, good agreement is obtained in all cases.

2.2.2 Adjoint Flow Analysis and Calculation of Shape Gradient

In this subsection, the derivation of adjoint flow equations and shape gradient function is described [7]. For the following derivations, it is convenient to adopt the convention of indicial notation where a repeated index *i* implies summation over *i* = 1 to 2. In this study, pressure drop in a microchannel is treated as cost function I, which is expressed by

$$I(\Gamma_w) = -\int_{\Gamma_i} \tilde{p}\tilde{u}_i n_i ds - \int_{\Gamma_o} \tilde{p}\tilde{u}_i n_i ds \tag{2.11}$$

where $\tilde{u}_i$ is the *i*th component of flow velocity, n_i the *i*th component of the unit normal vector, and Γ_w the part of the microchannel wall that is to be shaped. The goal is to determine the microchannel shape that minimizes the above cost function. Here, the variation of the cost

function with respect to the variations of the boundary is derived by a perturbation analysis. Let each point on Γ_w be moved by ε along the outer normal direction. The new curve constructed in this way is denoted by $\Gamma_{w,\varepsilon}$, as shown in **Fig. 2.2**. Let $(\tilde{u}_i^{\varepsilon}, \tilde{p}^{\varepsilon})$ be the solution of **Eqs. (2.7)**, **(2.8)**, and **(2.9)** in the new flow domain. Let $(\hat{u}_i, \hat{p})$ be defined as follows:

$$\hat{u}_i = \lim_{\varepsilon \to 0} \varepsilon^{-1} \left[\tilde{u}_i^{\varepsilon} - \tilde{u}_i \right] \in \Omega, \tag{2.12}$$

$$\hat{p} = \lim_{\varepsilon \to 0} \varepsilon^{-1} \left[\tilde{p}^{\varepsilon} - \tilde{p} \right] \in \Omega, \tag{2.13}$$

Then $(\tilde{u}_i^{\varepsilon}, \tilde{p}^{\varepsilon})$ can be expressed as

$$\tilde{u}_i^{\varepsilon} = \tilde{u}_i + \varepsilon \hat{u}_i, \quad \tilde{p}^{\varepsilon} = \tilde{p}_i + \varepsilon \hat{p} \tag{2.14}$$

Since both $(\tilde{u}_i^{\varepsilon}, \tilde{p}^{\varepsilon})$ and $(\tilde{u}_i, \tilde{p})$ satisfy the Navier-Stokes equations, it can be shown that $(\hat{u}_i, \hat{p})$ satisfy the following set of equations:

$$\hat{u}_{i,i} = 0 \tag{2.15}$$

$$\tilde{u}_j \hat{u}_{i,j} + \hat{u}_j \tilde{u}_{i,j} + \hat{p} - \frac{1}{\mathrm{Re}} \hat{u}_{i,jj} = 0 \tag{2.16}$$

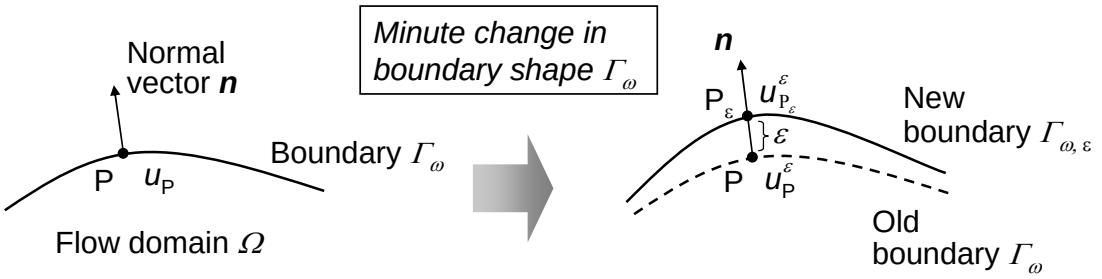

Fig. 2.2 Schematic diagram of a microchannel surface.

The next step is to derive the conditions satisfied by $\hat{u}_i$ on Γ_w. Consider a point P on Γ_w, and a corresponding point P_ε on $\Gamma_{w,\varepsilon}$ such that P_ε lies on the outward normal n, as shown in **Fig. 2.2**. Assume that P_ε is positive. A Taylor series expansion of u_i^ε about the point P along the normal direction n is

$$\tilde{u}_i^\varepsilon\Big|_{P_\varepsilon} = \tilde{u}_i^\varepsilon\Big|_P + \varepsilon\left(\frac{\partial \tilde{u}_i^\varepsilon}{\partial n}\right)_P + O\left(\varepsilon^2\right)$$

$$= \tilde{u}_i\Big|_P + \varepsilon\,\hat{u}_i\Big|_P + \varepsilon\left(\frac{\partial \tilde{u}_i}{\partial n}\right)_P + O\left(\varepsilon^2\right) \tag{2.17}$$

Since the velocities satisfy the no-slip condition on Γ_w,

$$\hat{u}_i = -\left(\frac{\partial \tilde{u}_i}{\partial n}\right)_P \quad \text{on } \Gamma_w. \tag{2.18}$$

The case of ε negative also yields the same expression. In this case, however, the Taylor series expansion is carried out for $\tilde{u}_i$, since $\tilde{u}_i^\varepsilon$ is not defined beyond $\Gamma_{w,\varepsilon}$ whereas $\tilde{u}_i$ is defined in the region of interest.

Next, the first variation of the objective function *I* is obtained. The value of the cost function *I* for the new domain is given by,

$$I\left(\Gamma_{w,\varepsilon}\right) = -\int_{\Gamma_i} \tilde{p}^\varepsilon \tilde{u}_i^\varepsilon n_i ds - \int_{\Gamma_o} \tilde{p}^\varepsilon \tilde{u}_i^\varepsilon n_i ds\,. \tag{2.19}$$

The first variation of the objective function, δI, is defined by the relation

$$I\left(\Gamma_{w,\varepsilon}\right) - I\left(\Gamma_w\right) = \varepsilon\,\delta I + O\left(\varepsilon^2\right), \tag{2.20}$$

and can be shown to be

$$\delta I = -\int_{\Gamma_i} \hat{p}\tilde{u}_i n_i ds - \int_{\Gamma_o} \hat{p}\tilde{u}_i n_i ds \,, \tag{2.21}$$

which is an integral expression over the inlet and exit boundaries.

The subsequent step is the transformation of this integral from one that is over inlet boundary Γ_i and exit boundary Γ_o to one that is over Γ_w. This is achieved through the introduction of an adjoint variable problem. The adjoint problem consists of a set of partial differential equations and boundary conditions and is derived below. Since $\tilde{u}_i n_i$ vanishes on the walls, **Eq. (2.21)** can be written as

$$\delta I = \oint \hat{p}\tilde{u}_i n_i ds \,, \tag{2.22}$$

The inner product of the perturbation **Eqs. (2.15)** and **(2.16)** and adjoint variables (u_i^*, p^*), integrated over the domain, and added to **Eq. (2.22)**, gives

$$\begin{aligned} \delta I = & \oint \hat{p}\tilde{u}_i n_i ds + \iint p^* \hat{u}_{i,i} dA \\ & + \iint u_i^* \left(\frac{1}{\mathrm{Re}} \hat{u}_{i,jj} - \tilde{u}_j \hat{u}_{i,j} - \hat{u}_j \tilde{u}_{i,j} - \hat{p} \right) dA \end{aligned} \tag{2.23}$$

The above expression can be rewritten by using Gauss divergence theorem and yields

$$\begin{aligned} \delta I = & \oint \hat{p}\left(\tilde{u}_i - u_i^*\right) n_i ds + \frac{1}{\mathrm{Re}} \oint \left(u_i^* \frac{\partial \hat{u}_i}{\partial n} - \hat{u}_i \frac{\partial u_i^*}{\partial n} \right) ds \\ & + \oint \left(p^* \hat{u}_i n_i - \hat{u}_i u_i^* \tilde{u}_j n_j - \tilde{u}_i u_i^* \hat{u}_j n_j \right) ds + \iint \hat{p} u_{i,i}^* dA \\ & + \iint u_i^* \left(\frac{1}{\mathrm{Re}} u_{i,jj}^* + \tilde{u}_j u_{i,j}^* + \tilde{u}_j u_{j,i}^* - p^* \right) dA \end{aligned} \tag{2.24}$$

The adjoint problem has to be defined such that the domain integrals in **Eq. (2.24)** vanish identically. The choice of boundary conditions for these equations is made such that the only non-zero terms are those that are integrals over Γ_w, the wall that is to be shaped. Let us define the following adjoint equations:

$$\frac{\partial u^*}{\partial x}+\frac{\partial v^*}{\partial y}=0 \tag{2.25}$$

$$\frac{\partial u^*}{\partial \tilde{t}}-\left(2\tilde{u}\frac{\partial u^*}{\partial \tilde{x}}+\tilde{v}\frac{\partial u^*}{\partial \tilde{y}}+\tilde{v}\frac{\partial v^*}{\partial \tilde{x}}\right)+\frac{\partial p^*}{\partial \tilde{x}}-\frac{1}{\mathrm{Re}}\nabla^2 u^*=0 \tag{2.26}$$

$$\frac{\partial v^*}{\partial \tilde{t}}-\left(\tilde{u}\frac{\partial v^*}{\partial \tilde{x}}+\tilde{u}\frac{\partial u^*}{\partial \tilde{y}}+2\tilde{v}\frac{\partial v^*}{\partial \tilde{y}}\right)+\frac{\partial p^*}{\partial \tilde{y}}-\frac{1}{\mathrm{Re}}\nabla^2 v^*=0 \tag{2.27}$$

The above adjoint equations can be discretized by using the same schemes employed for the flow analysis.

Based on **Eqs. (2.25)** to **(2.27)** and boundary conditions, **Eq. (2.24)** can be written as

$$\begin{aligned}\delta I=&\frac{1}{\mathrm{Re}}\int_{\Gamma_w}\left(\frac{\partial \tilde{u}_i}{\partial n}\right)\left(\frac{\partial u_i^*}{\partial n}\right)ds+\frac{1}{\mathrm{Re}}\int_{\Gamma_i+\Gamma_o}u_i^*\frac{\partial \hat{u}_i}{\partial n}\\&-\frac{1}{\mathrm{Re}}\int_{\Gamma_w}p^*\left(\frac{\partial \tilde{u}_i}{\partial n}\right)n_i ds.\end{aligned} \tag{2.28}$$

Since the second and third terms on the right hand side of **Eq. (2.28)** vanish, **Eq. (2.28)** is reduced to

$$\begin{aligned}\delta I=&\frac{1}{\mathrm{Re}}\int_{\Gamma_w}\left(\frac{\partial \tilde{u}_i}{\partial n}\right)\left(\frac{\partial u_i^*}{\partial n}\right)ds\\=&\frac{1}{\mathrm{Re}}\int_{\Gamma_w}\left(\frac{\partial \tilde{u}}{\partial n}\frac{\partial u^*}{\partial n}+\frac{\partial \tilde{v}}{\partial n}\frac{\partial v^*}{\partial n}\right)ds=G\end{aligned} \tag{2.29}$$

The shape gradient function $\boldsymbol{G}$ is calculated from flow analysis which finds the distributions of flow velocity $\tilde{u}$ and $\tilde{v}$ and adjoint flow analysis which finds the distributions of adjoint flow velocity u^* and v^*.

2.3 Case Studies

Flow in microchannels is driven by the pressure difference or the electric potential between inlet and outlet. For pressure-driven flow, an important issue is how to reduce the pressure drop required to realize a desired flow rate in a microchannel. U-shaped microchannels and/or branched microchannels are often used to provide long flow passage in a compact device. Modification of the shape of U-shaped channels and/or branched channels may decrease the pressure drop. In this study, two design examples are presented to demonstrate the effectiveness of the developed system for microchannel shape optimization problems. The adjoint variable method is applied to all gradient computations. For convenience, the physical coordinates system is transformed to computational coordinates in the flow and adjoint flow analysis. The two-dimensional computations in these case studies are performed on Windows Intel® 3.0 GHz processors.

2.3.1 U-shaped Microchannel

The first design example is a shape optimization problem of U-shaped microchannels in incompressible flows. The goal of the optimization is to minimize pressure drop for various inlet Reynolds numbers: Re = 0.1, 1, 10, and 100. The cost function is written as

$$I = -\int_{\Gamma_i+\Gamma_o} \tilde{p}\tilde{u}_i n_i ds\,, \tag{2.30}$$

which means the pressure drop between inlet and outlet. The initial shape of the U-shaped microchannel and the main design conditions are shown in **Fig. 2.3**. The width of the initial shape is 100 μm. The curved channel is connected with inlet and outlet straight channels. The total number of mesh is 864. The design boundaries are assigned to Γ_{w1} and Γ_{w2}, which correspond to the wall of the curved channel, and the design variables are associated with the grid points on both design boundaries. For pressure-driven liquid flow in a microchannel, the no-slip boundary condition is usually valid. The streamwise velocity component at the entrance is specified, and the transverse velocity component at the entrance is assumed to be zero. The prescribed pressure $p = 0$ is assumed at the exit boundary.

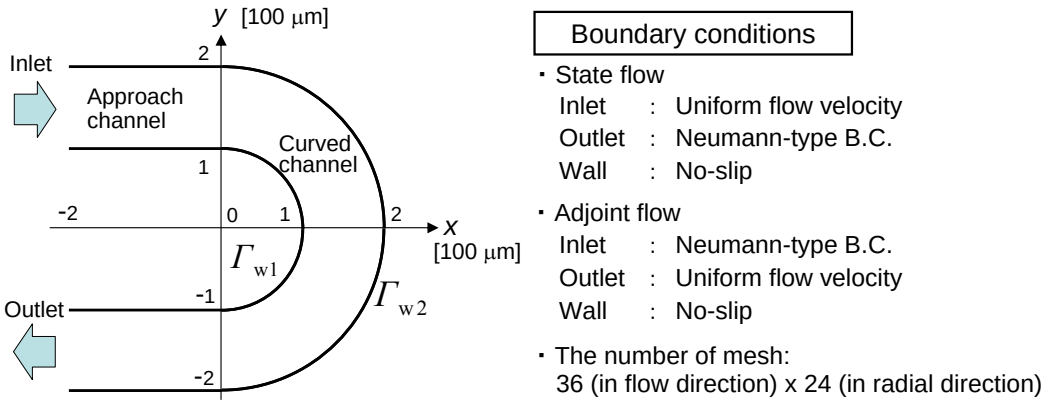

Fig. 2.3 Analytical domain and boundary condition for a U-shaped microchannel

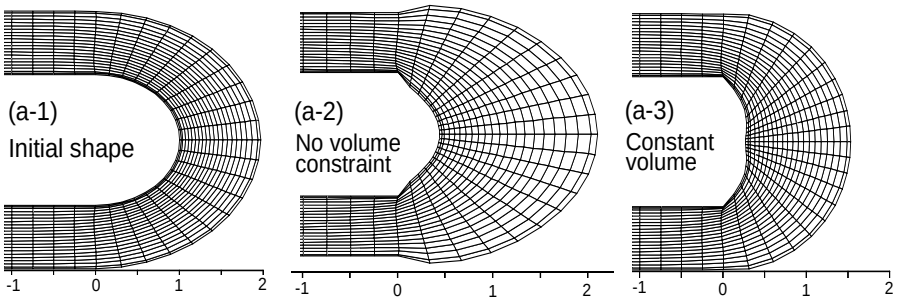

Fig. 2.4 Design results: (a-1) initial shape, (a-2) final shape under no volume constraint at Re = 10, (a-3) optimal shape under a constant volume constraint at Re = 10. Reference frame is prepared below each shape.

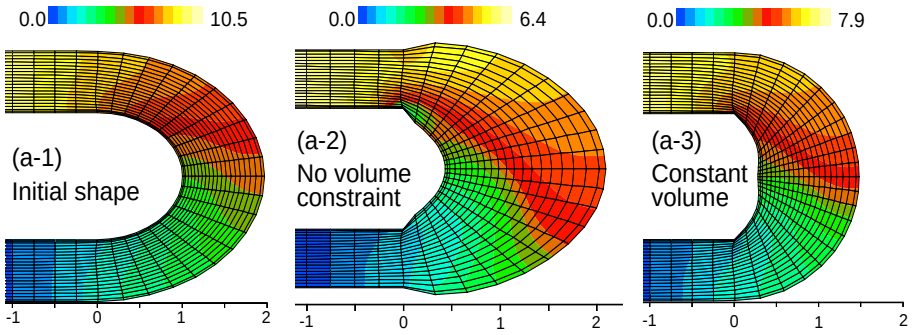

Fig. 2.5 Results of pressure distribution for initial and converged shape. Yellow and blue represents high and low pressure, respectively.

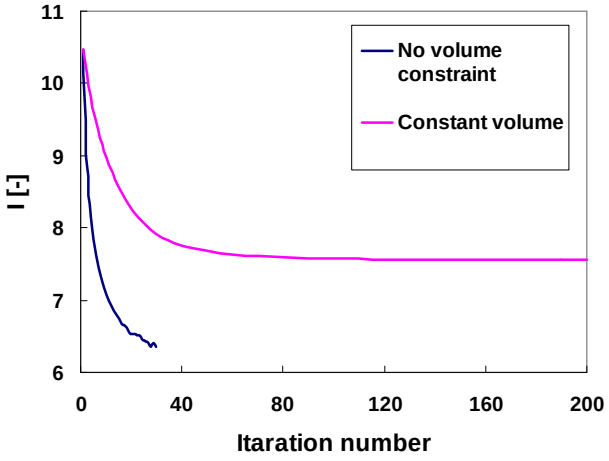

Fig. 2.6 Nondimensionalized cost function evolution (Design cycles vs. Cost function).

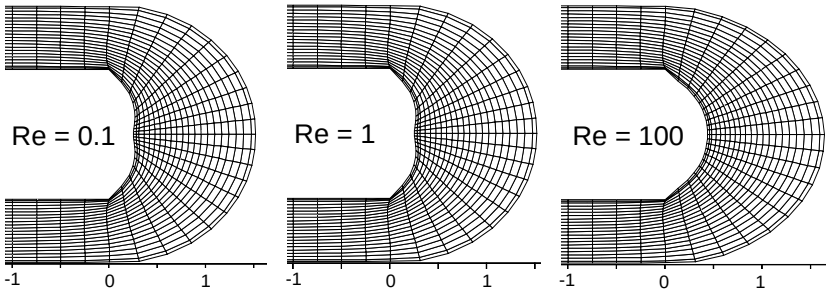

Fig. 2.7 Optimal shape at Re = 0.1 (left), 1 (middle), and 100 (right). Reference frame is prepared below each shape.

Design results at Re = 10 are presented here. **Figure 2.4** shows the initial shape, the final shape under no volume constraint, and the converged shape under a constant volume constraint. **Figure 2.5** illustrates the pressure distributions respectively. As seen in **Fig. 2.4**, under no volume constraint, the width of the curved channel is widened, and the shape of the channel is significantly modified. The wider channel makes the flow velocity lower, and a large reduction of pressure drop can be achieved. On the other hand, under a constant volume constraint, both the inside and outside surfaces of the curved channel are moved toward the inlet and outlet, and the flow passage is shortened.

The monotonic convergence of the cost function is shown in **Fig. 2.6**. This indicates that the gradient computation provides sufficiently accurate search directions for the optimization. The convergence criterion is selected such that the decrease in the cost function per iteration is less than 0.01 %.

Under a constant volume constraint, the cost function is converged in 92 design iterations and pressure drop is reduced by 27.6 %, as compared with that of the initial curved shape. Each design iteration requires approximately 10 seconds. On the other hand, if not under volume constraint, the design cycles are stopped in 30 design iterations due to the fluctuation of the cost function, and pressure drop is decreased by 39.3 %, as compared with that of initial curved shape.

In addition, the influence of Re on the result of shape optimization is investigated. **Figure 2.7** shows the optimal shapes at Re = 0.1, 1, and 100 under the constant volume constraint. On the basis of these results, the corresponding reductions in pressure drop are 29.0 %, 28.9 %, and 19.6 %, respectively, as compared with that of initial curved shape. The optimal shapes at Re = 0.1 and 1 are almost the same as that at Re = 10. The optimal shape at Re =100 is different from the others, and its curvature is small due to large flow inertia.

2.3.2 Branched Microchannel

The second design example targets the shape optimization of a branched microchannel. The cost function of the optimization is to decrease the pressure drop. Fluid is fed into the branched channel through a boundary Γ_i and comes out from two boundaries Γ_{o1} and Γ_{o2}. Uniform flow u_{in} is assumed at the inlet boundary, and prescribed pressure $p = 0$ is assumed at the exit boundaries. A no-slip condition is imposed on the bounding wall. The design boundaries are assigned to Γ_{w1}, Γ_{w2}, and Γ_{w3}, and the design variables are associated with the grid points on the design boundaries. The Reynolds number is defined by the uniform flow velocity u_{in} and the width of inlet boundary Γ_i. The mesh consists of 1000 elements. The numerical results of this design problem at Re = 1 and Re = 100 are presented in **Fig. 2.9**. In case of Re = 1, although 70 rounds of design cycles are required till convergence for 101 design variables, which are assigned on the channel surface, after 50 design cycles the decrease in pressure drop is small. The pressure drop of the optimally designed branched channel is decreased by about 33.1 % as compared with that of the initial shape. The design result at Re = 100 shows a 38.0 % reduction of pressure drop. As Re becomes large, the T-branched channel is transformed into Y-branched channel, in which fluid flows more smoothly without collision with wall. According to the

results of two design examples of U-shaped microchannels and branched microchannels, the validity of the developed shape optimization system is confirmed.

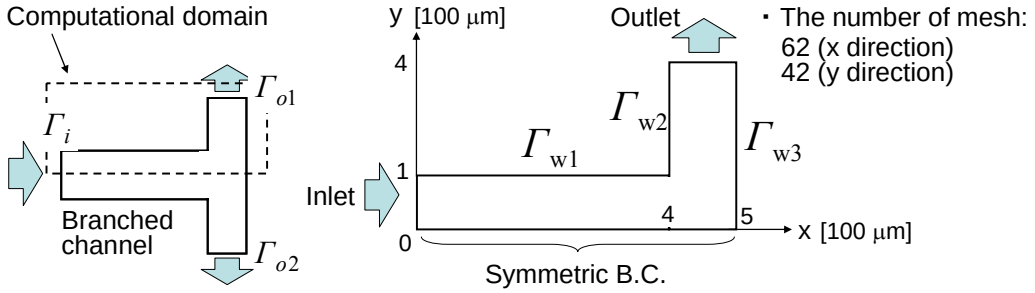

Fig. 2.8 Design conditions and assumptions of a branched microchannel

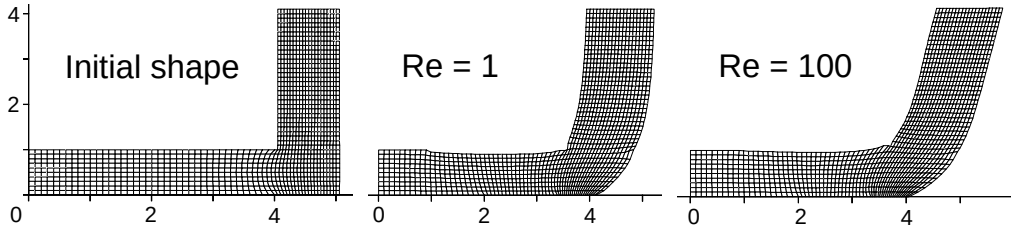

Fig. 2.9 Initial shape (left) and final shapes at Re = 1 (middle) and 100 (right) under the constant volume constraint.

2.4 Conclusions

Most of the previous work on numerical shape optimization for fluid flow can be found in the field of aerodynamics. The nonlinear optimization problems are often solved by using descent algorithms based on gradient information. However, the computation of the gradient of the cost function with respect to the design variables is usually very heavy. Recently, the adjoint variable method, which enables us to obtain gradients in a more expeditious manner, has been focused on. In this work, an automatic shape optimization system based on the adjoint variable method was developed by using C language on a Windows platform.

Since the pressure drop in microchannels is an important characteristic related to the energy

demand for process optimization, the developed system is applied to the pressure drop minimization problems of microchannels. The last section demonstrated by representative examples that the adjoint variable method can be used to formulate computationally feasible procedures for the shape design of pressure-driven microchannels. The computational time of each design cycle is of the same order as two flow solutions, since the adjoint equation is of comparable complexity to the flow equation. The developed system is quite general and is not limited to particular choice of cost function. Our future work will focus on the extension of the developed system to shape optimization problems of thermo-fluidic microdevices.

References

[1] S. Kim, J. Alonso, A. Jameson, "Multi-element high-lift configuration design optimization using viscous continuous adjoint method," Journal of Aircraft, **41**, 1082-1097 (2004)

[2] O. Soto, R. Löhner, C. Yang, "An adjoint-based design methodology for CFD problems," International Journal of Numerical Methods for Heat & Fluid Flow, **14**(6), 734-559 (2004)

[3] A. Jameson, L. Martinelli, N.A. Pierce, "Optimum aerodynamic design using the Navier-Stokes equations," Theoretical Computational Fluid Dynamics, **10**, 213-237 (1998)

[4] D.C. Tretheway and C.D. Meinhart, "Apparent fluid slip at hydrophobic microchannel walls," Physics of Fluids, **14**(3), L9-L12 (2002)

[5] F. Harlow and E. Welch, "Numerical calculation of time-dependentviscous incompressible flow of fluid with free surface," Physics of Fluids, **8**, 2182–2189 (1965)

[6] A.J. Chorin, "Numerical solution of the Navier-Stokes equations," Mathematics of Computation, **22**, 745-762 (1968)

[7] H. Cabuk and V. Modi, "Optimum plane diffusers in laminar flow," Journal of Fluid Mechanics, **227**, 373-393 (1992)

Chapter 3

Shape Design Using Simplified Model

Recent advances in CFD enable us to know both flow and temperature distributions in a microdevice precisely without conducting any experiments. However, it is not practical to apply CFD simulations directly to the optimal design problem of microreactors, since they require too much computational time and effort. From this viewpoint, a new systematic design approach based on a simplified thermo-fluid model is introduced in this chapter.

3.1 Design Problem of Plate-fin Microreactors

In this section, an optimal design problem of a plate-fin microreactor (see **Fig. 3.1**) is investigated. It is typically composed of three sections: inlet manifold section for flow distribution, parallel microchannels' section for reaction, and outlet manifold section for mixing. An optimal design problem of the plate-fin microreactor is formulated as shown in **Table 3.1**. It is not practical to apply CFD simulation directly to the optimal design problem due to the large number of degrees of freedom. In the following sections, a new systematic design approach is explained.

3.2 Thermo-fluid Design Approach

The proposed thermo-fluid design approach for a plate-fin microreactor mainly consists of two stages [1, 2]. The flowchart is shown in **Fig. 3.2**. In the first stage, the optimal microchannel

shape is derived by using a thermal compartment model: the “thermal design stage.” In the second stage, the optimal manifold shape is determined by using a pressure drop compartment model: the “fluid design stage.” After these two design stages, the obtained shape of the microreactor is validated by CFD simulation. The proposed approach will accelerate the microreactor design.

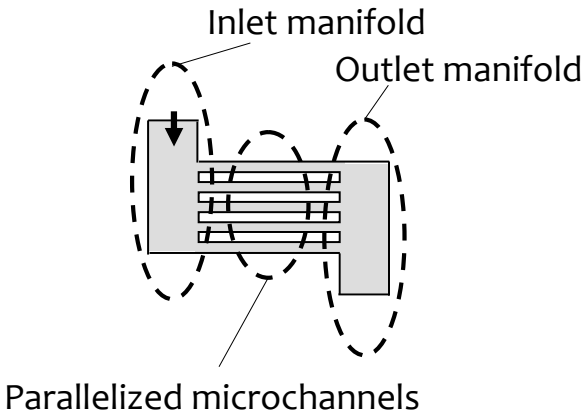

Fig. 3.1 A plate-fin microreactor.

Table 3.1 An optimal design problem of a plate-fin microreactor

Objective function	Maximization of product yield
	Maximization of production rate
Optimization variables	Microchannel shape and size
	Manifold shape and size
	Number of microchannels
	Feed flow rate & Inlet temperature
	Coolant temperature
Constraints	Mass balance for a given species
	Energy balance for fluid and wall
	Reaction temperature conditions
	Minimum product yield
	Total flow rate
	Residence time distribution among microchannels
	Maximum pressure drop (Pump performance)
	Upper and lower limits of reactor dimensions

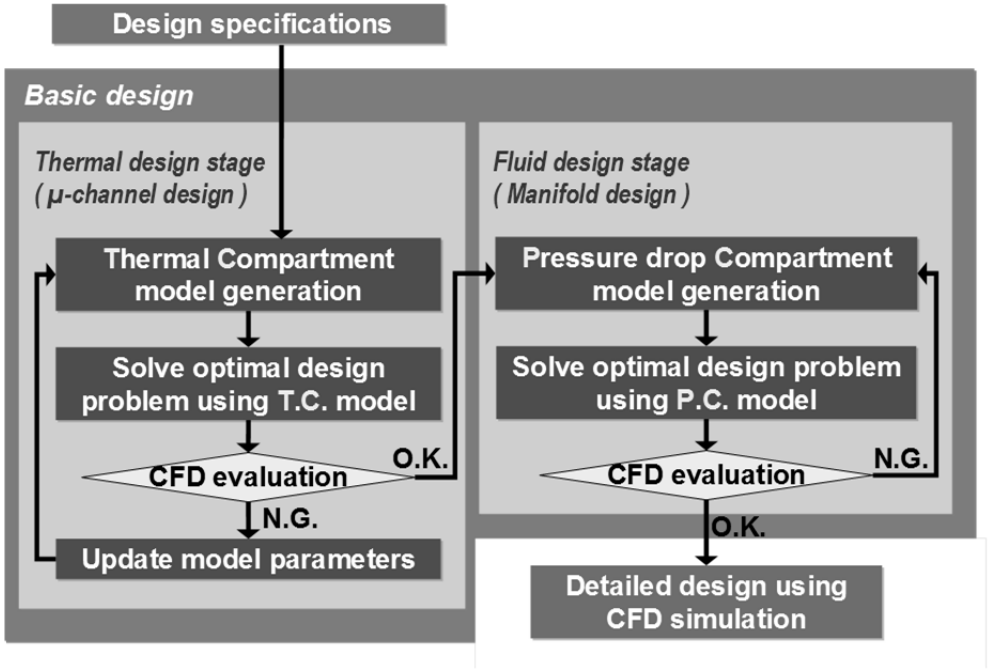

Fig. 3.2 Flowchart of proposed design approach

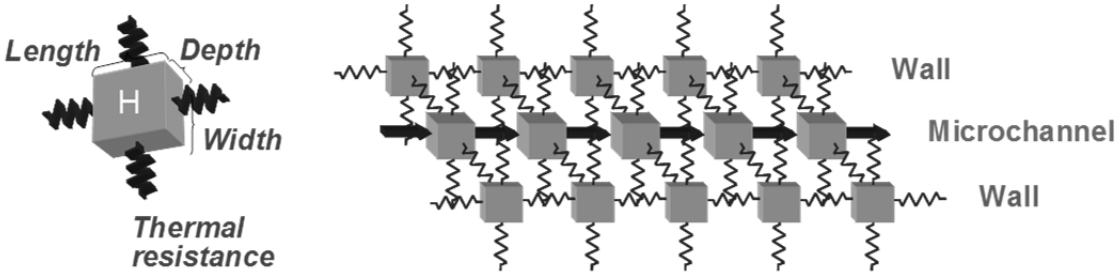

Fig. 3.3 Thermal compartment (left) and thermal compartment model (right)

3.2.1 Thermal Design Stage

In the thermal design stage, the parallel channels' section in a microreactor are divided into an adequate number of thermal compartments to describe heat transfer between fluids and walls. Each compartment is regarded as a lumped parameter system and has information on its shape and size, physical properties, and heat transfer coefficients between connected compartments. **Figure 3.3** represents a thermal compartment model for one microchannel and walls which surround it.

In a thermal compartment model, the longitudinal heat conduction inside the walls is considered, which is neglected in the conventional models. A microchannel and its walls can be representative of the parallel microchannels' section on the assumption that flow distribution is uniform. Energy balances of a microchannel compartment *i* and a wall compartment *i* are given by **Eqs.(3.1)** and **(3.2)**:

$$C_p(F_{in}^i T_{in}^i - F_{out}^i T_{out}^i) - Q^{ii} + \Delta Hr^i = 0 \tag{3.1}$$

$$k_w A_w^i (T_w^{i-1} + T_w^{i+1} - 2T_w^i)/\Delta x + Q^{ii} - Q_w^{ii} = 0 \tag{3.2}$$

where F^i, T^i, C_p and ΔHr^i are flow rate, temperature, specific heat and reaction heat generated in the microchannel compartment *i*. Q^{ii} is heat transfer rate from the microchannel compartment i to the wall compartment i. T_w^i, A_w^i, k_w and Δx are temperature, cross-sectional area, thermal conductivity and compartment length in the wall compartment *i*. Q_w^{ii} is heat transfer rate from the wall compartment *i* to the surrounding. The total thermal balance of the microreactor is solved under given boundary conditions.

Microchannel width is optimized as a function of the longitudinal position by taking into account the constraints related to thermal balance, pressure drop, reaction yield, temperature, and reactor dimensions. By changing the channel width, that is, by controlling residence time of fluid at each longitudinal position, a uniform temperature distribution with no hot-spot is realized even for a rapid exothermic reaction. The thermal design result is evaluated by CFD simulation. If the derived shape of the microchannel does not satisfy the given design specifications, model parameters, such as heat transfer coefficients, are adjusted to the value obtained by CFD simulation, and thermal design is repeated.

3.2.2 Fluid Design Stage

The detailed fluid dynamics of a microreactor is expressed by Navier-Stokes equations. However, it is difficult to solve those equations under the various boundary conditions. The pressure distribution usually determines the flow pattern at low Reynolds number. Therefore, the fluid design problem is regarded as a problem to find an appropriate pressure distribution over a microreactor.

In the fluid design stage, a pressure drop compartment model is used to estimate the pressure distribution over the microreactor including the inlet and outlet manifolds. Four types of pressure drop compartments with three design parameters (length, depth, and width) are introduced to describe the fluid dynamics in the microreactor: 1) a distributor dividing one stream into two streams, 2) a junction joining two streams into one, 3) a microchannel, and 4) a reaction-microchannel. A reaction-microchannel differs from a microchannel in having reaction kinetic models. In this investigation, each compartment is assumed to be a rectangular duct. For laminar flow in channels of rectangular cross-section, the velocity profile can be determined analytically. Pressure drop (ΔP) is calculated by **Eqs. (3.3)** and **(3.4)**:

$$\Delta P = \lambda\left(\frac{Z}{4m}\right)\left(\frac{\rho\bar{u}^2}{2}\right) \tag{3.3}$$

$$\lambda = \frac{64}{\mathrm{Re}} \times \frac{3/2}{(1+\varepsilon)^2\left[1-\frac{48}{\pi^5}\varepsilon\sum_{k=1,3,5,\cdots}^{\infty}\frac{4}{k^5}\tanh\left(\frac{k\pi}{2\varepsilon}\right)\right]} \tag{3.4}$$

Here, λ is the friction factor, Z the duct length, m the hydraulic diameter, ρ the density of fluid, $\bar{u}$ the average flow velocity, ε the aspect ratio of cross-section, and Re the Reynolds number.

The pressure distribution over a microreactor is modeled by combining compartments, which have design parameters. **Figure 3.4** shows an example of a combination of pressure drop compartments. While being distributed into each reaction-microchannel, the input stream passes through distributor compartments. The partitioned fluid is put together and becomes the output stream, while passing through junction compartments. Pressure balance equations are formulated for the combination of pressure drop compartments. **Equation (3.5)** represents the pressure balance among four compartments within the light gray region in **Fig. 3.4**.

$$\Delta P_C^{n-2} + \Delta P_O^3 = \Delta P_I^{n-1} + \Delta P_C^{n-1} \tag{3.5}$$

By repeating the derivation of pressure balance among other sets of compartments, algebraic equations which determine the relation between design parameters and pressure distribution are obtained.

Through the fluid design, the shapes of the inlet and outlet manifolds and the number of parallel microchannels are determined so as to optimize a given performance index such as the minimization of the total volume in the microreactor. Many constraints related to the pressure and mass balances, flow uniformity, pressure drop, total flow rate and reactor dimensions are considered in this design stage. The fluid design result is evaluated by CFD simulation. The compartment model is regenerated, and fluid design is repeated until the derived shape of manifold does not satisfy the design specifications.

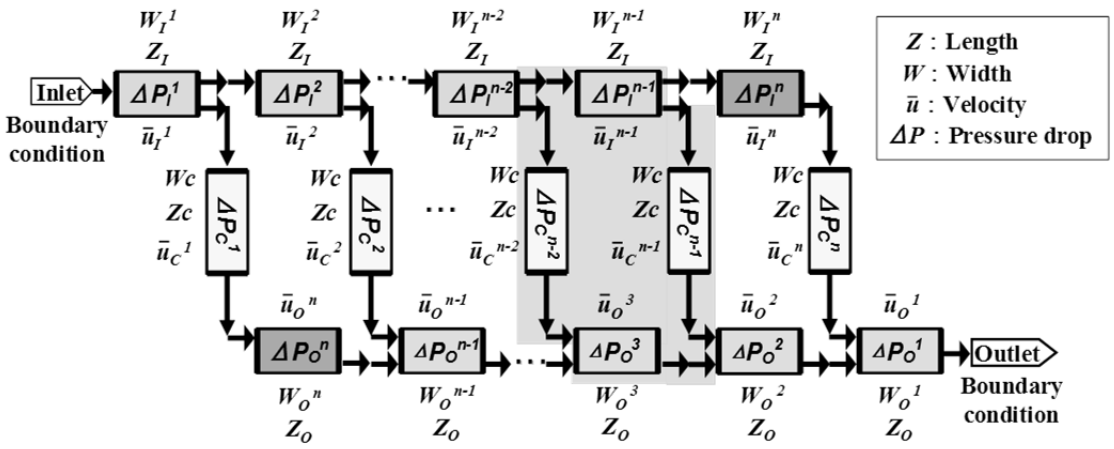

Fig. 3.4 Pressure drop compartment model

3.2.3 Detailed Design Stage

In the above-mentioned approach, the thermo-fluid design of the plate-fin microreactor is divided into two successive optimization problems. Therefore, the final shape of the microreactor, which is obtained by combining the thermal design and fluid design results, needs to be validated rigorously by CFD simulations.

3.3 Case Study

3.3.1 Design Conditions and Formulation

The thermo-fluid design approach is applied to a microreactor design problem. The objective of the design is to realize uniform temperature and residence time distributions. An exothermic first-order reaction A → B is taken up in this case study.

In the thermal design problem, it is assumed that a perfect flow distribution among parallel microchannels can be achieved, which means that all microchannels have the same temperature profiles axially. Therefore, symmetric boundary conditions are introduced into the thermal design problem of the plate-fin microreactor. These conditions can reduce the design region from the whole channel part to the one microchannel with a surrounding wall. In the case study, the basic design region is defined as a rectangular glass. To calculate the temperature distribution, the basic design region is divided into many thermal compartments representing the microchannel and the wall. The objective function of the thermal design problem is minimizing the integrated temperature error along the microchannel. The integrated temperature error I.E. is calculated by **Eq. (3.6)** where *x* means the axial position in the microchannel and *Tset* is a desired reaction temperature.

$$I.E. = \int (T(x) - Tset)dx \tag{3.6}$$

For a conventional macro reactor, it is not common to optimize tube diameter as a function of the tube position. However, a microchannel with varying width is not so difficult to fabricate by the techniques developed in the field of micro electro mechanical systems (MEMS).

In a fluid design problem, the microreactor including the inlet and outlet manifolds is compartmentalized as shown in **Fig. 3.4**. In this case study, it is assumed that pressure compartment configuration is point symmetry and that manifold shape is a trapezium. In addition, the first distributor compartment width (i.e., reactor inlet width), channel depth, and outlet pressure are fixed at constant value. The *n* th distributor compartment width and the number of microchannels are optimized under the constraints related to the pressure and mass balances, the flow uniformity, pressure drop, and reactor dimensions.

3.3.2 Design Results and Discussion

Figure 3.5 illustrates the thermal design result. The solid line in the upper graph shows the optimal channel width along the microchannel, and the dashed line shows the channel width which is optimized as a constant value. The optimal channel width increases gradually along the channel except for the inlet zone. The inlet width is slightly wider to preheat the feed stream. The width of the middle part becomes narrower due to faster reaction rate. The width of the last part becomes wider due to slower reaction rate. The bottom figure illustrates that the optimal microchannel shape is effective to keep the fluid temperature distribution uniform along the microchannel. On the other hand, the conventional straight channel has the hot-spot near inlet even if it is optimized.

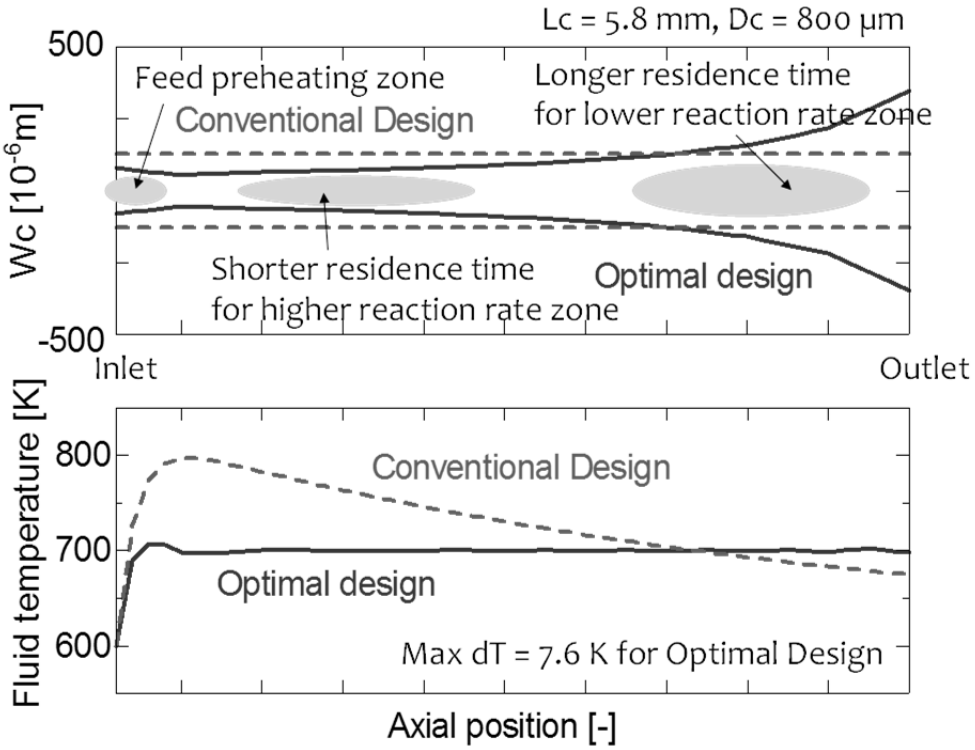

Fig. 3.5 Optimal channel width (upper) and temp. profiles (lower)

To assess the validity of the thermal compartment model, the design results obtained by using the thermal compartment model are compared with CFD simulation results. In this work, Fluent® code is used to calculate three-dimensional temperature distribution in the microchannel. The finite-volume method is used in Fluent® to solve conservation equations for mass, momentum, and energy. The equations are solved by using the SIMPLE algorithm. **Figure 3.6** shows the contour plots of temperature distribution in the microchannel including walls, which are obtained through CFD simulation. In the conventional channel, there is an area near the inlet, which means the existence of a hot-spot. On the other hand, the temperature distribution in the optimized channel is more uniform than that in the conventional channel.

Finally, the fluid design result is discussed. **Figure 3.7** shows a schematic drawing of the final shape of a plate-fin microreactor and the normalized flow distribution among parallel microchannels. The circle points correspond to the optimal design, and the triangle points represent the conventional design. The optimal manifold shape can realize flow equipartition in all parallel channels and avoid deterioration in the reactor performance.

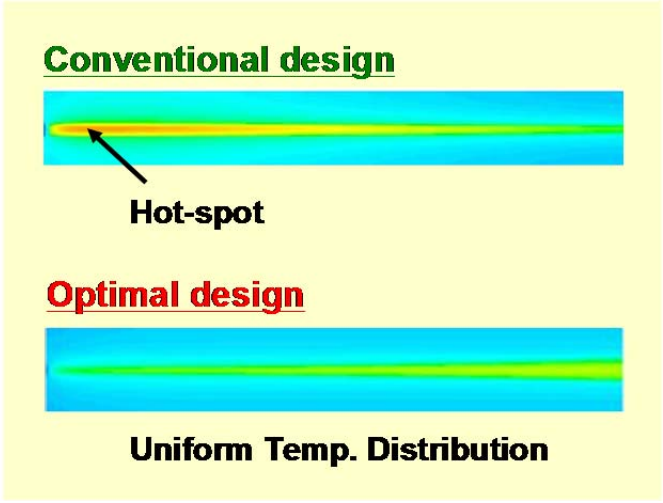

Fig. 3.6 Temperature contour plots by CFD

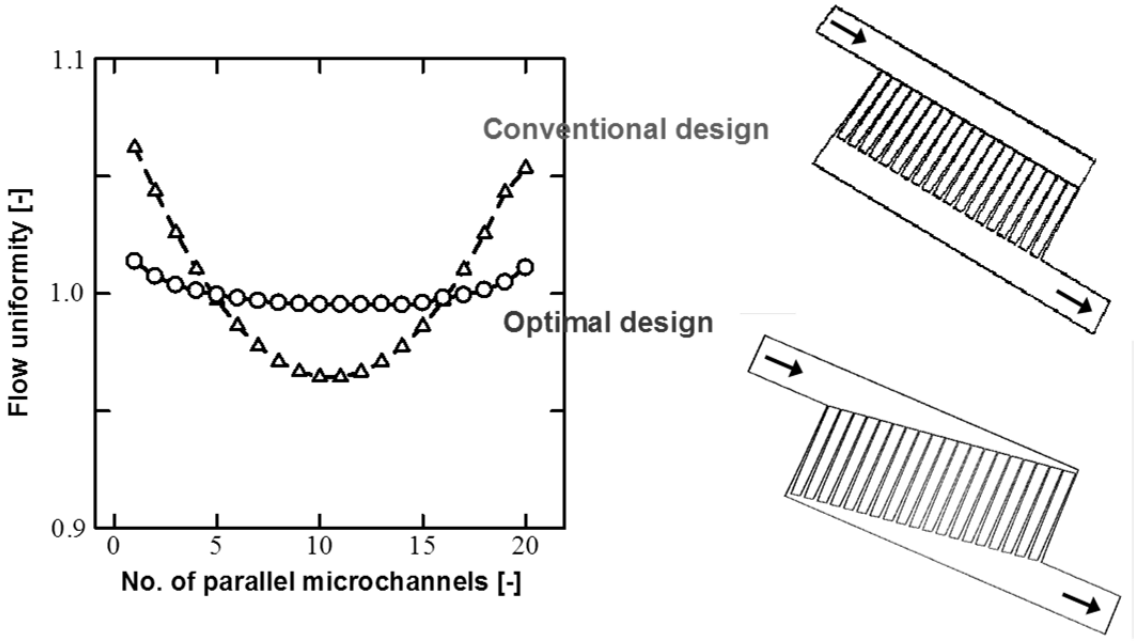

Fig. 3.7 Fluid design results

3.4 Conclusions

The thermo-fluid design approach was applied to the optimal design problem of a microreactor with uniform temperature and residence time distributions. In most of the conventional design approaches, the cross-sectional area of each microchannel is assumed to be constant, and the channel design under that condition sometimes causes an unnecessary increase of pressure drop. In the design strategy shown in Sec. 3.3, the fluid temperature along the microchannel is equalized by changing channel width, that is, the fluid residence time is controlled. In addition, the optimally designed manifold shape ensures the same residence time in all parallel microchannels and avoids deterioration in the reactor performance. The thermo-fluid compartment model is a very simple but powerful tool to shorten the computational time of microreactor design.

References

[1] O. Tonomura, M. Noda, M. Kano, S. Hasebe, “Optimal design approach for microreactors with uniform residence time distribution,” 10th Asian Pacific Confederation of Chemical Engineering (APCChE), Kitakyushu, Japan, Oct. 17-21 (2004)

[2] M. Noda, O. Tonomura, M. Kano, and Shinji Hasebe, “Systematic approach for thermal-fluid design of microreactors,” 10th Asian Pacific Confederation of Chemical Engineering (APCChE), Kitakyushu, Japan, Oct. 17-21 (2004)

Part II

Operation of Microreactors

Chapter 4

Operation Policy for Microreactors with External Numbering-up Structure

The performance of micro chemical plants with numbering-up structure depends on the flow distribution among the parallelized microchannels/microreactors [1]. One of the critical operational issues of micro chemical plants with external numbering-up structure is to keep a uniform flow distribution among parallelized microreactors even when blockage occurs in one or more microreactor. Since it is not practical to install flow controllers in all the microreactors, a simple and effective operation policy against blockage occurrence needs to be developed. In this chapter, micro chemical plants having four or eight parallelized microreactors are constructed to analyze the influence of blockage on the flow distribution among the parallelized microreactors under two types of operation policies, pressure drop control and total flow control. In addition, two control structures based on pressure drop control, pumping pressure control and pressure drop control over the parallelized section, are investigated through both simulations and experiments.

4.1 Total Flow Control and Pressure Drop Control

To maintain the desired product quality, it is important to keep uniform flow rate in each microreactor of the micro chemical plant when blockage occurs because the flow maldistribution makes the performance of the micro chemical plant worse. In this research, pressure drop control is proposed to achieve the uniform flow distribution. A micro chemical

plant consisting of four parallelized microreactors in **Fig. 4.1** is used to demonstrate the difference of two operation policies, total flow control and pressure drop control. When blockage occurs in microreactor 2, the flow distribution under the pressure drop control is derived by simulation and compared with that under the total flow control. In **Fig. 4.1**, reactant is fed to the parallelized microreactors at 12 mL/min in the normal condition. The physical properties of the reactant are assumed to be the same as water (293 K).

The results are shown in **Fig. 4.2**. In the case of blockage occurrence, mass flow rates of unblocked microreactors are significantly increased under the total flow control (**Fig. 4.2** left), while they are kept constant at the value in the normal condition under pressure drop control (**Fig. 4.2** right). These results show that the proposed pressure drop control is effective in making flow distribution uniform even when blockage occurs.

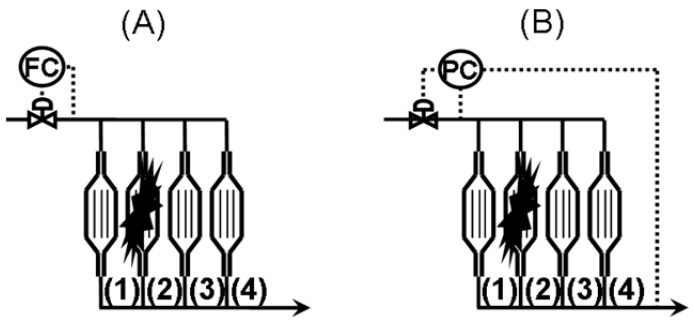

Fig. 4.1 Parallelized microreactors under two operation policies:
(A) total flow control and (B) pressure drop control

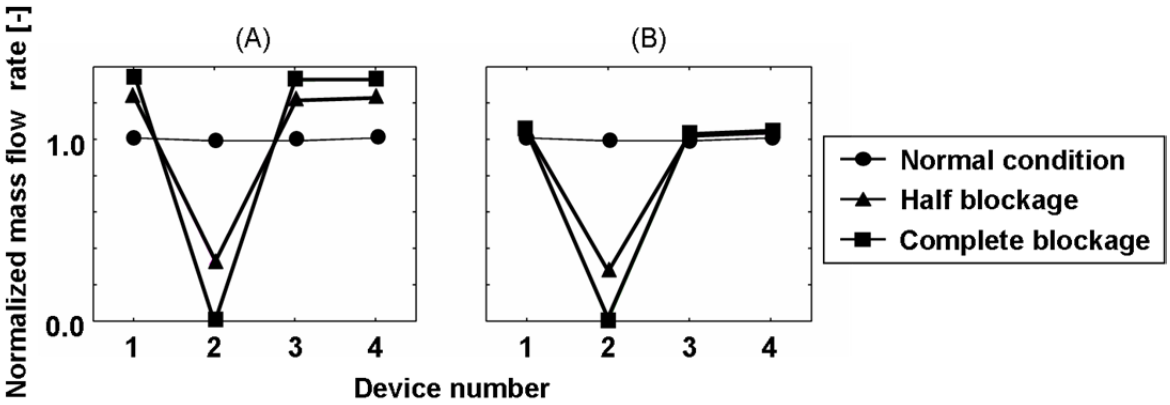

Fig. 4.2 Mass flow rate of each microreactor under blockage occurrence:
(A) total flow control and (B) pressure drop control

4.2 Comparison of Control Structures in Pressure Drop Control

In the previous section, it is confirmed that pressure drop control is superior to total flow control in realizing uniform flow distribution among unblocked microreactors when blockage occurs. In this section, two different control structures based on pressure drop control, pumping pressure control and pressure drop control over the parallelized section, are investigated.

4.2.1 Experimental Apparatus

Micro chemical plants having four or eight parallelized microdevices are used to grasp the distinction between two control structures. The schematic drawing of the micro chemical plant having four parallelized microdevices is shown in **Fig. 4.3**. Reactant is fed by using a double plunger pump. The product line is open to atmosphere. Flow rate of each microreactor is measured by using an in-line mass flow meter, and blockage in each microreactor is artificially realized by closing the valve located between the pump and each microreactor. Each microreactor consists of SUS tube having 0.3 mm in inner diameter and 2 m in length. In addition, a SUS tube with 0.5 mm in inner diameter and various lengths is installed after the parallelized microreactors to represent units that are not necessary to be parallelized. Hereafter, this section is referred to as a residence time section. The pressure drop over the parallelized section and the residence time section are denoted by ΔP_a and ΔP_b, respectively. The ratio of ΔP_a to ΔP_b is changed by adjusting the length of the residence time section.

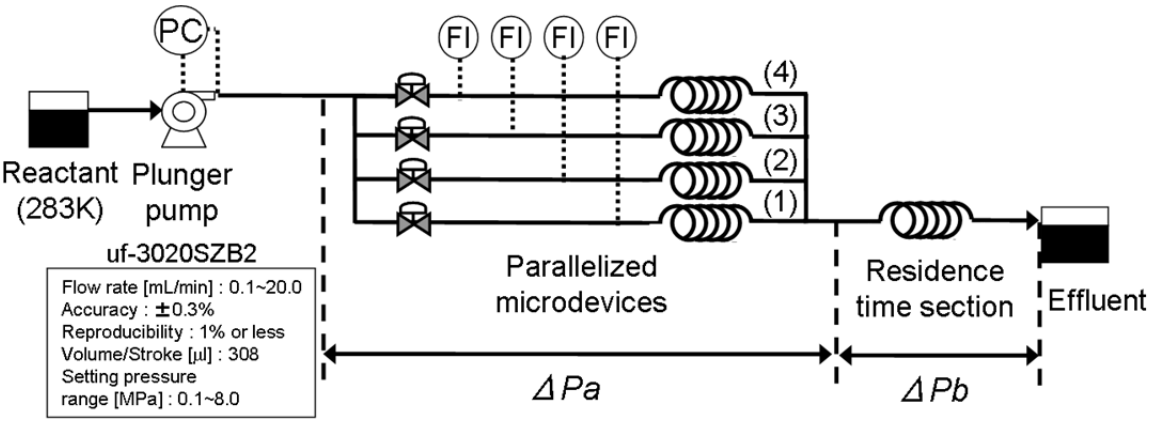

Fig. 4.3 Micro chemical plant under pumping pressure control

4.2.2 Pumping Pressure Control

Under pumping pressure control, the double plunger pump is operated at constant pumping pressure. In experiments, pumping pressure is kept at gauge pressure of 500 kPa to 1 MPa. Pressure drop over the whole micro chemical plant is kept constant under pumping pressure control, because the product line is open to atmosphere.

The influence of blockage on flow distribution under pumping pressure control is investigated through both simulations and experiments with changing the ratio $\Delta P_a/\Delta P_b$ in the range of one-fifth to seven. The first step in the experimental procedure is to adjust the pumping pressure to realize the total flow rate of 12 mL/min. This operating condition is regarded as the normal condition. Then, microreactor 1 is artificially blocked by closing the valve. In 300 seconds, the micro chemical plant is returned to the normal condition by opening the valve. These procedures are repeated for the other valves to imitate blockage in the other microreactors.

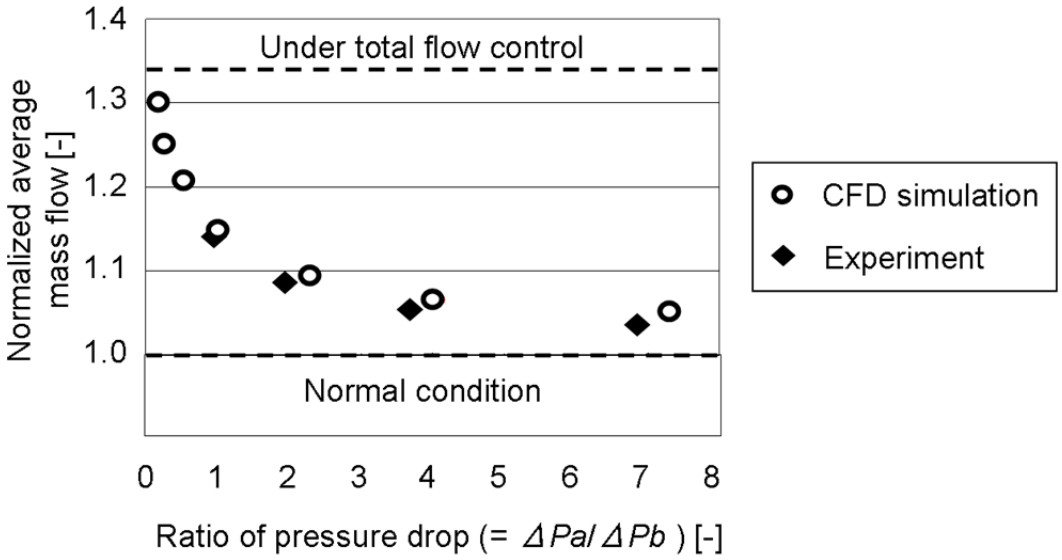

Fig. 4.4 Influence of blockage on the mass flow rate

Figure 4.4 shows the normalized average mass flow rate, which is defined as the ratio of average mass flow rate of unblocked microreactors under blockage occurrence to that under the normal condition at each $\Delta P_a/\Delta P_b$. There is little difference between the results of experiments and those of CFD simulations. The normalized average mass flow rate becomes closer to the flow rate under the normal condition as $\Delta P_a/\Delta P_b$ becomes larger. In other words, ΔP_a should be significantly larger than ΔP_b to keep the flow rate of unblocked microreactors unchanged when blockage occurs.

In laminar flow, pressure drop is proportional to flow rate and flow resistance. Therefore, ΔP_a and ΔP_b are expressed by

$$\Delta P_a = \frac{1}{\sum_{i=1}^{4} \frac{1}{k_i}} F \tag{4.1}$$

$$\Delta P_b = k_b F \tag{4.2}$$

where k_i (i = 1, 2, 3, 4) is a coefficient of resistance in each microreactor, k_b is a coefficient of resistance in the residence time section, and F is the total flow rate. The pressure drop over the whole chemical plant, ΔP, is calculated by

$$\Delta P = \Delta P_a + \Delta P_b = \left(\frac{1}{\sum_{i=1}^{4} \frac{1}{k_i}} + k_b \right) F \tag{4.3}$$

When ΔP_a is much larger than ΔP_b, the second term in the right side of **Eq. (5.3)** can be neglected. When blockage occurs in the i th microreactor, k_i becomes the infinite. Consequently, the total flow rate under blockage occurrence becomes three-fourth times as much as that under the normal condition, provided that all the coefficients of flow resistance in the parallelized section are the same. Therefore, the flow rates of unblocked microreactors do not change when $\Delta P_a/\Delta P_b$ is sufficiently large. On the other hand, when $\Delta P_a/\Delta P_b$ is equal to 1,

the total flow rate under blockage occurrence becomes six-seventh times, and the flow rate of each unblocked microreactor under blockage occurrence becomes eight-seventh times as much as that under the normal condition. These results correspond to the results of CFD simulations and experiments. It is concluded that pumping pressure control is effective to realize uniform flow distribution when the pressure drop over the parallelized section is dominant.

4.2.3 Pressure Drop Control over the Parallelized Section

The flow uniformity achieved by pumping pressure control depends on $\Delta P_a/\Delta P_b$, which is the ratio of the pressure drop over the parallelized section to that over the residence time section. The flow uniformity in the parallelized microreactors deteriorates when the $\Delta P_a/\Delta P_b$ is small. In this subsection, another pressure drop control structure where ΔP_a is directly controlled by manipulating the flow rate of the bypass line is proposed.

The performance of the proposed control structure is evaluated experimentally by using the micro chemical plants with four (Type A) and eight (Type B) parallelized microdevices. **Figure 4.5** shows an experimental setup of Type A plant. A bypass line is equipped around the plunger pump. A mass flow controller, which is a PID controller, is installed in the bypass line to keep the pressure drop over the parallelized section (ΔP_a) constant at its set-point. The experimental condition is summarized in **Table 4.1**. The plunger pump is operated so that the total flow rate is kept constant. The other conditions are the same as those in the previous subsection.

The experimental results for Type A plant is shown in **Fig. 4.6**. The top and bottom figures correspond to the case where $\Delta P_a/\Delta P_b = 50$ and $\Delta P_a/\Delta P_b = 1$, respectively. In the range of 0 to 300 seconds, the micro chemical plant is operated under the normal condition. The difference in flow rate between microreactors 1 and 2 is due to the degree of precision in the fabrication. When blockage occurs in microreactor 1 at 300 seconds, the flow rate of microreactor 1 goes to zero instantaneously and the flow rate of microreactor 2 deviates from its set-point. However, the flow rate of microreactor 2 returns to the normal level in a few tens of seconds. The deviation of the flow rate becomes small when blockage occurs gradually. The transient responses of microreactors 3 and 4 are similar to that of microreactor 2, and they are not shown in **Fig. 4.6** to identify the transient response of each microreactor easier. The top and bottom figures in **Fig. 4.6** show almost the same profiles. This result shows that the efficiency of the proposed control structure does not depend on $\Delta P_a/\Delta P_b$.

The experimental result of Type B plant is shown in **Fig. 4.7**, and it is almost the same as that of Type A plant. These results show that the proposed control structure has a function of keeping the flow rate of the unblocked devices constant regardless of the changes in $\Delta P_a/\Delta P_b$ and the number of parallelized microreactors.

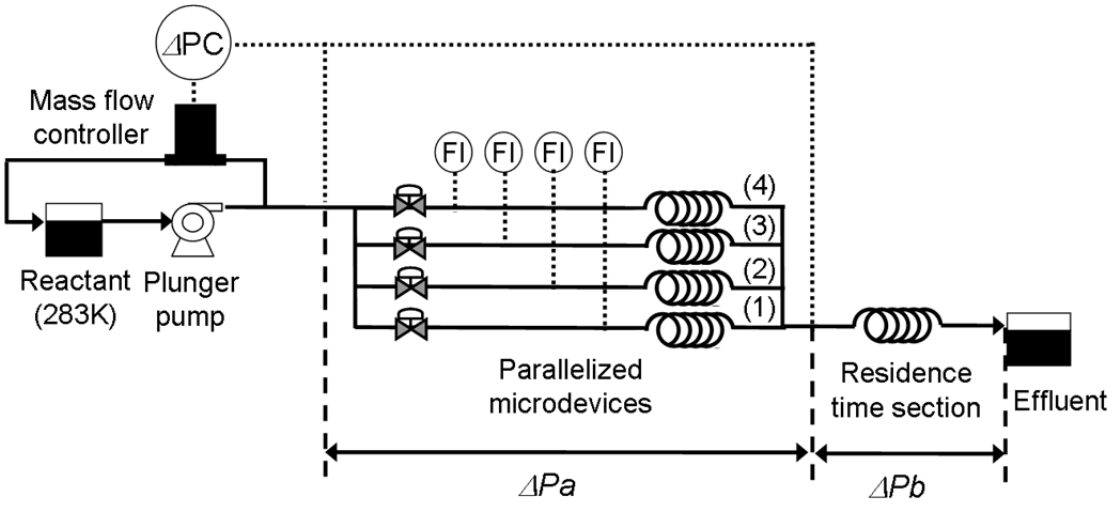

Fig. 4.5 Micro chemical plant under pressure drop control over the parallelized section

Table 4.1 Experimental condition

Flow rate of the double plunger pump [mL/min]	Pressure drop over the parallelized section [kPa]	PID controller			Residence time section		
		Proportional band [%]	Integral time [s]	Derivative time [s]	Inner diameter [mm]	Length (Type A) [m]	Length (Type B) [m]
18	500	34.6	7	1	0.5	0.1	4

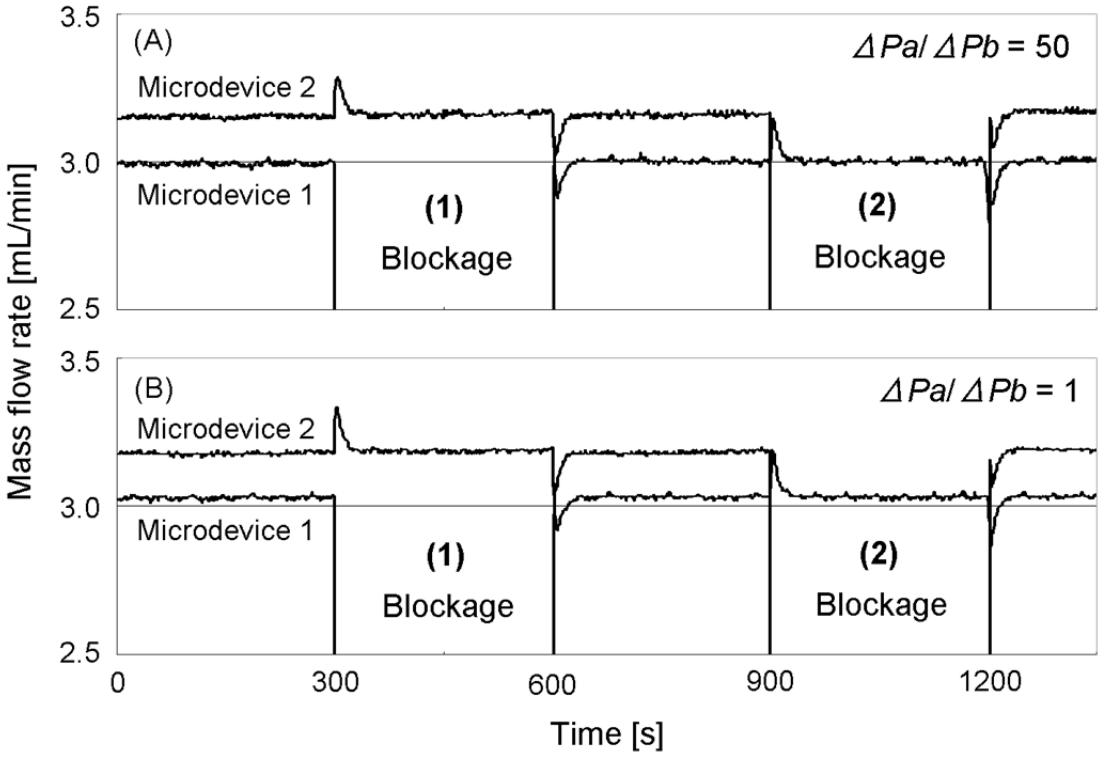

Fig. 4.6 The time series of mass flow rate in each microdevice in Type A: (A) $\Delta P_a/\Delta P_b = 50$ and (B) $\Delta P_a/\Delta P_b = 1$

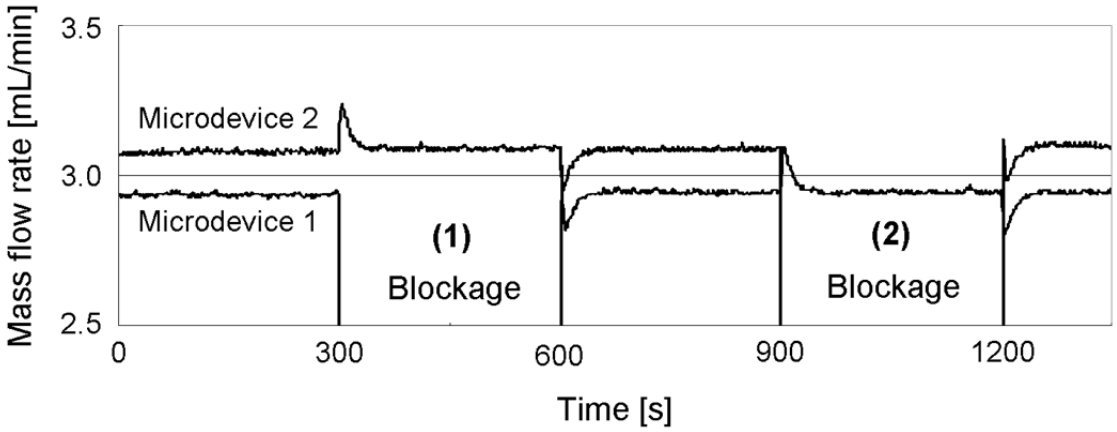

Fig. 4.7 The time series of mass flow rate in each microdevice in Type B

4.3 Blockage Occurrence in Three Microreactors

Provided that more than one microreactor is blocked at the same time, the effectiveness of the proposed pressure drop control over the parallelized section is investigated by using the micro chemical plant shown in **Fig. 4.5**.

Figure 4.8 represents the time series of flow rates of microreactors 1 and 2. In the range of 150 to 480 seconds, it is apparent that the flow rate of microreactor 1 violently oscillates when microreactors 2, 3, and 4 are blocked simultaneously. This result is explained as follows: the feed flow rate F_{Total} of the plunger pump under the normal condition is expressed by

$$F_{Total} = 4F_{MD} + F_{Bypass} \tag{4.4}$$

where F_{MD} and F_{Bypass} denote the flow rate in each microreactor and that in the bypass line, respectively. F_{Bypass} is assumed to be perfectly controlled by the mass flow controller. When one microreactor is blocked (Case 1), the flow rate of the bypass line $\hat{F}_{Bypass}$ is represented by

$$\hat{F}_{Bypass} = F_{Total} - 3F_{MD} \tag{4.5}$$

At this time, F_{Total} and F_{MD} in Case 1 are the same as those under the normal condtion. On the other hand, when three microreactors are blocked (Case 2), the flow rate of the bypass line $\hat{\hat{F}}_{Bypass}$ is represented by

$$\hat{\hat{F}}_{Bypass} = F_{Total} - F_{MD} \tag{4.6}$$

Under these conditions, when the flow rate in the bypass line changes slightly, **Eqs (4.5)** and **(4.6)** are expressed by

$$F_{Total} = 3\left(F_{MD} + \delta\hat{F}_{MD}\right) + \hat{F}_{Bypass} - \delta F_{Bypasss} \tag{4.7}$$

$$F_{Total} = \left(F_{MD} + \delta\hat{\hat{F}}_{MD}\right) + \hat{\hat{F}}_{Bypass} - \delta F_{Bypasss} \tag{4.8}$$

According to **Eqs. (4.7)** and **(4.8)**, the relationship between the change of the flow rate of the bypass line and that of each microreactor are expressed by

$$\delta\tilde{F}_{MD} = \frac{\delta F_{Bypasss}}{3} \tag{4.9}$$

$$\delta\tilde{\tilde{F}}_{MD} = \delta F_{Bypasss} \tag{4.10}$$

Judging from **Eqs. (4.9)** and **(4.10)**, the effect of $\delta F_{Bypasss}$ on the flow rate of each microreactor in Case 2 becomes three times as much as that in Case1. Since F_{MD} is proportional to ΔP_a, the stady-state gain of the process in Case 2 is three times larger than that in Case1. This change in the steady-state gain affects the control performance significantly and causes oscillatory behavior in Case 2 as shown in **Fig. 4.8**. In general, the control action becomes stronger and the controlled and manipulated variables become more oscillatory as the number of blocked microdevices increases as long as the same controller is used.

The influence of blockage on the control performance depends greatly on the ratio of the number of blocked microreactors to the number of parallelized microreactors. The influence is smaller as the ratio is smaller. As shown in this experimental study, the influence will be

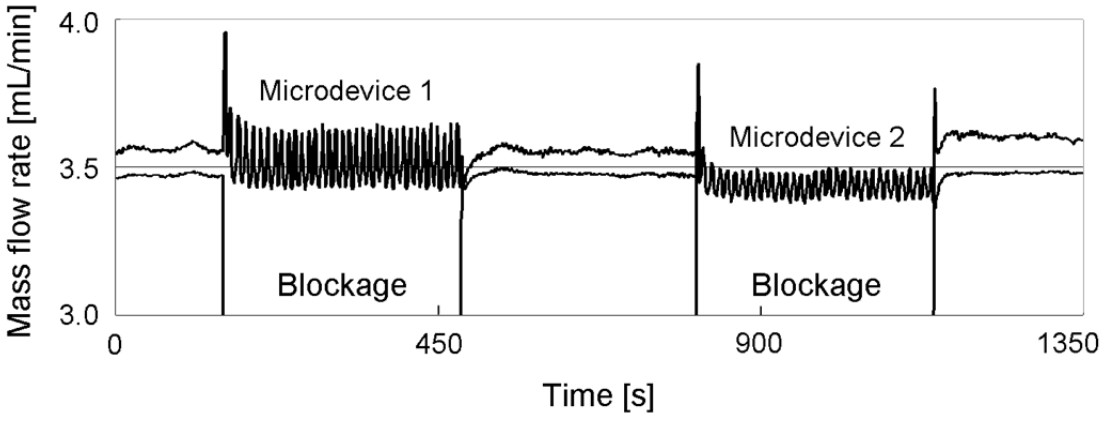

Fig. 4.8 The time series of mass flow rate under blockage occurrence in three microdevices

significant when there are a few parallelized microreactors. In such a situation, it is necessary to design a controller that is robust against the degree of blockage. For example, control parameters might need to be changed appropriately according to the number of blocked microreactors.

4.4 Conclusions

Two operation policies, total flow control and pressure drop control, are compared, and the simulation result shows that the pressure drop control is effective to keep uniform flow distribution among the parallelized microreactors even when blockage occurs. In addition, two control structures based on pressure drop control, pumping pressure control and pressure drop control over the parallelized section, are investigated experimentally. The former control structure is simple. However, this structure functions only when the ratio of pressure drop over the parallelized section to that over the residence time section, $\Delta P_a/\Delta P_b$, is large. On the other hand, the latter control structure can make the flow distribution uniform for any $\Delta P_a/\Delta P_b$.

The investigations mentioned above are conducted on the assumption that a microreactor is completely blocked and its flow rate becomes zero. In the actual process, there is a possibility that microreactors are partially blocked. In such a case, the uniformity of the residence time in the parallelized microreactors cannot be achieved, and the flow maldistribution deteriorates reaction selectivity, heat transfer efficiency, and so on. When blockage in a microreactor is detected, it is preferable to stop the production in the blocked microreactor and to replace it with a new microreactor. Meanwhile, the flow rates of the other unblocked microreactors are kept constant at the normal level by the pressure drop control over the parallelized section.

The proposed pressure drop control over the parallelized section is proved to be highly effective for the operation of micro chemical plants with external numbering-up structure. However, in addition to the control method, it is necessary to develop an effective monitoring method that can detect and diagnose abnormal conditions such as blockage.

References

[1] N. Kockmann, “Micro process engineering: fundamentals, devices, fabrication, and applications,” Wiley, VCH, Weinheim (2006)

Chapter 5

Data-based and Model-based Blockage Diagnosis for Stacked Microrectors

This research focuses on blockage diagnosis of stacked microreactors. Stacked microreactors consist of a number of plates and are widely used as heat exchangers or reactors. Since it is not practical to install sensors into every single plate, an abnormal plate needs to be specified with as few sensors as possible when blockage occurs. In thist work, two types of blockage diagnosis systems, a data-based blockage diagnosis system (DB-BDS) and a model-based blockage diagnosis system (MB-BDS), are proposed. DB-BDS is preferable to MB-BDS when experiments can be performed to obtain operation data under complete blockage in each plate. On the other hand, MB-BDS is preferable to DB-BDS when experiments are not desired to obtain operation data under blockage and a process model can be built. The performance of the proposed systems is evaluated with their applications to a stacked microreactor.

5.1 Stacked Microreactors

This work focuses on blockage diagnosis of stacked microreactors, and all data are generated from simulations. Therefore, first of all, the simulation model of the stacked microreactor and the simulation settings are explained in this section. The microreactor is modeled by using the microchemical process simulator (μCPS) developed by Fujioka et al. [1].

A part of the microreactor investigated in this work is shown in **Fig. 5.1**. Simulation settings are

as follows:

(1) The microreactor is made of stainless steel and insulated from the environment.
(2) A total of 20 plates are stacked. Plates are numbered from the bottom. A cover plate of 100 μm thickness is set on the top.
(3) Each plate has one microchannel.
(4) Reactant in the odd plates and coolant in the even plates flow in parallel.
(5) Pressure drop between inlet and outlet is controlled and kept constant.
(6) The following exothermic reaction takes place:

$$\mathrm{A} \rightarrow \mathrm{B}$$
$$-r_A = 5C_A$$
$$\Delta H_R = -10$$

where ΔH_R $[\mathrm{kJ \cdot mol^{-1}}]$ is heat of reaction, r_A $[\mathrm{kmol \cdot m^{-3} \cdot s^{-1}}]$ is reaction rate, and C_A $[\mathrm{kmol \cdot m^{-3}}]$ is mole concentration of reactant A.

(7) Each plate is compartmentalized into 30 compartments as shown in **Fig. 5.2**.
(8) The microreactor is operated at the steady state as shown in **Table 5.1**. Reactant and coolant have the same physical properties as water.
(9) The temperature of the device wall between reactant and coolant is measured. All sensors are located near the inlet.

A number of simulations are executed to obtain temperature data under various degrees of blockage including complete blockage in each plate. In this case study, blockage degree (BD) is defined as

$$BD = \frac{F_N - F_B}{F_N} \times 100 \ [\%] \tag{5.1}$$

where F_N and F_B denote flow rate in the blocked plate under normal operating condition and under blockage occurrence, respectively.

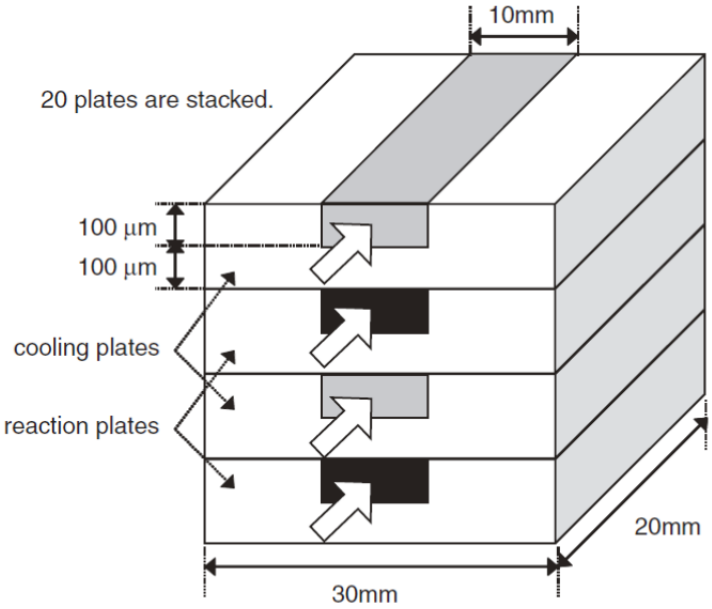

Fig. 5.1 A part of the stacked microreactor consisting of 10 reaction plates and 10 cooling plates.

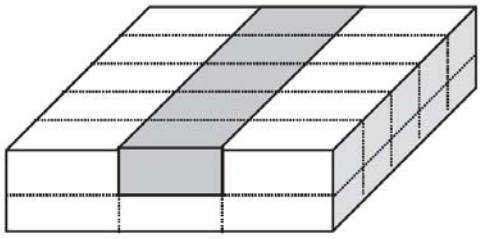

Fig. 5.2 Compartments of each plate of the stacked microreactor

Table 5.1 Steady-state operating condition of the stacked microreactor

	Reactant	Coolant
Inlet temperature (°C)	40.0	20.0
Outlet temperature (°C)	46.5	45.8
Mean velocity ($m\,s^{-1}$)	0.020	0.097
Flow rate ($g\,s^{-1}$)	0.20	0.96
Conversion (%)	96.7	–
Pressure drop (Pa)	300	1500

5.2 Data-based Blockage Diagnosis System

In this section, the DB-BDS is explained in detail. DB-BDS is developed by using operation data obtained under complete blockage in each plate. In DB-BDS, only temperature measurements are used to identify blockage location. As described in Sec. 5.1, this work focuses on stacked microreactors consisting of a number of plates. In a stacked microreactor, hot or cold fluid flows in each plate for efficient heat transfer. Such stacked microreactors are widely used in the field of micro chemical process technology.

5.2.1 Assumptions and System Development Policy

To develop DB-BDS, the following assumptions are introduced:

(1) Temperature of the device wall between the hot fluid and the cold fluid is measured.
(2) Temperature sensors are set up at regular intervals.
(3) Temperature data are obtained under blockage in each plate.

Under these assumptions, DB-BDS is constructed by adopting the following policy:

(i) The system is built from operation data. No first principle model is required.
(ii) The system uses only two temperature measurements, which changes the most when blockage occurs.
(iii) The system identifies the blocked plate that is assumed to be located between the two sensors selected in (2).

When blockage occurs in a plate of the stacked microreactor, a change in temperature measurement is larger as the sensor is closer to the blockage location. Therefore, blockage must occur between two sensors at which temperature changes are the largest. In other words, only two temperature measurements are sufficient to identify the blockage location. In addition, since temperature sensors are set up at regular intervals, the stacked microreactor has a repetitive structure of a unit module that consists of several plates with two temperature sensors at both ends. Therefore, DB-BDS can be developed by analyzing one particular unit module even if the microreactor consists of a huge number of plates. Experimental data under blockage in each plate of the whole stacked microreactor is not necessary.

However, the top plate and the bottom plate of microreactors exchange heat through only a single side and also they are affected by heat radiation. Therefore, DB-BDS is to be constructed separately for such parts of the process if necessary.

5.2.2 Procedure

Various degrees of blockage are expected in real microreactors and blockage needs to be detected and diagnosed as early as possible. To realize efficient diagnosis for various degrees of blockage, the proposed DB-BDS uses the ratios of temperature differences between normal and abnormal operating conditions at one sensor to those at the other sensor.

The procedure for building DB-BDS is as follows:

(1) Obtain temperature data under complete blockage in each plate by experiment. The total number of plates between two sensors is K.
(2) Calculate the temperature differences between normal and abnormal operating conditions at two sensors

$$\Delta T_{1,k} = T_{1,k,\mathrm{B}} - T_{1,k,\mathrm{N}} \tag{5.2}$$

$$\Delta T_{2,k} = T_{2,k,\mathrm{B}} - T_{2,k,\mathrm{N}} \tag{5.3}$$

where T denotes temperature, k (k = 1, 2, . . . , K) is the blockage location. In addition, B and N denote blockage and normal, respectively
(3) Calculate the ratio of temperature difference

$$R_k = \frac{\Delta T_{1,k}}{\left|\Delta T_{2,k}\right|} \tag{5.4}$$

The denominator is an absolute value of temperature difference because the sign of temperature difference makes it possible to judge whether blockage occurs in a hot fluid plate or a cold fluid plate.

At the first step, complete blockage is simulated for generating data although the completeness of the blockage is not strictly necessary.

After blockage is detected, the blockage location is identified through the following procedure:

(1) Identify two temperature sensors whose measurements change the most of all.
(2) Calculate the temperature differences between normal and abnormal operating conditions at the two sensors:

$$\Delta T_1 = T_{1,\mathrm{B}} - T_{1,\mathrm{N}} \tag{5.5}$$
$$\Delta T_2 = T_{2,\mathrm{B}} - T_{2,\mathrm{N}} \tag{5.6}$$

(3) Calculate the ratio of temperature difference:

$$R = \frac{\Delta T_1}{|\Delta T_2|} \tag{5.7}$$

(4) Identify the plate that has the smallest difference between the prepared ratio and the actual ratio as a blocked plate:

$$\Delta R = R_k - R \tag{5.8}$$

It is expected that the ratio of two temperature differences remains unchanged even if the degree of blockage varies. Therefore, various degrees of blockage can be identified by using the proposed DB-BDS as shown in **Fig. 5.3**. The black circles are temperature measurements during the system development stage, and they are plotted in the two-dimensional $\Delta T_1 - \Delta T_2$ space. In this illustrative example, six solid half lines are drawn because the total number of plates between two sensors, K, is six. The cold fluid flows through three of six plates: 1st, 3rd, and 5th plates. On the other hand, the hot fluid flows through the other three plates: 2nd, 4th, and 6th plates. Both $\Delta T_{1,k}$ and $\Delta T_{2,k}$ become positive when blockage occurs in a cold fluid plate, while they become negative when blockage occurs in a hot fluid plate. The ratio R_k corresponds to the directions of the half lines. When blockage occurs, ΔT_1 and ΔT_2 are calculated and plotted in the same $\Delta T_1 - \Delta T_2$ space (outline circle in **Fig. 5.3**). The direction of the dotted half line corresponds to the ratio R. The blocked plate can be identified by comparing differences between the dotted half line and the other solid half lines. In this example, the 3rd plate is

identified as the most suspicious plate. In addition, the degree of blockage can be roughly estimated via **Fig. 5.3** because the distance from the origin corresponds to the degree of blockage.

DB-BDS not only can diagnose the blockage location but also can estimate the degree of blockage. It is also intuitively understandable. DB-BDS has such attractive features even though it can be easily developed. In fact, the application results have shown that the proposed DB-BDS functions better than another statistical method based on a linear discriminant model.

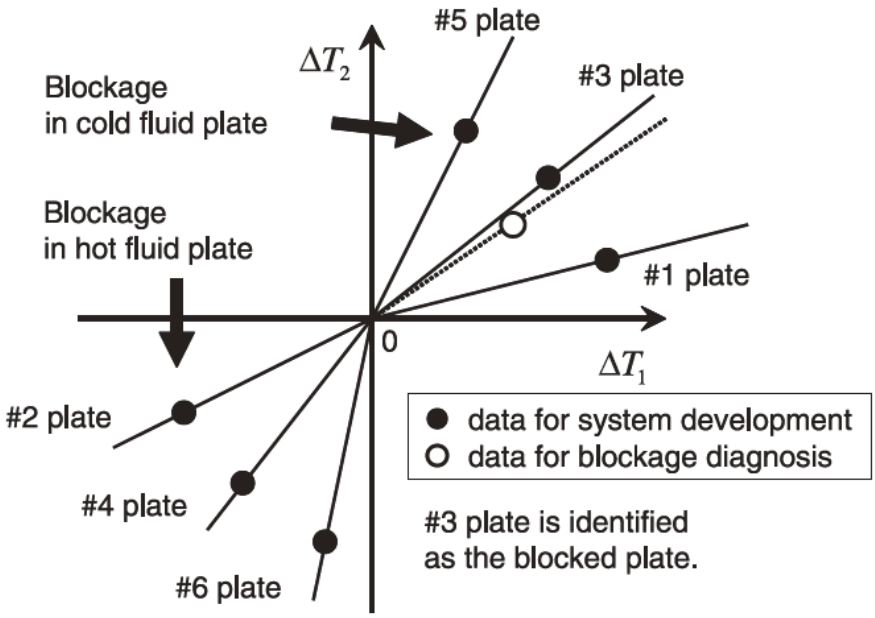

Fig. 5.3 Concept of data-based blockage diagnosis system (DB-BDS) for stacked microreactors

5.3 Model-based Blockage Diagnosis System

In this section, the MB-BDS is explained in detail. MB-BDS uses physical models of the process operated under a normal condition and under blockage occurrence in each plate. The inputs of the models are pressure drop and inlet temperature, and the outputs are the temperatures of the plates where sensors are set up. Although these variables are used in this work, inputs and outputs vary with applications. In MB-BDS, operation data of an actual

process under blockage occurrence is not required in advance, while a simplified process model is required.

5.3.1 Assumptions and System Development Policy

To develop MB-BDS, the following assumptions are introduced:

(1) The temperature of the device wall between the hot fluid and the cold fluid is measured.
(2) A physical model is available to calculate temperature.

Under these assumptions, MB-BDS is constructed by adopting the following policy:

(1) The system is built on the basis of a simplified process model.
(2) The system uses all temperature measurements available.
(3) The system identifies the blocked plate in a whole stacked microdevice.

In general, compartment models can be used as a process model for MB-BDS. The models used in this work are explained in the next application section.

5.3.2 Procedure

The procedure for building MB-BDS is as follows:

(1) Build a physical model that can simulate the process operated under a normal condition and a complete blockage condition in each plate.
(2) Calculate temperature distribution under the normal condition and the complete blockage condition in each plate.
(3) Calculate the temperature difference.

$$\Delta \breve{\boldsymbol{T}}_k = \breve{\boldsymbol{T}}_{k,\mathrm{B}} - \breve{\boldsymbol{T}}_{\mathrm{N}} \tag{5.9}$$

where $\breve{\boldsymbol{T}}_{\mathrm{N}} \in \Re^S$ denotes a vector consisting of temperature measurements at S sensors under the normal condition and $\breve{\boldsymbol{T}}_{k,\mathrm{B}} \in \Re^S$ under the complete blockage condition in the k th plate. The temperature is estimated through the physical model.

After blockage is detected, the blockage location is identified through the following procedure:

(1) Calculate the temperature difference from temperature measurements of the real process

$$\Delta \boldsymbol{T} = \boldsymbol{T}_{\mathrm{B}} - \boldsymbol{T}_{\mathrm{N}} \tag{5.10}$$

(2) Judge whether blockage occurs in hot fluid plates or cold fluid plates. Blockage occurs in cold fluid plates when $\Delta \boldsymbol{T} > \boldsymbol{0}$. On the other hand, blockage occurs in hot fluid device when $\Delta \boldsymbol{T} < \boldsymbol{0}$.

(3) Identify the plate that has the highest correlation between $\Delta \boldsymbol{T}$ and $\Delta \breve{\boldsymbol{T}}_k$ as a blocked device. The correlation is defined as

$$R_k = \frac{(\Delta \boldsymbol{T} - \Delta \overline{\boldsymbol{T}})^T (\Delta \breve{\boldsymbol{T}}_k - \Delta \overline{\breve{\boldsymbol{T}}}_k)}{\| \Delta \boldsymbol{T} - \Delta \overline{\boldsymbol{T}} \| \| \Delta \breve{\boldsymbol{T}}_k - \Delta \overline{\breve{\boldsymbol{T}}}_k \|} \tag{5.11}$$

where $\Delta \overline{\boldsymbol{T}}$ and $\Delta \overline{\breve{\boldsymbol{T}}}_k$ denote a mean vector of $\Delta \boldsymbol{T}$ and $\Delta \breve{\boldsymbol{T}}_k$, respectively.

The performance of MB-BDS will not be strongly affected by the accuracy of the physical models because calculated temperature distribution is to be similar in spite of the model accuracy.

5.4 Application to Microreactor

In this section, the proposed DB-BDS and MB-BDS are applied to blockage diagnosis problems of the stacked microreactor described in Section 5.1 to validate their performance.

5.4.1 Results of DB-BDS

To build a DB-BDS, temperature data under a normal operating condition and under complete blockage in each plate are used. Temperature sensors are set up at regular intervals about every 1–10 plates. In this case study, it is assumed that the stacked microreactor consists of a sufficiently large number of plates and the influence of the top and the bottom plates can be neglected.

A part of the diagnosis results is summarized in **Table 5.2**. The identified plate in each case is shown in the table for various blockage locations, blockage degrees, and sensor intervals. The diagnosis is successful when the identified plate is the same as the blockage location. The developed DB-BDS was able to identify the blockage location successfully by using only two temperature sensors even when blockage degree was less than 10% and sensors are set up every 10 plates. No misdiagnosis occurred. The results clarify the usefulness of the proposed DB-BDS.

Table 5.2 Diagnosis results of data-based blockage diagnosis system (DB-BDS)

Blockage location	Blockage degree (%)	Sensor interval			
		4	6	8	10
1	100	1	1	1	1
	70	1	1	1	1
	36	1	1	1	1
	9	1	1	1	1
2	100	2	2	2	2
	62	2	2	2	2
	30	2	2	2	2
	8	2	2	2	2
5	100		5	5	5
	69		5	5	5
	36		5	5	5
	9		5	5	5
6	100		6	6	6
	64		6	6	6
	32		6	6	6
	8		6	6	6
9	100				9
	69				9
	36				9
	9				9
10	100				10
	63				10
	32				10
	8				10

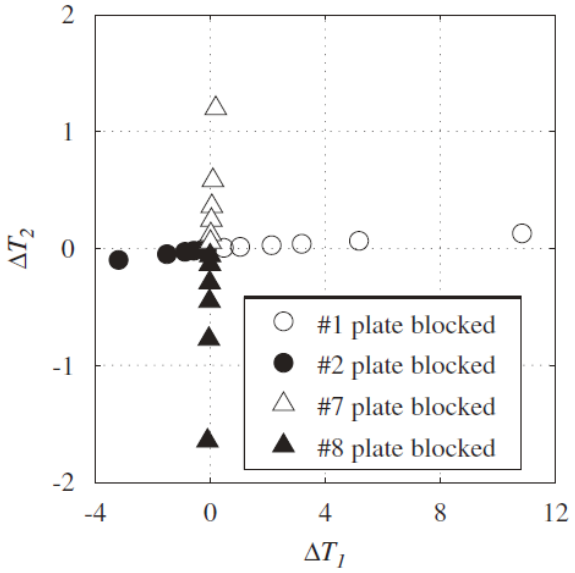

Fig. 5.4 Temperature differences under various blockage degrees and locations. Temperature sensors are set up every 10 plates.

DB-BDS can identify blockage location successfully for various blockage degrees because the ratio of two temperature differences remains unchanged even if blockage degree varies. To confirm this advantageous feature of DB-BDS, temperature differences under various blockage degrees and locations are plotted in **Fig. 5.4**. As expected, the plotted points, which correspond to various blockage degrees but the same blockage location, are on the same half line. The results confirm that the ratio of two temperature differences remains unchanged when blockage degree varies.

5.4.2 Simplified Model for MB-BDS

MB-BDS requires physical models of the process operated under a normal condition and under complete blockage in each plate. In this case study, models for MB-BDS are derived by simplifying the microreactor model described in Sec. 5.1. The characteristics of the simplified model are as follows:

(1) Each plate is compartmentalized into only six compartments as shown in **Fig. 5.5**.
(2) Temperature dependency of physical properties of reactant and coolant is ignored. The properties are constant.

The other settings are the same as the original ones described in Sec. 5.1. In the simplified model, each plate should be compartmentalized into at least two compartments in the flow direction to describe counter current flow. In this case study, each plate is compartmentalized into two compartments in the flow direction although cocurrent flow is investigated.

5.4.3 Results of MB-BDS

To build MB-BDS, temperature data under normal operating condition and under complete blockage are generated by using the simplified models. Temperature sensors are set up at regular intervals about every 1 to 10 plates. A part of diagnosis results is summarized in **Table 5.3**. The temperature sensors are set up at the 1st, 5th, 9th, 13th, 17th, and 21st (cover) plates when the interval is four, the 2nd, 8th, 14th, and 20th when the interval is six, and the 1st, 11th, and 21st when the interval is 10. The developed MB-BDS was able to identify the blockage location successfully in many cases, but several misdiagnoses occurred. In particular, MB-BDS could not identify the blocked plate when the 5th plate is blocked and the sensor interval is 10. Misdiagnosis tends to occur when the temperature sensor interval is six or more regardless of blockage degree. MB-BDS can diagnose correctly whether blockage occurs in reaction plates or cooling plates even when it misdiagnoses. In such cases, MB-BDS identifies the plate near the blocked plate. Therefore, the performance of blockage diagnosis can be improved if MB-BDS provides two or three candidates, including the most doubtful microdevice and its neighboring microdevices. Such modification is not essential from the theoretical viewpoint, but it might be useful from the practical viewpoint.

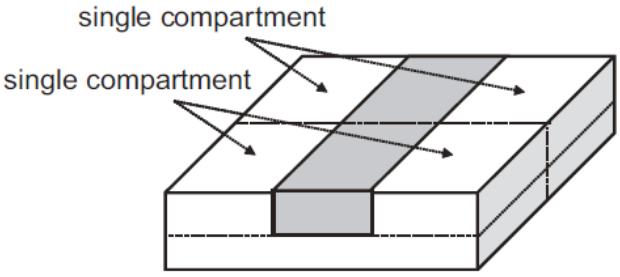

Fig. 5.5 Simplified compartment model of each plate for model-based blockage diagnosis system (MB-BDS).

Table 5.3 Diagnosis results of model-based blockage diagnosis system (MB-BDS)

Blockage location	Blockage degree (%)	Sensor interval			
		2	4	6	10
1	100	1	1	1	1
	70	1	1	1	1
	36	1	1	1	1
	9	1	1	1	1
2	100	2	2	2	2
	62	2	2	2	2
	30	2	2	2	2
	8	2	2	2	2
5	100	5	5	7	1
	69	5	5	7	1
	36	5	5	7	1
	9	5	5	7	1
6	100	6	6	8	6
	64	6	6	8	6
	32	6	6	8	6
	8	6	6	8	6
9	100	9	9	9	11
	69	9	9	9	11
	36	9	9	9	11
	9	9	9	9	11
10	100	10	10	10	10
	63	10	10	10	10
	32	10	10	10	10
	8	10	10	10	10

5.4.4 Discussion

The results show that the diagnosis performance of MB-BDS was worse than that of DB-BDS. However, this comparison is not fair, because it is assumed that the stacked microreactor consists of a sufficiently large number of plates and the influence of the top and the bottom plates on temperature distribution is neglected in DB-BDS while such an influence is taken into account in MB-BDS. It should be emphasized here that both systems are useful and a suitable system should be adopted on the basis of process characteristics. DB-BDS is preferable to MB-BDS when experiments can be performed to obtain operation data under blockage in each plate. On the other hand, MB-BDS is preferable to DB-BDS when experiments are not desired and a process model can be built.

Both DB-BDS and MB-BDS diagnose blockage on the basis of temperature data. Therefore, detectable changes in temperature are required for the success of the proposed diagnosis systems. Although the proposed diagnosis systems are shown to be effective through the case study and will be effective in many practical applications, they will not function well if temperature of a whole microdevice is ideally kept constant. Such an ideal situation may occur when the microdevice with high heat conductivity is soaked in a water/oil bath and the reaction heat is not significant. From this viewpoint, the proposed blockage diagnosis system can be applied to various types of stacked microprocesses, regardless of their plate design, material, and reaction, as long as temperature is affected by blockage.

5.5 Conclusions

Two types of diagnosis systems, a data-based blockage diagnosis system (DB-BDS) and a modelbased blockage diagnosis system (MB-BDS), were proposed. The performance of the proposed systems was evaluated with their applications to a stacked microreactor. DB-BDS and MB-BDS were applied to various types of blockage, i.e., various locations and degrees. The results showed that both DB-BDS and MB-BDS could diagnose the blockage location successfully even when blockage degree was less than 10%.

References

[1] T. Fujioka, O.Tonomura, M. Kano, M. Noda, S. Hasebe, “Development of micro chemical process simulator: design and operation of plate-fin microdevice,” 10th Asian Pacific Confederation of Chemical Engineering (APCChE), Kitakyushu, Japan (2004)

Chapter 6

Detection and Diagnosis of Blockage in Parallelized Microreactors

The split-and-recombine-type flow distributors (SRFDs) proposed by Tonomura et al. [1] are rigorously analyzed by using CFD simulation, and the SRFDs are re-designed to increase robustness to changes in operating conditions such as inlet flow velocity. In addition, a blockage detection and diagnosis system is developed. In the developed system, a small number of flow sensors are embedded in the SRFDs to isolate a blocked microreactor as early as possible from the parallelized microreactors. The effect of sensor location on blockage diagnosis is also investigated. Finally, the performance of blockage diagnosis by using the developed SRFD having two flow sensors is assessed through experiments.

6.1 Flow Distribution in Parallelized Microreactors

This section shows the basic structures and characteristics of micro chemical plants with parallelized microreactors. In addition, the characteristics of a specific flow distributor developed by Tonomura et al. [1] are rigorously analyzed through CFD simulations.

6.1.1 Split-and-recombine-type Flow Distributors (SRFDs)

The well-known strategy for increasing the production capacity of micro chemical plants is the parallelization of the optimally designed identical microreactors. A schematic diagram of a micro chemical plant with externally parallelized microreactors is shown in **Fig.6.1**. The

parallelized section where microreactors are running in parallel is connected to a distribution section and a confluence section. The distribution section carries out a function of distributing a reactant flow among the parallelized microreactors. The distributed flows pass through microreactors and are collected into one flow at the confluence section. A lack of uniformity in the flow distribution lowers the plant's performance.

Flow distributors, which are used at the distribution section in **Fig. 6.1**, are typically classified into two types: manifold-type and bifurcation-type. Unlike such flow distributors, Tonomura et al. [1] have developed SRFDs that have three or more bifurcation points and one or more junction points. **Figure 6.2** shows an example of SRFDs, in which one flow is divided into four flows. The SRFD consists of channels having a length of L [mm] and a width of d [mm]. It is assumed that $L_1 = L_4 = L$ and $L_2 = L_3 = a\ L$. a is introduced to achieve the uniform flow distribution among the parallelized microreactors under a normal operating condition and determined by CFD simulation. u_{in} [m/s] is the averaged flow velocity at the inlet, and u_k [m/s] (k is channel number) is the averaged flow velocity at the outlet of each channel. The outlet of SRFD is opened to atmosphere. In this research, the commercial CFD software "COMSOL Multiphysics® 3.4" is used to estimate the flow distribution of water (293 K) in the SRFD. The normalized flow velocity u_k*, which is given by u_k / u_{in}, is used to evaluate the flow distribution.

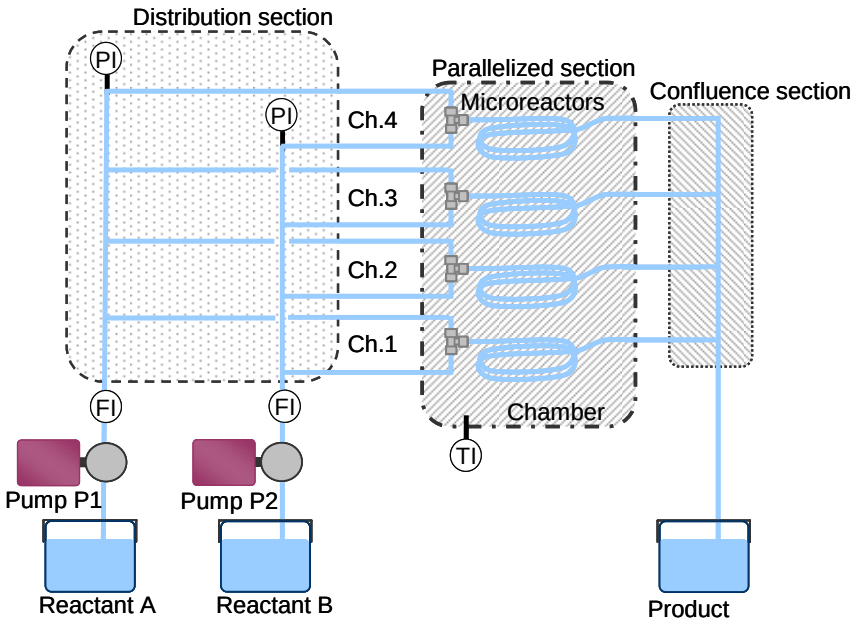

Fig. 6.1 Schematic diagram of micro chemical plants with parallelized microreactors

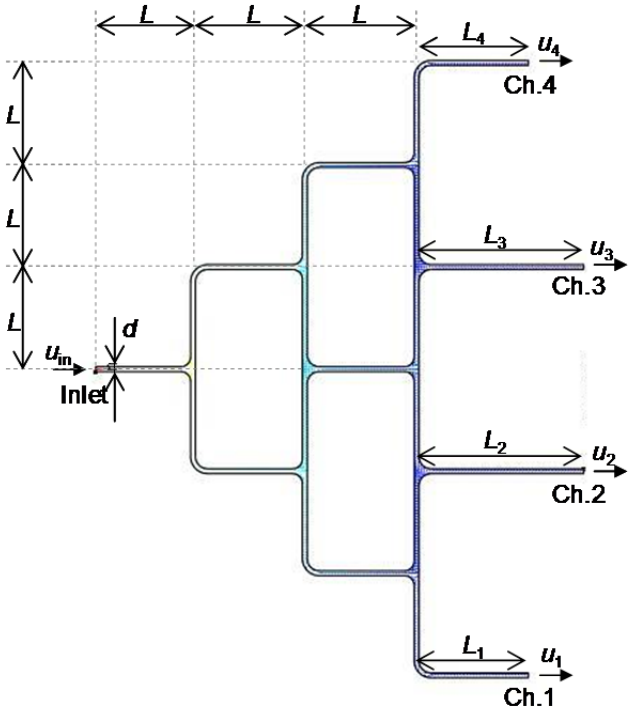

Fig. 6.2 Split-and-recombine-type flow distributors (SRFDs)

6.1.2 Effects of Design Parameters and Reynolds Number on Flow Distribution

It is preferable that the uniform flow distribution in the SRFD is maintained even when the inlet flow velocity or the material properties of the fluid change. In this section, L and d are selected as design parameters. **Table 6.1** shows the representative simulation conditions for SRFDs. When a circular channel having L = 10 mm and d = 1.0 mm is adopted, u_{in} = 0.2 m/s corresponds to inlet volumetric flowrate V_{in} = 10 mL/min. In this section, the effects of design parameters on the flow distribution are investigated by using CFD simulation. **Figure 6.3** shows the results of CFD simulation. L/d and Reynolds number, Re, are used as parameters to systematically investigate the flow distribution of the SRFD. Re is calculated from given information on channel diameter, flow velocity, density, and viscosity. In **Fig. 6.3**, the vertical axis denotes the differences between two normalized flow velocities, u_2* and u_1*, and the flow distribution is highly uniform when each plotted point on **Fig. 6.3** is located near zero. The uniform flow distribution is achieved independently of L/d, when Re is less than 100. At higher Re, the difference in flow velocity between Ch. 2 and Ch. 1 becomes large. In such a case, the SRFD needs to be re-designed so as to realize the uniform flow distribution. The alternative approach is to use flow controllers. However, the installation of flow controllers in all the channels requires high cost and extra space.

Table 6.1 Representative simulation conditions for SRFDs

L/d	L [mm]	d [mm]	a	u_{in} [m/s]	Re
5	10	2.0	1.80	0.05	100
10	10	1.0	1.75	0.2	200
20	10	0.5	1.78	0.8	400
40	40	1.0	1.67	0.2	200

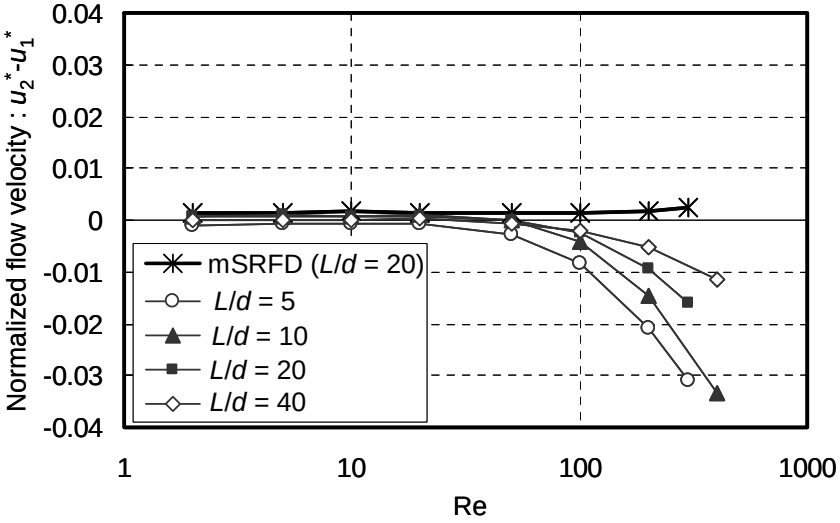

Fig. 6.3 CFD simulation results: Effects of Re and L/d on flow distribution.

6.1.3 Design Modification of SRFD

Figure 6.3 indicates that the difference between u_2* and u_1* is reduced at higher Re, according as L/d becomes large. An increase in L/d usually leads to a larger pressure drop of flow in the SRFD (ΔP_{SRFD}). To further improve the uniformity in the flow velocities without increasing ΔP_{SRFD}, the modified SRFD (mSRFD) where the channel width of Ch. 0 is enlarged, as shown in **Fig. 6.4**, is proposed in this research. CFD simulation result of mSRFD (L/d = 20) is added to **Fig. 6.3**, and it is clarified that mSRFD gives a more uniform flow distribution in the wide range of Re.

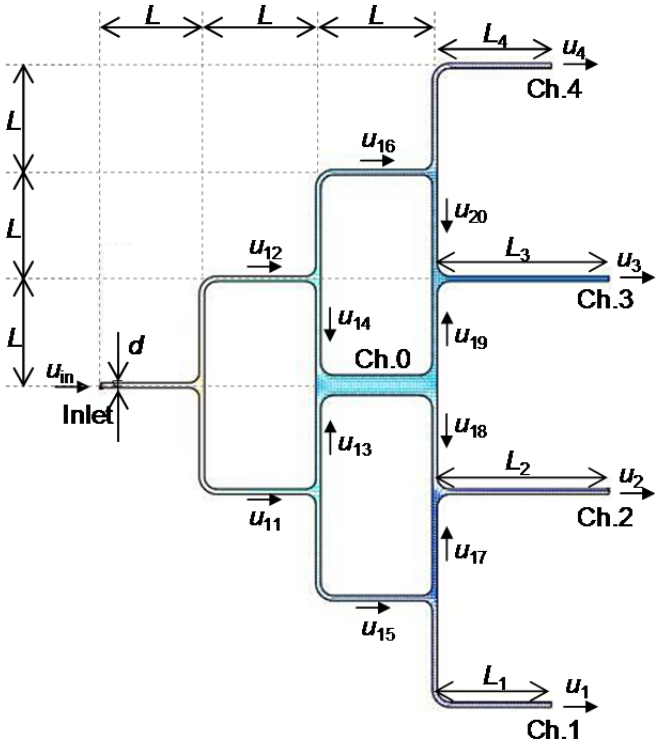

Fig. 6.4 Modified split-and-recombine-type flow distributor (mSRFD)

6.2 Detection and Diagnosis of Blockage

Blockage is the most recognized problem in MCPs, because the diameter of microchannels is less than 1 mm. A process monitoring system that can detect and diagnose blockage is indispensable for effective and stable operation of MCPs. In this research, just two flow sensors are embedded in mSRFDs, and a blockage diagnosis system (BDS) is developed to identify a blocked microreactor among the parallelized microreactors.

6.2.1 Concept of Blockage Diagnosis System

Reactants are supplied to micro chemical plants at a constant flowrate. Micro chemical plants have a symmetric structure and are designed beforehand so that flow distribution is uniform. Under these assumptions, the developed BDS uses the ratios of flow velocity (or flowrate) differences between normal and abnormal operating conditions at one sensor to those at the other sensor. In this work, to simplify the problem, two sensors are symmetrically located in SRFDs or mSRFDs. The procedure for building BDS is as follows: 1) Obtain flow velocity data

under normal operating conditions through CFD simulation, 2) Obtain flow velocity data under blockage in each microreactor through CFD simulation, 3) Calculate the flow velocity difference between normal and abnormal operating conditions at two sensors, and 4) Calculate the ratio of flow velocity differences. Sensor location is determined so as not to deteriorate the performance of BDS even when the fluid properties and the microreactor characteristics change. After blockage is detected, the blockage location is identified through the following procedure: 1) Calculate the flow velocity difference between normal and abnormal operating conditions at two sensors, 2) Calculate the ratio of flow velocity differences, and 3) Identify the microreactor that has the smallest difference between the prepared ratio and the actual ratio as a blocked reactor. The performance of the developed system is evaluated with its application to four parallelized microreactors in the following section.

6.2.2 Application to Four Parallelized Microreactors

The developed BDS is applied to blockage diagnosis problems of the four parallelized microreactors, which are connected to mSRFD described in Sec. 6.1. Through the system development, the results of flow velocity measurements are plotted in the two-dimensional Δu_{15} and Δu_{16} space (**Fig. 6.5** (a)) and Δu_{17} and Δu_{20} space (**Fig. 6.5** (b)). In both figures, ΔP_{MR} and $\Delta P_{\mathrm{mSRFD}}$ represents the pressure drop of microreactors and mSRFD, respectively. The ratios of flow velocity differences under the blockage in microreactor connected to Ch.i (i = 1, 2, 3, 4) correspond to square, diamond, triangle, and circle, respectively. As each point deviates from the origin, the total flowrate in the process becomes large. **Figure 6.5** shows that the ratio of two flow velocity differences remains unchanged even when total flow rate of the process varies, without reference to ΔP_{MR}. In addition, it is clarified that the blockage location is successfully identified on the basis of the ratios of two flow velocity differences. These simulation results suggest that the developed BDS has robustness to changes in the total flowrate and ΔP_{MR}.

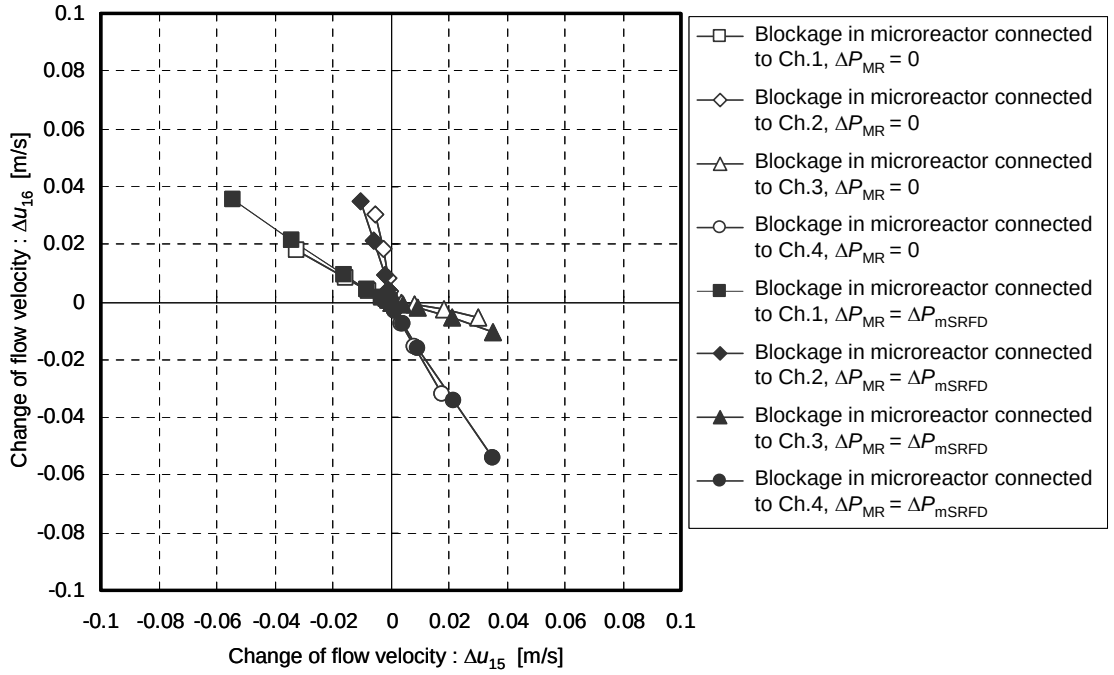

(a) Flow sensors are located at u_{15} and u_{16}, as shown in **Fig. 6.4**.

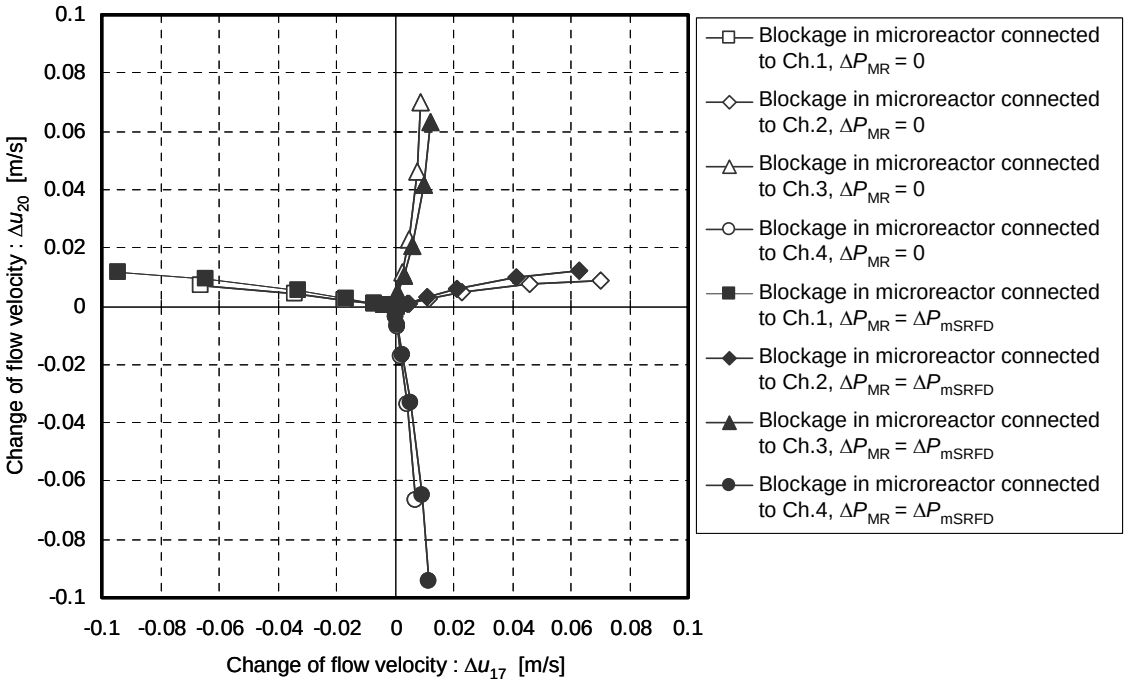

(b) Flow sensors are located at u_{17} and u_{20}, as shown in **Fig. 6.4**.

Fig. 6.5 Blockage diagnosis results of mSRFD (CFD simulation)

6.3 Experimental Validation

In this section, the effectiveness of the developed BDS is assessed through experiment.

6.3.1 Measurement of Pressure Drop in Flow Sensors

Before applying the developed BDS to an experimental setup of micro chemical plant having SRFDs and parallelized microreactors, the performance of flow sensors is evaluated. The mass flowmeters (MFMs) for liquids produced by Horiba STEC Co. (LF series) are used as the flow sensors. When MFMs are embedded in SRFDs, the pressure drop of MFMs influences the pressure distribution over the SRFDs. Therefore, the pressure drop of MFMs is measured for various flowrates. **Figure 6.6** shows an experimental setup for measuring the pressure drop of MFM. Water (293 K) is fed into MFM by using a syringe pump (Harvard PHD2000 series), and the pressure drop of MFM is measured by two pressure sensors (Yokogawa Electric Co. FP101 series). A Scope Coder (Yokogawa Electric Co. DL750) is used to acquire the measurement signals. Inlet flowrate is varied from 0 mL/min to 4 mL/min to examine the relationship between flowrate and pressure drop of MFM. As seen in **Fig. 6.7**, the pressure drop of MFM is proportional to flowrate. The experimental results show that the pressure drop of MFM is equivalent to that of the circular tube with 0.8 mm in inner diameter and 120 mm in length. Therefore, in this research, an SRFD is built with Teflon® tubes with 0.8 mm in inner diameter and 120 mm in length, as shown in **Fig. 6.8**.

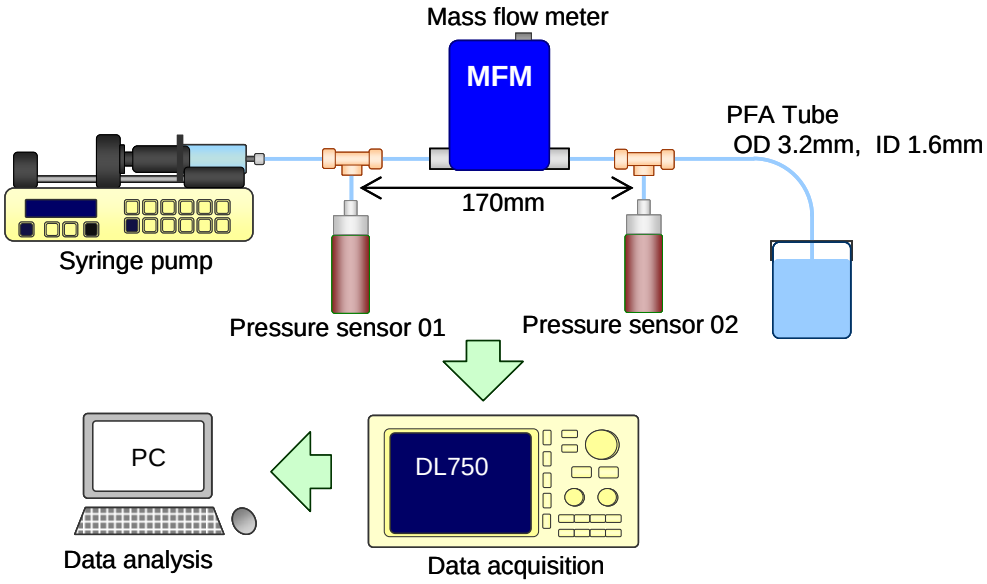

Fig. 6.6 Experimental setup for measuring the pressure drop of mass flowmeter

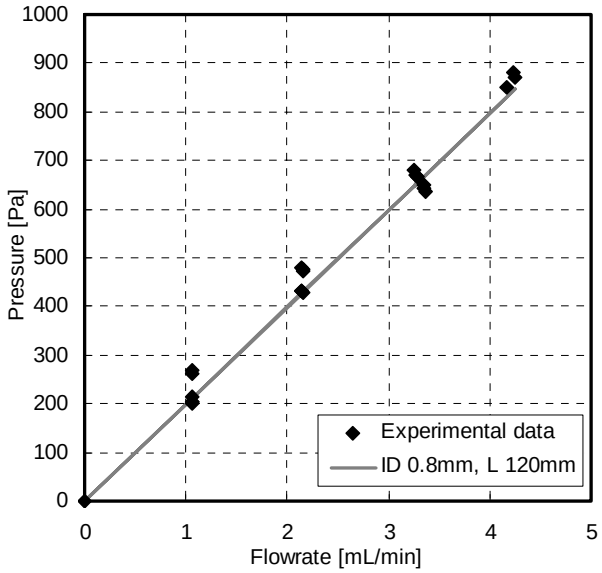

Fig. 6.7 Experimental results: Pressure drop of mass flowmeter for various flowrates

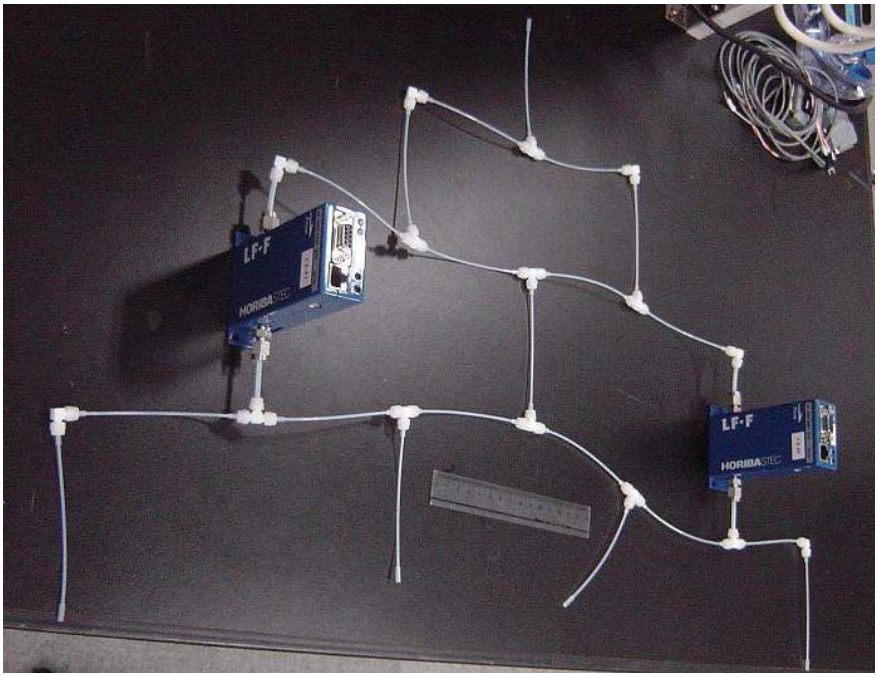

Fig. 6.8 SRFD having two mass flowmeters

6.3.2 Application to Experimental Setup of Micro Chemical Plant

Figure 6.9 shows an experimental setup of micro chemical plant with numbering-up structure. MFMs are installed into SRFD to measure the flowrates of V_{15} and V_{16}. L/d of SRFD is 150 (=120 mm / 0.8 mm) on the basis of Sec. 6.3.1. A gear pump (HNP Mikrosysteme mzr-2905) is used to feed water (293 K) continuously. A pressure sensor (Yokogawa Electric Co. FP101 series) is attached to the inlet of SRFD. MFMs mentioned in Sec. 6.3.1 are installed in the parallelized section as well as the distribution section in micro chemical plant. The Scope Coder (Yokogawa Electric Co. DL750) is used to acquire each measurement signal. In addition, the blockage in microreactors is artificially realized by closing the valves. The performance of blockage diagnosis is evaluated for all the combination of V_{in} = 5.4 mL/min and 7.2 mL/min and ΔP_{MR} = 2 x ΔP_{SRFD}, 6 x ΔP_{SRFD}, 15 x ΔP_{SRFD}, and 30 x ΔP_{SRFD}. The experimental results are plotted in the two-dimensional ΔV_{15} and ΔV_{16} space (**Fig. 6.10** (a)). In addition, the flowrates of V_1 and V_4, which have been used in our work [1], are measured and the results are plotted in ΔV_1 and ΔV_4 space (**Fig. 6.10** (b)). As seen in **Fig. 6.10** (b), it is clear that when ΔP_{MR} becomes large, it is more difficult to distinguish between the blockage in microreactors connected to Ch.2 and Ch.3. On the other hand, as seen in **Fig. 6.10** (a), the developed BDS makes it possible to successfully identify the blocked microreactor even when ΔP_{MR} becomes large and the inlet flowrate of SRFD varies.

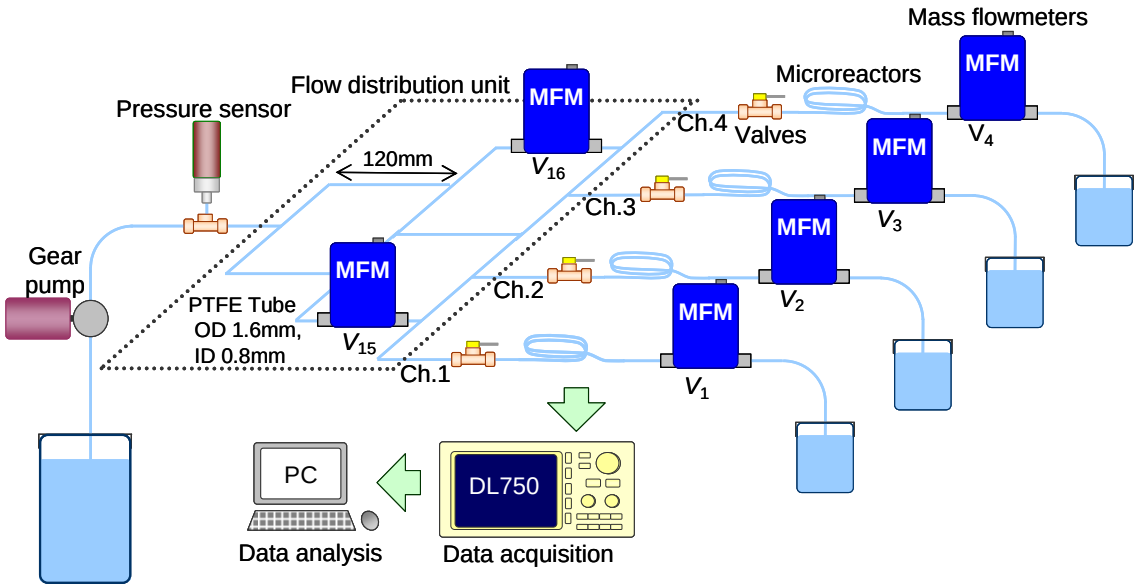

Fig. 6.9 Experimental setup of MCP with four parallelized microreactors

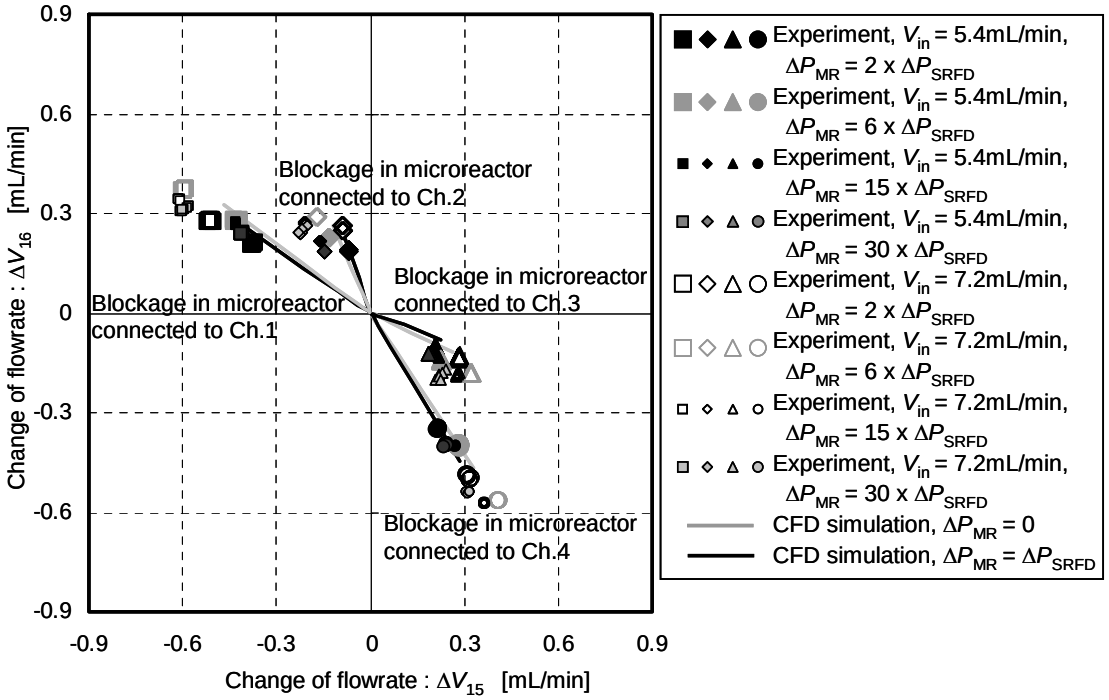

(a) Flowrates V_{15} and V_{16} are measured, as shown in **Fig. 6.9**.

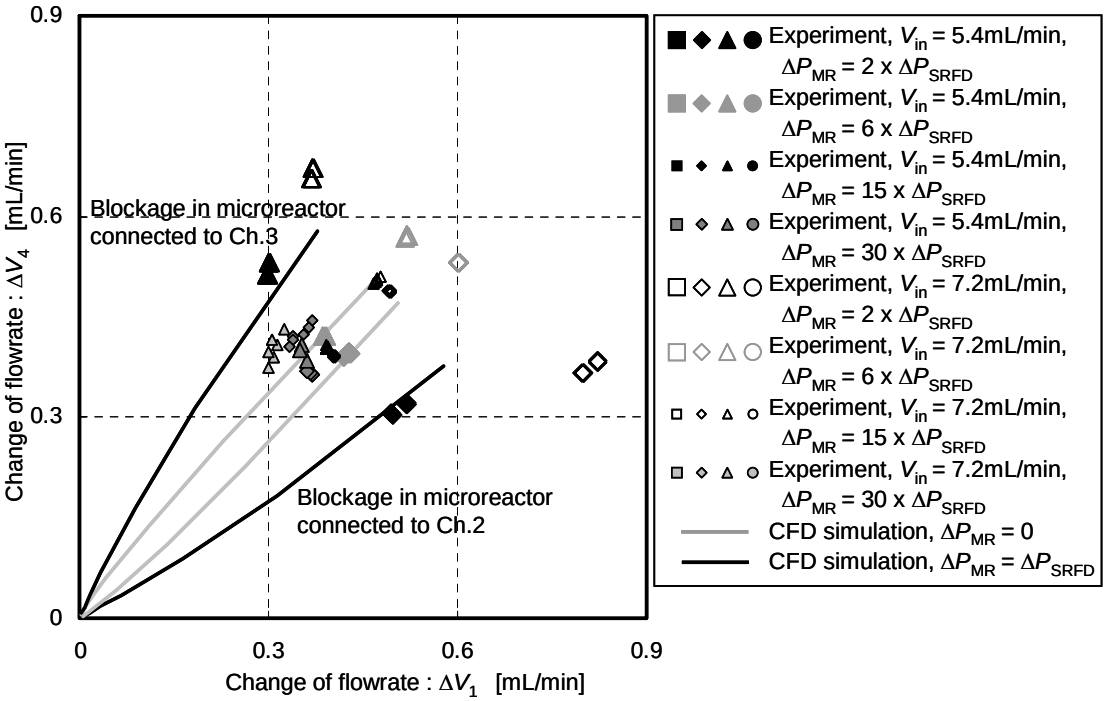

(b) Flowrates V_1 and V_4 are measured, as shown in **Fig. 6.9**.

Fig. 6.10 Blockage diagnosis results of SRFD (Experiment and CFD simulation)

6.4 Conclusions

The flow uniformity in SRFDs, which have three or more bifurcation points and one or more junction points, was examined through CFD simulation, and the design of SRFDs is modified to achieve a uniform flow distribution in the wide range of Re. In addition, the blockage detection and diagnosis system that can identify a blocked microreactor by using a small number of flow sensors was developed, and its effectiveness was demonstrated numerically and experimentally. The results showed that the developed system has high robustness to changes in the fluid properties and the microreactor characteristics such as pressure drop. The developed system will be applicable to various types of micro chemical plants with parallelized microreactors.

References

[1] O. Tonomura, S. Nagahara, M. Kano, S. Hasebe, Fluid distribution and blockage diagnosis in parallel microchannel configurations, Proceedings of 10th International Conference on Microreaction Technology (IMRET) / AIChE Spring National Meeting, New Orleans, US (2008) 128d.

Chapter 7

Blockage Detection and Stable Operation of Parallelized Microreactors

When the production capacity of micro chemical plants is increased by numbering-up approach, it is important to realize the uniform flow distribution among the parallelized microreactors. In addition, a blocked microreactor needs to be identified as early as possible to achieve the stable long-term operation of micro chemical plants. In Chapter 4, the pressure drop control method was developed to keep uniform flow distribution among the parallelized microreactors even when blockage occurs. In Chapter 6, the blockage detection and diagnosis system was developed to identify a blocked microreactor by using two flow sensors and SRFD. In this chapter, two methods developed in Chapters 4 and 6 are combined to keep continuous operation of a plant without shutdown until it is returned to normal condition after detecting a blocked microreactor. In addition, the performance of the developed system is maximized by adjusting the channel size and sensor placement in the flow distributors. The effectiveness of the developed system and the optimal design result is demonstrated through simulation and experiment.

7.1 Developed Method for Monitoring and Control

In the blockage detection system explained in Chapter 6, two flow sensors are embedded in SRFDs and is used to identify a blocked microreactor among the parallelized microreactors. In addition, as explained in Chapter 4, the pressure drop control method can achieve the uniform flow distribution even when blockage occurs. Therefore, a combination of the pressure drop

control method and the blockage detection method holds the possibility of continuous operation as shown in **Fig. 7.1**. If a blocked device is identified, the production in the blocked device is stopped. And then, the blocked device is replaced with a new device. During this replacement of the blocked device, the pressure drop control method can keep the flow rates of unblocked devices constant at the normal level. To minimize the influence of the blockage on the productivity of micro chemical plants, a blocked device needs to be identified as early as possible.

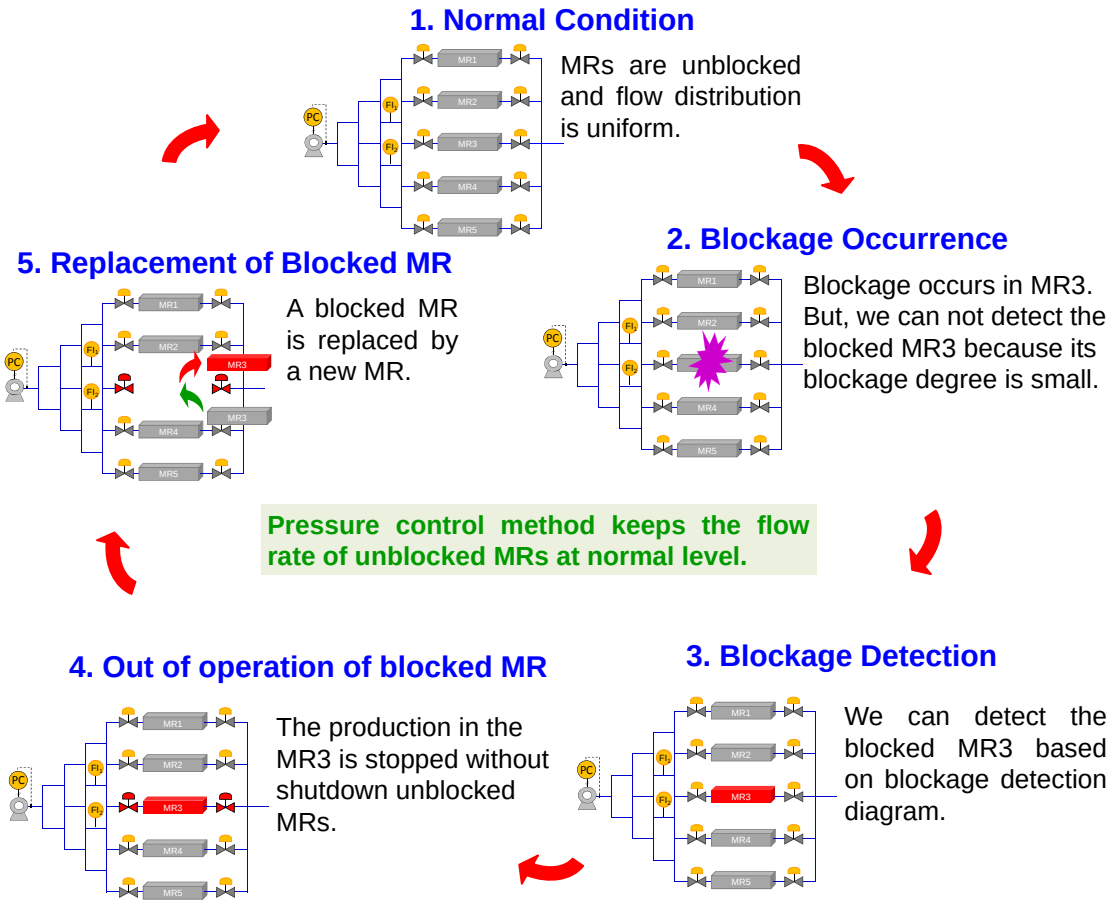

Fig. 7.1 Continuous operation policy (MR stands for microreactor)

7.2 Case Study: Five Parallelized Microreactors

The proposed blockage diagnosis performance depends on the channel design of SRFD and sensor placement. Therefore, in this section, an optimal design problem of SRFD with five

parallelized micoreactors is investigated. The objective of this problem is to maximize the blockage diagnosis performance by adjusting channel sizes and sensor placement.

7.2.1 Design Problem Formulation

Flow distribution in micro chemical plants with/without blockage can be estimated by CFD model or compartment model [1]. In this research, an optimal channel design and sensor placement problem is solved on the basis of compartment model, which requires less computational time than CFD model. The compartment model is explained in Chapter 3.

Five parallelized microreactors connected to SRFD is shown in **Fig. 7.2**. Its design condition and assumption are summarized in **Table 7.1**. In the problem formulation, the channel resistance and sensor placement in SRFD are determined to maximize the adjacent angles between lines in the diagram used for blockage diagnosis, as shown in **Fig. 7.3**, within constraints on the total flowrate, the flow uniformity under normal and abnormal operating conditions, the number of available sensors, the number of parallelized microreactors and their pressure drop, and the channel resistance boundaries.

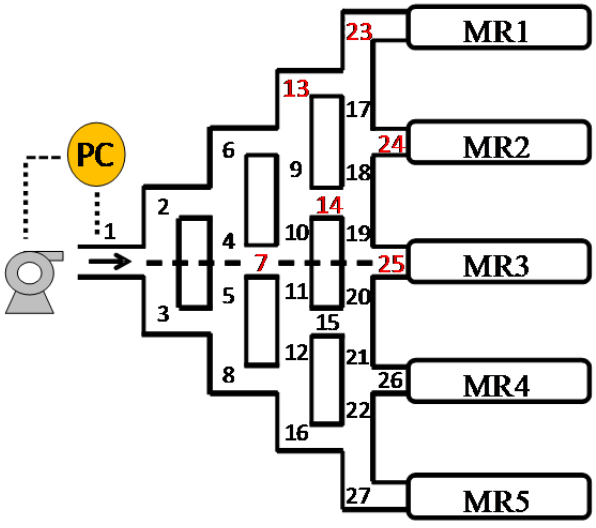

Fig. 7.2 Five parallelized microreactors connected to SRFD

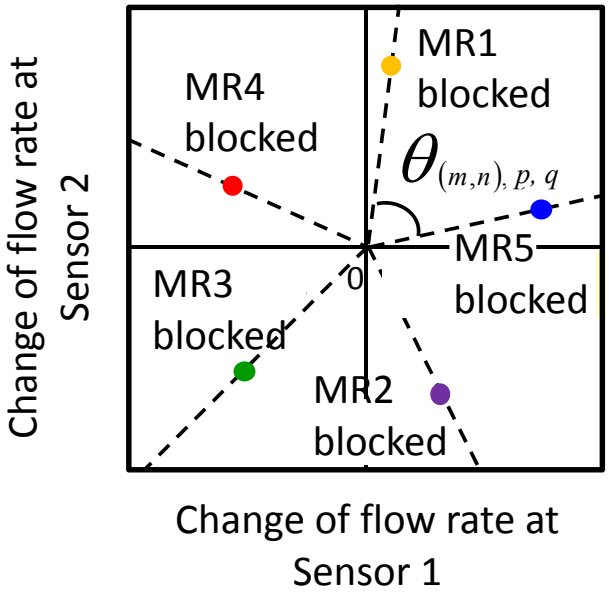

Fig. 7.3 Blockage diagnosis diagram

Table 7.1 Design condition and assumption

Design variables	Resistance of Ch. 7, 13. 14, 23, 24, 25 Sensor allocation in SRFD	
Design Conditions	The number of parallelized microreactors	5
	Flowrate of each microreactor at normal condition, V_0 [mm^3/s]	50
	Channel resistance of normal microreactor, R_M [mm^{-3}]	1000
	Fluid viscosity, μ [Pa s]	1.0×10^{-3}
	Fixed channel resistance, R_o [Pa s mm^{-3}]	52
	Flow uniformity at normal condition, f_U [mm^3/s]	1.0×10^{-3}
	Flow uniformity at abnormal condition, F_U [mm^3/s]	1.5
	Lower & upper boundaries of design variables, r_L, r_U [Pa s mm^{-3}]	[1, 1000]
	Minimum detectable flowrate, VF_L [mm^3/s]	0.5
Assumptions	Fully-developed laminar flow at inlet of SRFD Open to atmosphere at exit of every microreactor Channel resistance of a blocked microreactor equal to $R_M \times 2$ No multiple blockage No resistance of flow sensors	

The formulation of this design problem is shown as follows:

$$\min_{\boldsymbol{r},(m,n)} \max_{p_1,p_2} \cos\theta_{(m,n),p_1,p_2} \tag{7.1}$$

s.t.

$$\sum_{\mathrm{i}=23}^{27} \left|V_0 - v_{i,0}\right| \leq f_{\mathrm{U}} \tag{7.2}$$

$$\sum_{\substack{i,j=1 \\ i\neq j}}^{5} \left|V_0 - \mathrm{v}_{i+22,j}\right| \leq F_U \tag{7.3}$$

$$r_{\mathrm{L}} \leq r_i \leq r_{\mathrm{U}} \tag{7.4}$$

$$\left|\boldsymbol{VF}_{(m,n),p_1}\right| \geq VF_{\mathrm{L}} \tag{7.5}$$

$$\Delta P_{tot} = const \tag{7.6}$$

$$\boldsymbol{g} = \mathbf{0} \tag{7.7}$$

where

$\boldsymbol{r}$	: Channel resistance vector	[Pa s mm^{-3}]
r_i	: Channel resistance of Ch.*i*	[Pa s mm^{-3}]
$\cos\theta_{(m,n),p,q}$	: Adjacent angles between lines in the blockage diagnosis diagram (sensor location : *m*, *n* ; blockage scenario : *p, q*)	[-]
V_0	: Inlet flowrate at each microreactor	[mm^3 s^{-1}]
$v_{i,j}$	: Flowrate in Ch. *i* under scenario *j*	[mm^3 s^{-1}]
f_{U}	: Allowable flow uniformity under normal condition	[mm^3 s^{-1}]
$\sigma_{i,j+22}$	: $\sigma = 1$ for $i = j + 22$, $\sigma = 0$ for $i \neq j + 22$	[-]
F_{U}	: Allowable flow uniformity under abnormal condition	[mm^3 s^{-1}]
r_{L}, r_{U}	: Upper and lower boundaries of channel resistance	[Pa s mm^{-3}]
$\boldsymbol{VF}_{(m,n),p}$	: Flowrate change at Ch. *m* and *n* under blockage scenario *p*	[mm^3 s^{-1}]
VF_{L}	: Detectable minimum flowrate	[mm^3 s^{-1}]
$\boldsymbol{g}$	: Mass and pressure balance	[-]
ΔP_{tot}	: Total pressure drop	[Pa]

Objective function of Eq. (7.1) is to maximize the minimum of a set of angles shown in **Fig. 7.3**. Equation (7.1) is expressed as follows:

$$\cos\theta_{(m,n)p_1,p_2} = \frac{\boldsymbol{VF}_{(m,n)p_1} \cdot \boldsymbol{VF}_{(m,n)p_2}}{|\boldsymbol{VF}_{(m,n)p_1}||\boldsymbol{VF}_{(m,n)p_2}|} \tag{7.8}$$

$$\boldsymbol{VF}_{(m,n)p_1} = \begin{pmatrix} v_{m,p_1} - v_{m,0} \\ v_{n,p_1} - v_{n,0} \end{pmatrix} \tag{7.9}$$

7.2.2 Numerical and Experimental Results

Through the optimization, the obtained numerical results are as follows: **Table 7.2** shows the design results of channel resistances. **Table 7.3** shows the flowrates of the whole process and every microreactor under individual blockage scenario. **Tables 7.4** to **7.8** shows the flowrates of microreactors under individual blockage scenario when total flow control and pressure drop control methods are applied to the process. In addition, **Fig 7.4** shows the result of blockage diagnosis in this numerical case study.

Table 7.3 shows that the uniform flow distribution is realized under normal condition, and **Fig. 7.4** illustrates that the successful diagnosis of each blocked microreactor can be achieved. In addition, as shown in **Tables 7.4** to **7.8**, it is clarified that during this replacement of the blocked device, the pressure drop control method can keep the flow rates of unblocked devices constant at the normal level.

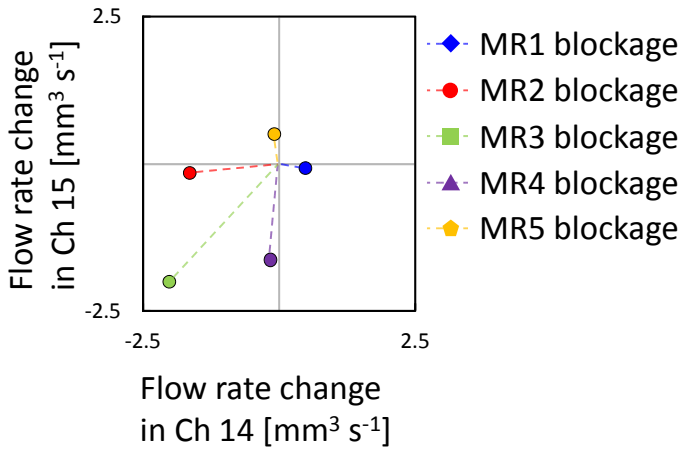

Fig. 7.4 Numerical result of blockage diagnosis

Table 7.2 Design results of channel resistances [Pa s mm^{-3}]

Ch 7	Ch 13	Ch 14	Ch 23	Ch 24	Ch 25
1000	1.80	1.00	302	261	246

Table 7.3 Flowrates under each blockage scenario [mm^3 s^{-1}]

Blokage scenario	Total flowrate	Flowrate				
		MR1	MR2	MR3	MR4	MR5
#0 (normal)	250.0	50.0	50.0	50.0	50.0	50.0
#1 (MR 1 blockage)	245.2	43.8	50.4	50.4	50.3	50.3
#2 (MR 2 blockage)	244.8	50.4	43.4	50.4	50.3	50.3
#3 (MR 3 blockage)	245.2	50.4	50.4	43.6	50.4	50.4
#4 (MR 4 blockage)	244.8	50.3	50.3	50.4	43.4	50.4
#5 (MR 5 blockage)	245.2	50.3	50.3	50.4	50.4	43.8

Table 7.4 Inlet flowrates of microreactors by different flow control methods under blockage scenario #1 (MR1 is blocked) [mm^3 s^{-1}]

Control method	MR1	MR2	MR3	MR4	MR5
Pressure drop control	43.8	50.4	50.4	50.3	50.3
Total flow control	43.7	51.8	51.6	51.5	51.4

Table 7.5 Inlet flowrates of microreactors by different flow control methods under blockage scenario #2 (MR2 is blocked) [$mm^3 s^{-1}$]

Control method	MR1	MR2	MR3	MR4	MR5
Pressure drop control	50.4	43.7	50.4	50.3	50.3
Total flow control	51.8	43.6	51.6	51.5	51.5

Table 7.6 Inlet flowrates of microreactors by different flow control methods under blockage scenario #3 (MR3 is blocked) [$mm^3 s^{-1}$]

Control method	MR1	MR2	MR3	MR4	MR5
Pressure drop control	50.4	50.4	43.6	50.4	50.4
Total flow control	51.6	51.6	43.6	51.6	51.6

Table 7.7 Inlet flowrates of microreactors by different flow control methods under blockage scenario #4 (MR4 is blocked) [$mm^3 s^{-1}$]

Control method	MR1	MR2	MR3	MR4	MR5
Pressure drop control	50.3	50.3	50.4	43.7	50.4
Total flow control	51.5	51.5	51.6	43.6	51.8

Table 7.8 Inlet flowrates of microreactors by different flow control methods under blockage scenario #5 (MR5 is blocked) [$mm^3 s^{-1}$]

Control method	MR1	MR2	MR3	MR4	MR5
Pressure drop control	50.3	50.3	50.4	50.4	43.8
Total flow control	51.4	51.5	51.6	51.8	43.7

In order to validate the effectiveness of numerical design results, an experimental system was developed as show in **Fig. 7.5** (left). Stainless steel tubes are used to construct SRFD and their dimensions are summarized in **Fig. 7.5** (right) and **Table 7.9**. The other experimental apparatus are shown in **Table 7.10**. Water (298 K) is continuously supplied to five parallelized microreactors by using a plunger pump and are distributed to reactors through SRFD. The outlets of this process are opened to atmosphere. Flow sensors are installed at Ch. 14 and 15 in **Fig. 7.2**. A valve is closed in each line to artificially realize blockage in a microreactor.

As shown in **Fig. 7.6**, it is shown that the experimental results are in good agreement with simulation results in terms of the blockage diagnosis. The usefulness of the developed method was confirmed through this experiment.

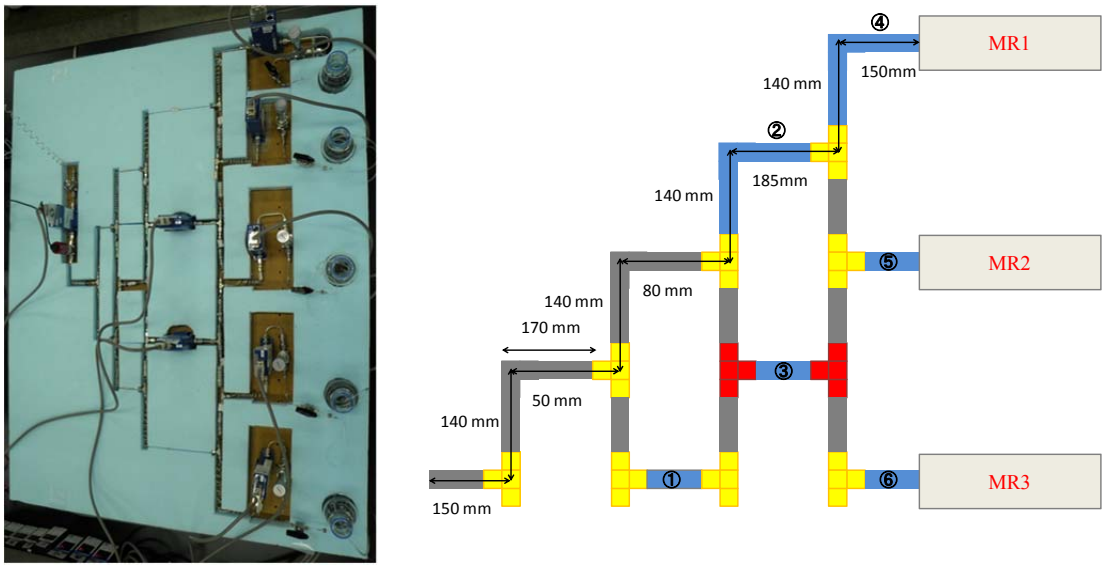

Fig. 7.5 Experimental system (left) and constructed SRFD (right)

Table 7.9 Channel diameter and length of SRFD (Channel number corresponds to **Fig. 7.5**.)

Channel number	Inner diameter [mm]	Length [mm]
①	0.1	29.5
②	1.0	530.1
③	1.0	294.5
④	0.3	462.8
⑤	0.3	498.6
⑥	0.3	596.4
Others	0.5	957.2

Table 7.10 Experimental apparatus

Name	Manufacture	Model number
Pump	Uniflows	uf-3000B2
Flow sensor	HORIBA STEC	LF-40, LF-50
Pressure sensor	KEYENCE / YOKOGAWA	APV80 / FP101-E31-L20A
Valves	Swagelock	ss-4BMG
Electronic scale	A&D Company	FX-1200i

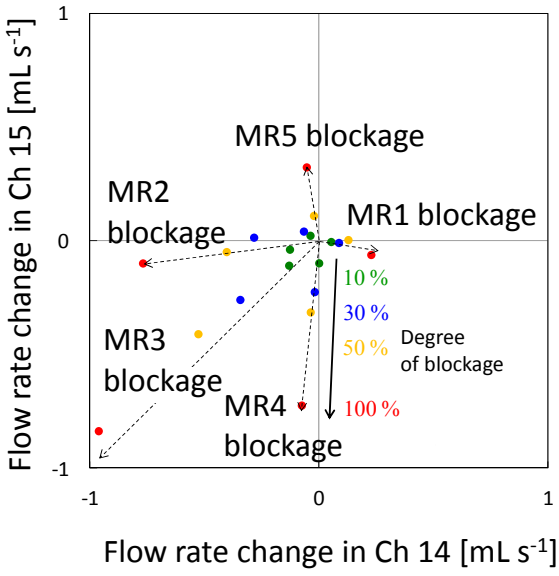

Fig. 7.6 Blockage diagnosis results: simulation (dashed line) vs. experiment (closed circle)

7.3 Conclusions

In Chapter 6, the method that can diagnose a blocked microreactor by using the split-and-recombine-type flow distributor and just two flow sensors was developed, and the pressure drop control method, in Chapter 4, was also developed to keep the flow rates of unblocked microreactors constant at the normal level even when blockage occurs. In this research, both methods were combined to achieve continuous operation of micro chemical plants while the blocked microreactor is identified and replaced by a new one. An optimal design problem was formulated to maximize the blockage diagnosis performance by adjusting the channel resistance/size of the flow distributor as well as sensor location. The usefulness of the optimally designed flow distributor and the proposed continuous operation was demonstrated through numerical and experimental case studies on a plant having five parallelized microreactors.

References

[1] C. Amador, A. Gavriilidis, P. Angeli, “Flow distribution in different microreactor scale-out geometries and the effect of manufacturing tolerances and channel blockage,” Chemical Engineering Journal, **101**, 379-390 (2004)

Conclusions and Final Remarks

Future chemical production is determined by globalized, volatile markets with increased quality demand for fine and specialty products. The increasing product variety also needs more flexible production plants which can produce small amounts for laboratory as well as market supply up to several hundred tons per year. Micro chemical process technology promises breakthrough technology in such areas. In this thesis, it can be concluded that the developed methods are well suited to carry out shape design and stable operation of microreactors. Coming back to the requirements regarding the method described in the Introduction, the following can be concluded:

Part I. Shape design of microreactors

A plate-fin microreactor is one of the dominant devices to be used in a micro chemical plant. In this microreactor, the flow uniformity in branched channels is very important to realize the sharp residence time distribution. Flow distribution is strongly affected by shape of device. Therefore, in Chapter 1, effects of the design on the flow uniformity were discussed by using CFD simulation. In addition, it was demonstrated that the magnification of outlet manifold area makes the flow distribution uniform. However, the extension of the outlet manifold increases dead volume inside the microreactor, broadens residence time distribution, and makes space time long. Therefore, shape optimization problem to make space time small was solved under the constraint on flow uniformity. The result clarified that a plate-fin microreactor with optimal manifold shape can achieve uniform flow distribution while realizing minimum space time. To derive optimal shape automatically, a new optimization system was developed by integration the model and mesh generator with the CFD simulator.

Recently, the adjoint variable method, which enables us to obtain gradients in a more

expeditious manner, has been focused on. In Chapter 2, an automatic shape optimization system based on the adjoint variable method was developed by using C language on a Windows platform. Since the pressure drop in microchannels is an important characteristic related to the energy demand for process optimization, the developed system was applied to the pressure drop minimization problems of U-shaped and branched microchannels. It was demonstrated by representative examples that the adjoint variable method can be used to formulate computationally feasible procedures for the shape design of pressure-driven microchannels. The computational time of each design cycle is of the same order as two flow solutions, since the adjoint equation is of comparable complexity to the flow equation. The developed system is quite general and is not limited to particular choice of cost function. Our future work will focus on the extension of the developed system to shape optimization problems of thermo-fluidic microreactors.

In Chapter 3, the thermo-fluid design approach was applied to the optimal design problem of a microreactor with uniform temperature and residence time distributions. In most of the conventional design approaches, the cross-sectional area of each microchannel is assumed to be constant, and the channel design under that condition sometimes causes an unnecessary increase of pressure drop. In the design strategy, the fluid temperature along the microchannel was equalized by changing channel width, that is, the fluid residence time is controlled. In addition, the optimally designed manifold shape ensured the same residence time in all parallel microchannels and avoided deterioration in the reactor performance. The thermo-fluid compartment model is a very simple but powerful tool to shorten the computational time of microreactor design.

Part II. Operation of microreactors

When the scale of chemical processes is increased from the scale of the laboratory flask to the scale of industrial production, the numbering-up approach is basically adopted. In microreactors with numbering-up structure, fouling and clogging decrease the flow rates, increase the pressure drop, lead to maldistribution of flow, or even block the entire reactor.

In Chapter 4, two operation policies, total flow control and pressure drop control, were compared, and the simulation result showed that the pressure drop control is effective to keep uniform flow distribution among the parallelized microreactors even when blockage occurs. In addition, two control structures based on pressure drop control, pumping pressure control and pressure drop control over the parallelized section, were investigated experimentally. The

former control structure is simple. However, this structure functions only when the ratio of pressure drop over the parallelized section to that over the residence time section, $\Delta P_a/\Delta P_b$, is large. On the other hand, the latter control structure can make the flow distribution uniform for any $\Delta P_a/\Delta P_b$.

The proposed pressure drop control over the parallelized section was demonstrated to be highly effective for the operation of micro chemical plants with external numbering-up structure. However, in addition to the control method, it is necessary to develop an effective monitoring method that can detect and diagnose abnormal conditions such as blockage. Therefore, the following chapters described the monitoring method for blockage.

In Chapter 5, two types of diagnosis systems, a data-based blockage diagnosis system (DB-BDS) and a modelbased blockage diagnosis system (MB-BDS), were proposed. The performance of the proposed systems was evaluated with their applications to a stacked microreactor. DB-BDS and MB-BDS were applied to various types of blockage, i.e., various locations and degrees. The results showed that both DB-BDS and MB-BDS could diagnose the blockage location successfully even when blockage degree was less than 10%.

In Chapter 6, the flow uniformity in SRFDs, which have three or more bifurcation points and one or more junction points, was examined through CFD simulation, and the design of SRFDs was modified to achieve a uniform flow distribution in the wide range of Re. In addition, the blockage detection and diagnosis system that can identify a blocked microreactor by using a small number of flow sensors was developed, and its effectiveness was demonstrated numerically and experimentally. The results showed that the developed system has high robustness to changes in the fluid properties and the microreactor characteristics such as pressure drop.

In Chapter 7, two methods developed in Chapters 4 and 6 were combined to keep continuous operation of a plant without shutdown until it is returned to normal condition after detecting a blocked microreactor. In addition, the performance of the developed system was maximized by adjusting the channel size and sensor placement in the flow distributors. The effectiveness of the developed system and the optimal design result was demonstrated through simulation and experiment.

Chemical process engineering covers not only the design and implementation of process routes into chemical production plants, but also equipment design with appropriate materials, their

properties, operation and control. Physical and chemical phenomena involved in production processes are intrinsically multi-scale, since they operate at different time and length scales. The length scales range from the molecular scale up to the plants and environment scale. These length scales can be correlated with the time scales of phenomena involved, ranging from less than 1ns up to several years. All of the scales have an impact on the performance of a production process Systems engineering embraces process simulation, equipment design, and system oriented, cross-linked thinking for the multi-scale and multi-disciplinary fields such as micro chemical plants. A systems approach is generally model-based where mathematical models of different types and forms play increasingly important roles in process design and operation. A comprehensive model-based systematic approach needs a flexible framework for plug-and-play of knowledge bases, models, methods, and tools. In the future, product-process-device modeling will contribute to chemical and pharmaceutical research and development. First-principle and data-driven modelling approaches complement each other in such research and development. In addition, a systematic framework is needed to work efficiently with product-process-device models and to fully exploit their potential benefits.

List of Publications

Journal

1. Osamu Tonomura, Shotaro Tanaka, Masaru Noda, Manabu Kano, Shinji Hasebe, Iori Hashimoto, “CFD-based optimal design of manifold in plate-fin microdevices,” *Chemical Engineering Journal*, 101 (2004) 397–402 [Chapter 1]
2. Manabu Kano, Toku Fujioka, Osamu Tonomura, Shinji Hasebe, Masaru Noda, “Data-based and model-based blockage diagnosis for stacked microchemical processes,” *Chemical Engineering Science*, 62 (2007) 1073–1080 [Chapter 5]
3. Osamu Tonomura, Takayuki Tominari, Manabu Kano, Shinji Hasebe, “Operation policy for micro chemical plants with external numbering-up structure,” *Chemical Engineering Journal*, 135S (2008) S131–S137 [Chapter 4]
4. Yoshiaki Tanaka, Osamu Tonomura, Katsumi Isozaki, Shinji Hasebe, “Detection and diagnosis of blockage in parallelized microreactors,” *Chemical Engineering Journal*, 167 (2011) 483–489 [Chapter 6]
5. Osamu Tonomura, Tatsuya Takase, Shinji Hasebe, “Shape design of pressure-driven microchannels using adjoint variable method,” (in Preparation) [Chapter 2]
6. Osamu Tonomura, Shinji Hasebe, Masaru Noda, “Thermo-fluid design approach to microreactors with uniform temperature and residence time distribution,” (in Preparation) [Chapter 3]
7. Osamu Tonomura, Akira Morimoto, Shinji Hasebe, “Optimal channel design and sesor allocation of flow distribution for rapid blockage detection and stable operation of parallelized microreactors,” (in Preparation) [Chapter 7]

Conference Proceedings

1. Osamu Tonomura, Manabu Kano, Shinji Hasebe, Masaru Noda, "Optimal shape design and operation of microreactors," *7th World Congress of Chemical Engineering (WCCE)*, O35-003, Glasgow, Scotland, Jul. 10-14 (2005) [a part of Chapter 3]
2. Osamu Tonomura, Shinji Hasebe, "Shape Optimization of microchannels using CFD and adjoint method," *20th European Symposium on Computer Aided Process Engineering (ESCAPE)*, 37-42, Ischia, Italy, June 6-9 (2010) [a part of Chapter 2]
3. Osamu Tonomura, Shinji Hasebe, "Detection and diagnosis of blockage in externally parallelized microreactors," *AIChE Annual Meeting*, paper 325e, Pittsburgh, PA, Oct. 28-Nov. 2 (2012) [a part of Chapter 6]
4. Akira Morimotoi, Osamu Tonomura, Shinji Hasebe, "Optimal channel design and sesor allocation of flow distribution for rapid blockage detection and stable operation of parallelized microreactors", *2nd Flow Chemistry Asia Conference*, Singapore, Nov. 14-15 (2013) [a part of Chapter 7]

Patents

1. Osamu Tonomura, Satoshi Nagahara, Manabu Kano, Shinji Hasebe
   Fluid distribution device, micro plant, method of designing fluid distribution device, and method of detecting blockage of flow channel
   Japanese Patent Number: 5376602 (Registration date: October 4, 2013)
   US Patent Number: 8,549,907 (Registration date: October 8, 2013)
   [a part of Chapter 6]

2. Yoshiaki Tanaka, Osamu Tonomura, Katsumi Isozaki, Shinji Hasebe
   Flow distribution device and micro plant
   Japanese Patent Number: 5564723 (Registration date: June 27, 2014)
   [a part of Chapter 6]